The Thesis Committee for Jinkyoo Park
Certifies that this is the approved version of the following thesis:

On Characteristics of Stable Boundary Layer Flow Fields and Their Influence on Wind Turbine Loads

APPROVED BY
SUPERVISING COMMITTEE:

Supervisor:

Lance Manuel

Sukanta Basu

On Characteristics of Stable Boundary Layer Flow Fields and their Influence on Wind Turbine Loads

by

Jinkyoo Park, B.S.

THESIS

Presented to the Faculty of the Graduate School of
The University of Texas at Austin
in Partial Fulfillment
of the Requirements
for the Degree of

MASTER OF SCIENCE IN ENGINEERING

THE UNIVERSITY OF TEXAS AT AUSTIN
August 2011

Dedicated to my family.

Acknowledgments

I would like to express my deep gratitude to my advisor, Dr. Lance Manuel, for his encouragement and guidance during my research and graduate studies. Without his support, I would not have completed my graduate study. Special gratitude is also extended to Dr. Sukanta Basu at North Carolina State University for the numerical simulation work related to meteorology and for his advice on my research. I also would like to thank the faculty members in structural engineering who have shared me academic insight and inspiration.

I gratefully acknowledge the financial support of the National Science Foundation that I received through Grant No. CBET-0967816 (Program Manager: Dr. Gregory L. Rorrer).

Last but not least, I would like to offer my sincerest thanks to my parents and brothers for their love and their trust in me.

Jinkyoo Park
August 2011

On Characteristics of
Stable Boundary Layer Flow Fields
and their Influence on Wind Turbine Loads

Jinkyoo Park, M.S.E.
The University of Texas at Austin, 2011

Supervisor: Lance Manuel

Fourier-based stochastic simulation of wind fields commonly used in wind turbine loads computations is unable to account for contrasting states of atmospheric stability. Flow fields in the stable boundary layer (SBL), for instance, have characteristics such as enhanced wind shear and show noticeable wind veer (changing wind direction with elevation); the influence of such characteristics on utility-scale wind turbine loads has not been systematically studied. To investigate these influences, we use large-eddy simulation (LES) to generate inflow wind fields and to estimate load statistics for a 5-MW wind turbine model. In the first part of this thesis, we describe a procedure employing LES to generate SBL wind fields for wind turbine load computations. In addition, we study how large-scale atmospheric conditions as well as associated turbine-scale wind field characteristics affect turbine loads. In the second part, we study the contrasting characteristics of LES-SBL and stochastic neutral boundary layer (NBL) flow fields and their influences on wind turbine load statistics by isolating effects of the mean wind (shear) profile and of variation in wind direction and turbulence levels over the rotor sept area.

Among large-scale atmospheric conditions, the geostrophic wind speed and surface cooling rate have the greatest influence on flow field characteristics and, thus, on wind turbine loads. Higher geostrophic winds lead to increased mean and standard deviation values of the longitudinal wind speed at hub height, while attenuating wind shear. This generally increases fatigue and maximum loads on the wind turbine. A higher surface cooling rate makes the atmosphere more strongly stratified and, subsequently, increases the wind shear and decreases the level of turbulence. This generally decreases the fatigue and maximum tower-top yawing moment and base fore-aft tower bending moment. In the case of the blade root out-of-plane bending moment, however, higher surface cooling rates increase fatigue loads due to the enhanced shear which magnifies the amplitude of this blade bending moment.

In summary, our studies suggest that LES may be used very effectively to model wind fields in the SBL (that have contrasting characteristics from those in the NBL) and to assess turbine loads for conditions that are not typically examined in design standards.

Table of Contents

List of Tables

List of Figures

Chapter 1

Introduction

1.1 Background

As concerns about greenhouse gas emissions and increasing oil prices keep growing, renewable energy sources and wind power in particular have received increasing attention. By the first half of 2011, the total energy generated by wind power worldwide had reached 200GW. This is equivalent to 2.5% of global electricity consumption, according to the World Wind Energy Association (WWEA). The U.S. government has announced that wind energy will provide 20% of the U.S. Electricity needs by 2030. Currently, wind energy provides only 1% of total U.S. electricity generation (36 GW in 2010); thus, an additional capacity of 270 GW will need to be available by 2030 to achieve the target [16].

The expansion of wind power is accelerating due to the development of state-of-the-art wind turbine technologies; not only the efficiency but also the size of wind turbines is increasing. Large wind turbines (with hub heights of 80-100 meters and higher) are subjected to more severe atmospheric conditions such as low-level jets, stronger wind shear, and changing wind direction with elevation—all of which are experienced in the stable boundary layer.

1.2 Research Motivation

Wind conditions in the stable boundary layer (SBL) can offer a good source of power generation because they are faster and more consistent. However, abnormal wind inflow phenomena such as higher shear, coherent turbulence structures, and wind direction changes with elevation, which have been observed in the SBL, can cause harmful damage to a wind turbine structure. The International Electrotechnical Commission (IEC) sets design requirements for wind turbines in the standard, IEC 61400-1 [2]. This standard does not address SBL wind field simulation and SBL-associated wind field characteristics.

In recent years, many simulation methods for generating turbulent flow fields have been developed. Compared to stochastic methods commonly used for neutral boundary layer flow field generation where flows are stationary and usually derived from standard spectra, computational fluid dynamic (CFD) methods, based on solution of the Navier-Stokes equation, can more accurately capture the behavior of fluid motion and even account for turbulence. Among various CFD approaches, direct numerical simulation (DNS) can provide the most accurate behavior of wind fields, but the computational costs are prohibitive. Currently, large-eddy simulation (LES), which reduces the computational cost by employing filtering processes, is being used extensively in atmospheric science and other fields. In this research, LES will be applied to model wind fields in the SBL and to study associated wind turbine loads on a utility-scale machine.

1.3 Stable Boundary Layer

The stable boundary layer (SBL) is a stably stratified atmospheric layer that usually forms in the night over land when the earth cools as a result of a net loss of radiation. This net loss of radiation causes the temperature of the air to increase with height and this inversion of the lapse rate acts as a damper on the vertical movement of the air, eventually stratifying the wind flow layers. Generally, statically stable air tends to suppress turbulence while it induces strong shear.

Many interesting processes can occur within the SBL such as nocturnal low-level jets, patch sporadic turbulence, and wind direction veering with elevation [14]. Several researchers have attempted to study the impact of these SBL-associated features on utility-scale wind turbines. Sim et el. [12, 13] investigated the influence of SBL flow fields on wind turbine fatigue and extreme loads. Kelley [10] studied the influences of coherent turbulence structures, identified by high Reynolds stresses in the SBL, on a large wind turbine.

Figures 1.1(a) and 1.1(b) show the longitudinal wind speed variation and wind direction change with height in the stable boundary layer. The wind fields in these figure were simulated using LES. The wind speed and direction profiles are not in steady state as can be seen in the figures; they evolve with time during the night. Note that the thick red-colored layer that represents concentrated higher wind speeds in Fig. 1.1(a) shows the formation of a low-level jet (LLJ).

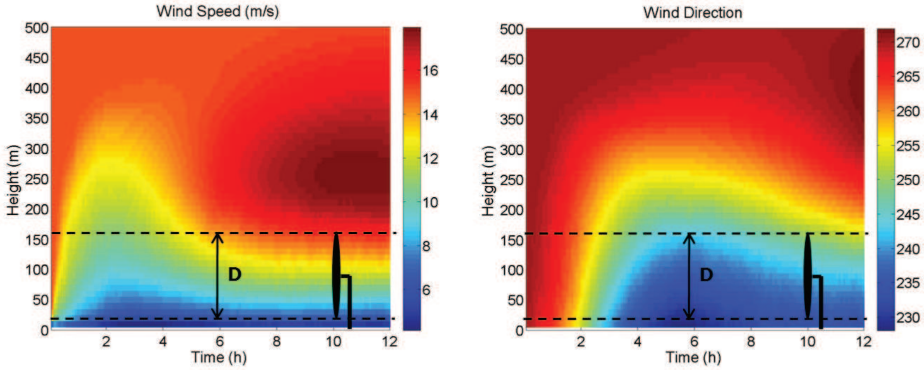

(a) Longitudinal wind speed

(b) Wind direction

Figure 1.1: Evolution of the wind field in SBL simulated by large-eddy simulation

1.4 Research Organization

This research is composed mainly of two parts. The first part (Chapter 2) is about the procedure for making use of LES in wind turbine loads estimation to understand the general characteristics of SBL wind fields and associated wind turbine loads. The organization of this topic is represented in Figure 1.2. Chapter 2 first studies the characteristics of LES-generated SBL wind inflows. We address the procedure for converting LES outputs into wind fields that are compatible to an open-source wind turbine loads simulation code, FAST [7]. In addition, we investigate the relation between large-scale environmental parameters and turbine-scale wind field characteristics. We also investigate how large-scale environmental conditions affect wind turbine load statistics.

The second part of this research (Chapter 3) is related to a comparison

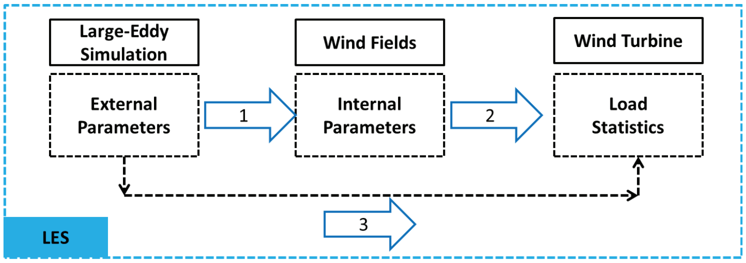

Figure 1.2: Procedure for using LES in wind turbine loads estimations

of SBL and NBL wind fields in terms of turbine-scale wind field characteristics and their effects on wind turbine loads. The organization of this work is represented in Figure 1.3. First we compare characteristics of SBL and NBL wind fields. Based on observed differences in the two types of flow fields, we isolate SBL-related features, observed in the LES-generated wind fields. Then, we investigate how these features contribute to wind turbine load processes as well as load statistics. Through this analysis, we can understand not only how the two types of wind fields, SBL and NBL, differ from each other, but also what specific characteristics of the simulated SBL-associated wind fields most directly influence wind turbine loads.

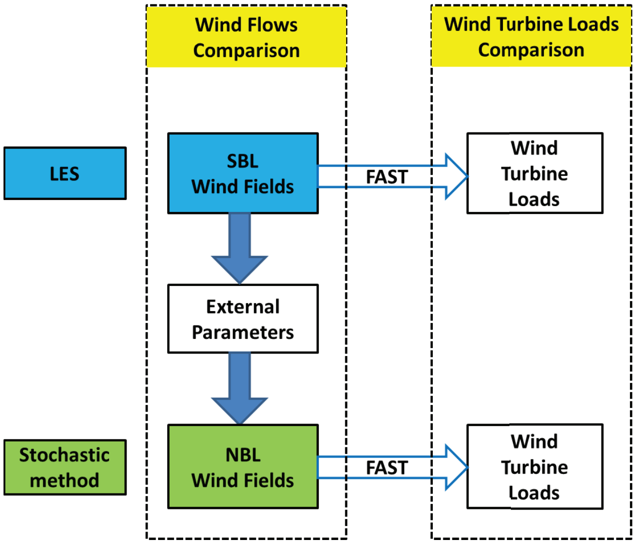

Figure 1.3: Procedure for comparison of NBL and SBL flow fields.

Chapter 2

Large-Eddy Simulation for Stable Boundary Layer Wind Fields and Associated Wind Turbine Loads

2.1 Introduction

Fourier-based stochastic simulation of wind fields commonly used in wind turbine loads computations is unable to discriminate between flow fields during periods of varying thermal stratification and stability in the atmospheric boundary layer. For instance, wind velocity flow fields in the stable boundary layer (SBL) have enhanced wind shear and are also accompanied by wind veer (i.e., wind direction changes with height above the ground). The influence of such flow characteristics on utility-scale wind turbines has not been systematically studied. To investigate such influences, we use large-eddy simulation (LES) to generate inflow wind fields under different SBL conditions and then extract load statistics from aeroelastic response simulations on a model of a 5-MW wind turbine. An extensive suite of LES flow fields are generated where the geostrophic winds, surface cooling rates, and other large-scale forcings are varied. Our overall study on turbine loads for SBL wind fields is organized as follows. First, we carry out a parametric study to relate large-scale environmental conditions (which we refer to as "external" wind field parameters) to wind field characteristics at the turbine scale (we refer to these as “internal” wind field parameters). Next, we investigate how the various turbine-scale internal parameters, separately and together, influence turbine loads. Finally, we attempt to establish a direct relationship between the large-scale environmental conditions (the external parameters) and the wind turbine load statistics.

2.1.1 Background on Large-Eddy Simulation

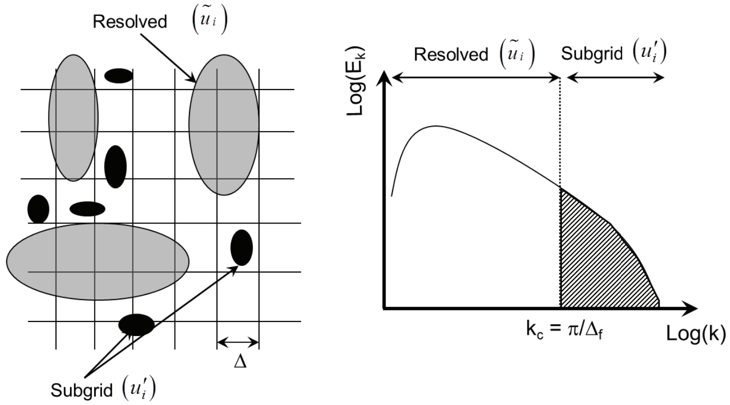

Figure 2.1: Resolved and sub-grid scales in physical space (left) and Fourier space (right) [4].

Large-eddy simulation (LES) is a state-of-the-art mathematical approach for modeling turbulence in computational fluid dynamics (CFD). LES is currently the most efficient method for modeling the turbulent motions of high Reynolds-number flows. In LES, low-pass filtering is applied to the Navier-Stokes equations to eliminate the small-scale motions of turbulence as represented in Fig. 2.1. In LES, one resolves large-scale flow field features;

sub-grid scale turbulence is parameterized based on various theoretical and empirical models. LES has been employed in previous studies to model wind fields for neutral and stable boundary layer conditions and to compare resulting flow fields with those generated using stochastic simulation (see Sim [12], Sim et el. [13]).

2.1.2 Computational Framework and Analysis Procedure

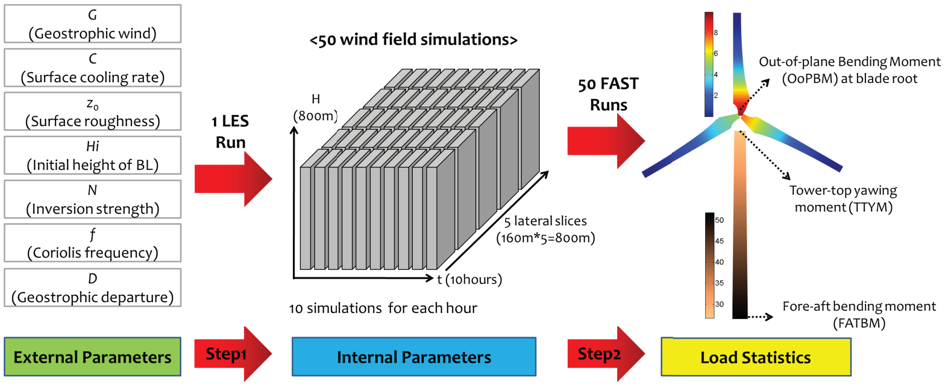

Figure 2.2: Procedure for using LES to study SBL wind fields and wind turbine loads.

Figure 2.2 shows the procedure undertaken in this study where we first attempt to relate the large-scale environmental conditions (external parameters) to turbine-scale wind field characteristics (internal parameters) and, next, we relate the internal parameters to wind turbine load statistics. The entire procedure can be divided into two parts: in the first part, for specific choices of external parameters (indicated in Fig. 2.2), LES wind fields are generated; next, from the simulated wind fields generated as the output from LES, wind field internal parameters of relevance at the turbine scale are extracted (these internal parameters are defined later) ; finally, from turbine response simulations with the various LES wind fields as input, wind turbine load statistics are estimated and related to the internal parameters. The ultimate goal is to examine how turbine loads are related to the internal parameters and how those internal parameters result from specific large-scale external parameters. Note that the external parameters (such as the geostrophic wind speed and the surface cooling rate as well as others) influence wind field changes mostly at longer time scales and larger spatial scales, while the internal parameters correspond to wind field parameters such as the hub-height mean wind speed and a wind shear parameter (the mean wind profile power-law exponent) that are averaged over shorter time scales (on the order of 10 minutes) and are relevant at spatial scales on the order of a turbine rotor diameter and smaller (the 5-MW turbine used in our study has a rotor diameter of 126 meters).

The output from the LES computations is a 3D-vector field (for the longitudinal, lateral, and vertical velocity components) provided over a 2D spatial grid (representing lateral and vertical coordinates) and as time series. There are a total of 80 grid points in the lateral (y) direction covering 800 m and 79 grid points in the vertical (z) direction extending 790 m above the ground. In the vertical direction, only the lowest 160 meters of the spatial domain are needed as this adequately covers the entire rotor swept area; in the lateral direction, the 800-meter extent allows us to make five lateral slices, each of which can be used in turbine response simulations. The LES computations are carried out to produce time series at 0.1 s (10 Hz) increments but are output at 0.4 s (2.5 Hz) for computational efficiency. Each LES output provides a 12-hour record. Thus, a total of 108,000 time steps result from each LES output file (108,000 × 0.4 s = 12 hours).

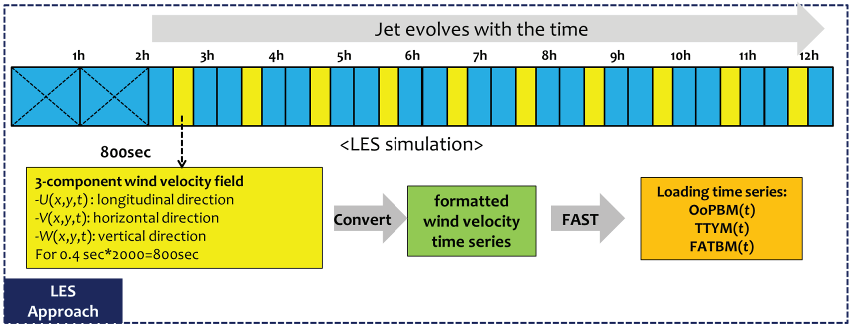

Figure 2.3: Temporal segmentation of a single LES output

Turbine loads are generally computed by running 10-minute simulations. Figure 2.3 describes how each 12-hour LES output is temporally segmented into 10-minute wind fields that may be used for turbine response simulations. Except for the first two hours of LES output that are discarded (to allow for some spin-up time), a ten-minute portion of the LES wind field is extracted from each of the remaining ten hours. Together with the five lateral slices that are extracted spatially, this yields a total of 50 simulated wind fields from each LES output that are used in turbine load calculations. Actually, each wind file taken from LES output for loads calculation is 800 seconds long so that transients can be extracted in the loads simulations and a full 600-second (10-minute) sample of loads can be obtained. Note that selecting wind fields covering ten whole hours allows us to study the effects of variation in wind field characteristics with evolution of the stable boundary layer. Figure 2.2 illustrates schematically how the lateral slices and the temporal segments are extracted from the LES output. The temporal segmentation is elaborated upon in Fig. 2.3.

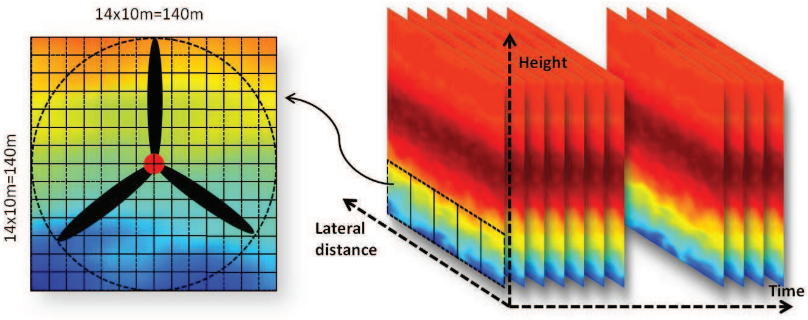

Figure 2.4: Spatial segmentation of a single LES output

As was mentioned before, the lateral and vertical grid spacings of the LES output are each 10 meters. Figure 2.4 illustrates how, from each of the five lateral slices, a 140 m × 140 m vertical plane centered at the turbine hub with 10 m grid spacing in lateral and vertical directions is used in the turbine response simulations that are carried out using the open-source software, FAST [7]. At each grid point, over the rotor plane, the velocity vector comprising velocities, U, W, and V, in the x, y, and z directions are part of the input to FAST. Rotor and tower loads are computed in FAST. Figures 2.2 and 2.3 indicate how 50 FAST analyses result from a single LES flow field output leading to various turbine load statistics. The three loads discussed in this work include OoPBM (the blade root out-of-plane bending moment), TTYM (the tower-top yawing moment), and FATBM (the fore-aft tower bending moment).

2.1.3 Wind Turbine Model for Load Calculations

Table 2.1: Key Properties and Dimensions of the NREL 5MW Baseline Wind Turbine.

Properties/Dimensions	Values
Power Rating	5 MW
Rotor Orientation, Configuration	Upwind, 3 Blades
Control	Variable Speed, Collective Pitch
Drivetrain	High Speed, Multiple-Stage Gearbox
Rotor Diameter	126 m
Hub height	90 m
Cut-In, Rated, and Cut-Out Wind Speeds	3 m/s, 11.4 m/s, 25 m/s
Cut-In and Rated Rotor Speeds	6.9 rpm, 12.1 rpm
Rated Tip Speed	80 m/s
Overhang, Shaft Tilt, Precone	5 m, 5^o, 2.5^o
Rotor Mass	110,000 kg
Nacelle Mass	240,000 kg
Tower Mass	347,460 kg

In this study, turbine loads simulations are carried out for the NREL 5MW Onshore Baseline Wind Turbine model [8]. This model describes a conventional three-bladed upwind variable-speed collective pitch-controlled turbine. Some of the turbine's key properties and dimensions are summarized in Table 2.1. We assume a turbine foundation fixed at the base for the 5MW turbine model.

2.1.4 Fatigue and Extreme Loads

In this study, we compute load statistics related to ultimate and fatigue limit states. For ultimate states, we consider either ten-minute maxima or, in some cases, one-minute block maxima computed from the output (load) time series from FAST. For fatigue limit states, we estimate equivalent fatigue load (EFL) statistics; this is done by first constructing a load range histogram using a rainflow cycle-counting algorithm [3] applied to the loads time series. Information from this histogram is converted to an estimate of cumulative damage based on Miner's rule; this finally yields an EFL estimate [15]. Miner's rule can be expressed as follows:

$$N_F \cdot S^m = K \tag{2.1}$$

where N_F is the number of cycles to failure at stress level, S; m is the Wöhler exponent, a property of the material; K is another material-related parameter related to the total fatigue resistance or capacity. To compute damage resulting from N stress cycles, S_i, each of different amplitude, Miner's rule can be used as follows:

$$D = \frac{\sum_{i=1}^{N} S_i^m}{K} \tag{2.2}$$

where D is the damage fraction; if D reaches unity, failure due to fatigue is assumed to occur. To compare different load time series, it is useful to define an "equivalent fatigue load" that represents the amplitude that a fixed number, N_0, of constant-amplitude stress cycles that would result in the same damage as that found for the N variable-amplitude stress cycles according to Eq. 2.2. This equivalent fatigue load (EFL) is defined as follows by equating Eqs. 2.1 and 2.2:

$$EFL = \sqrt[m]{\sum_{i=1}^{N} \frac{S_i^m}{N_0}} \tag{2.3}$$

In this study, we use a fixed number, N_0, equal to 1,000 in all EFL calculations; the actual number, N, of loading cycles will vary for each load time series resulting from the different wind fields. (An EFL, e, estimated from a ten-minute load time series, should be interpreted as: "The fatigue damage that results from this load time series is the same as would be caused by 1,000 load cycles of constant amplitude, e.") Generally, only load EFL estimates will be considered when comparing the influences of different SBL wind field characteristics on fatigue loads on the 5-MW turbine model; in some cases, full load cycle/range histograms are also presented.

2.2 The Effect of Environmental Conditions on Turbine-Scale Wind Field Characteristics

To simulate loads on a wind turbine for design, Fourier-based stochastic simulation is generally used. For instance, TurbSim [6], a stochastic, full-field, turbulent wind simulator developed at the National Renewable Energy Laboratory (NREL), can generate turbulent wind fields based on standard turbulence spectrum models. Such procedures have been routinely used for flow fields in the near-neutral atmospheric boundary layer. For the stable boundary layer, which is the focus of this study, we instead use LES to generate flow fields and represent the flow physics realistically. We specify large-scale environmental parameters as input in order to realize several stability regimes and turbine-level flow fields.

2.2.1 External Parameters

The large-scale atmospheric and surface conditions used as inputs or initial conditions for the LES computations are termed external parameters in this study. The following seven external parameters were varied as LES inputs:

- G, Geostrophic wind speed
- C, Surface cooling rate
- z_0, Surface roughness
- H_i, Initial height of boundary layer
- N, Inversion strength
- f, Coriolis frequency
- D, Geostrophic departure

Forty-four different combinations of these external parameters were considered in this study. These combinations are listed in Table 2.2. In particular, note that LES Run No. 12 (marked as CONTROL) represents a single case that we make special use of in discussing trends and carrying out some parametric studies.

Table 2.2: List of LES runs representing different combinations of external parameter values

No.	G(m-s^{-1})	C(K-h^{-1})	z_0(m)	H_i(m)	N(K-m^{-1})	f(s^{-1})	D(m-s^{-1})
1	9	0.75	0.03	200	0.003	0.00010	0
2	12	0.75	0.01	200	0.003	0.00010	0
3			0.03	200	0.003	0.00010	0
4			0.03	300	0.003	0.00010	0
5	12	2.00	0.03	200	0.003	0.00010	0
6	15	0.50	0.03	200	0.003	0.00010	0
7	15	0.75	0.01	200	0.003	0.00010	0
8			0.01	200	0.003	0.00012	0
9			0.03	50	0.003	0.00010	0
10			0.03	100	0.003	0.00010	0
11			0.03	200	0.003	0.00008	0
12 **(CONTROL)**	**15**	**0.75**	**0.03**	**200**	**0.003**	**0.00010**	**0**
13			0.03	200	0.003	0.00010	2
14			0.03	200	0.003	0.00010	4
15			0.03	200	0.003	0.00010	6
16			0.03	200	0.003	0.00010	8
17			0.03	200	0.003	0.00012	0
18			0.03	200	0.010	0.00008	0
19			0.03	200	0.010	0.00010	0
20			0.03	200	0.010	0.00012	0
21			0.03	300	0.003	0.00010	0
22			0.10	200	0.003	0.00010	0
23			0.10	200	0.003	0.00012	0
24	15	1.00	0.03	200	0.003	0.00010	0
25			0.10	200	0.003	0.00008	0
26			0.10	200	0.003	0.00012	0
27	15	1.25	0.03	200	0.003	0.00010	0
28	15	1.50	0.03	200	0.003	0.00010	0
29	15	2.00	0.03	200	0.003	0.00010	0
30	18	0.75	0.01	200	0.003	0.00010	0
31			0.03	50	0.003	0.00010	0
32			0.03	100	0.003	0.00010	0
33			0.03	200	0.003	0.00010	0
34			0.03	200	0.003	0.00010	2
35			0.03	200	0.003	0.00010	4
36			0.03	200	0.003	0.00010	6
37			0.03	200	0.003	0.00010	8
38			0.03	200	0.010	0.00010	0
39			0.03	300	0.003	0.00010	0
40			0.10	200	0.003	0.00010	0
41	18	1.00	0.03	200	0.003	0.00010	0
42	18	1.25	0.03	200	0.003	0.00010	0
43	18	1.50	0.03	200	0.003	0.00010	0
44	18	2.00	0.03	200	0.003	0.00010	0

2.2.2 Internal Parameters

Turbine-scale wind field parameters are referred to as internal parameters in this study. Traditionally, the hub-height longitudinal ten-minute mean wind speed and turbulence intensity (or standard deviation) have been considered as turbine-scale flow field parameters of interest when defining or simulating inflow fields for turbine load calculations. We consider these and a few others that are especially relevant for describing characteristics of SBL flow fields; stability-related parameters have been the subject of other studies where correlation of these to turbine loads has been discussed [5, 9, 11]. The following list of internal parameters are considered in some detail in the numerical studies and discussions that follow:

- U_h, mean of the longitudinal wind speed at hub height;
- σ_U, standard deviation of the longitudinal wind speed at hub height;
- α, exponent of the power law describing wind shear profile;
- Ri, Richardson number;
- $\Delta\theta$, mean wind direction change between the rotor top and bottom (an ad hoc indicator of wind veer).

The 44 different LES runs listed in Table 2.2 yielded a total of 2,200 wind fields that were used in turbine response simulations (since each LES run results in 50 ten-minute wind files for turbine loads studies). On the turbine rotor plane, the simulated wind velocities described on the grid shown in Fig. 2.4 are needed to compute internal parameters. Table 2.3 provides summary statistics of the internal parameters from the 2,200 wind fields resulting from the 44 LES runs.

In general, SBL wind fields are expected to have steeper mean wind profiles (larger values of α), lower turbulence levels (smaller values of σ_U), non-zero wind veer ($\Delta\theta$), and positive Richardson number (Ri) compared to

Table 2.3: Summary statistics of the internal parameters from 2,200 LES-generated wind fields.

	U_h (m/s)	α	σ_U (m/s)	Ri	$\Delta\theta$ (°)
Mean (m)	11.657	0.368	0.497	0.159	15.089
Std Dev (s)	1.526	0.065	0.171	0.063	6.174
Max	15.397	0.537	0.944	0.660	34.247
Min	6.551	0.198	0.118	0.112	4.341

neutral boundary layer (NBL) wind fields. For the SBL cases studied here, as expected, the wind shear exponent, α, of 0.368 is significantly higher than 0.2, a value often used for neutral conditions. Also, the mean turbulence intensity is less than 5%, which is quite low, the mean wind direction turning between the rotor top and bottom is more than 15°. The variability is seen to be greater in σ_U) than in α values. The largest variability is seen in Ri and $\Delta\theta$, both of which have coefficients of variation greater than 40%. Compared to U_h and σ_U, the variability in the remaining three parameters that are all more important in stable stratification is much larger.

Table 2.4: Correlation coefficients among the internal parameters (based on 2,200 LES-generated wind fields).

	U_h	α	σ_U	Ri	$\Delta\theta$
U_h	1.00	0.28	0.36	0.10	0.09
α	0.29	1.00	-0.59	0.50	0.88
σ_U	0.36	-0.59	1.00	-0.55	-0.77
Ri	0.10	0.50	-0.55	1.00	0.69
$\Delta\theta$	0.09	0.88	-0.77	0.68	1.00

Table 2.4 presents correlation coefficients among the internal parameters. We note that U_h is positively correlated with σ_U as well as with α. However, the correlation coefficient between α and σ_U is negative suggesting

a complex relationship among U_h, σ_U, and α which will be further investigated later. The Richardson number, which is widely used as an indicator of atmospheric stability, is positively correlated with α and $\Delta\theta$, and negatively correlated with σ_U. Stable conditions, indicated by a higher Ri number, appear to cause strong shear and large wind direction change with elevation, while reducing turbulence levels. Most notably, the correlation coefficient between α and $\Delta\theta$ is the largest; this indicates that strong wind shear and wind direction change (wind veer) occur together in the stable boundary layer.

It is clear that the various internal parameters are inter-related in a complicated manner; this is difficult to completely understand by studying correlation coefficients (i.e., pair-wise relation measures) alone. Accordingly, we next investigate relationships, together, of three of the internal parameters—U_h, σ_U, and α—by means of 3-D graphical representations. The three parameters selected are thought to be the most important because they are the most directly related to wind turbine loads and they are easier to measure and interpret compared with the other parameters such as Ri that requires understanding, for example, of temperature gradients.

Figure 2.6 shows all 2,200 combinations of the internal parameters, U_h, σ_U, and α, extracted from the 44 LES runs. Usually, wind fields are simulated by specifying internal parameters such as these (e.g., for stochastic simulation of wind fields in the neutral boundary layer); here, however, we *extract* these internal parameters from the LES-generated wind fields and they indicate to us the nature of turbine-scale flow field characteristics. The x-coordinate of

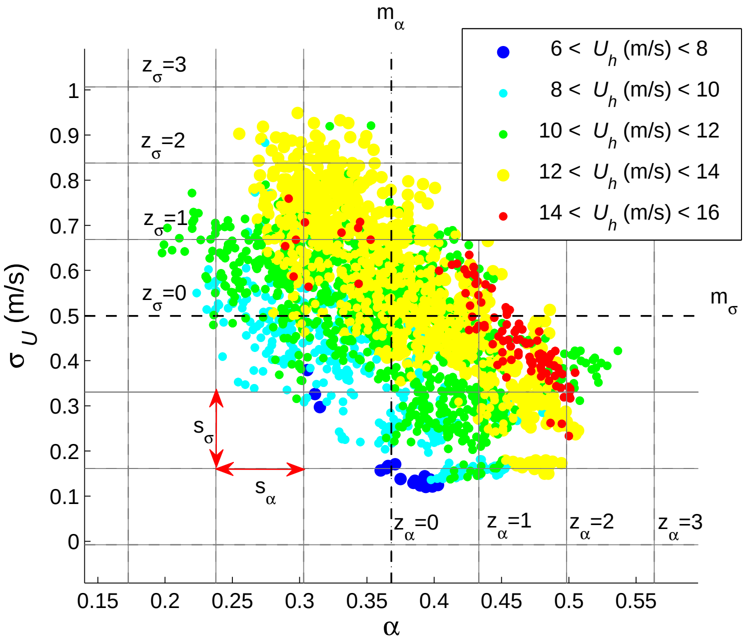

Figure 2.5: Relationships between U_h, σ_U, and α.

each point represents the value of α, while the y-coordinate represents the value of σ_U. The vertical and horizontal grid lines are spaced at one standard deviation for α and σ_U, respectively. The internal parameter, U_h, is also indicated by the color of each point; the color for each U_h value is indicated by ranges in the legend. This plot effectively describes how these three internal parameters occur together in the LES flow fields and helps to identify patterns of correlation at the same time.

It is convenient to normalize the parameters, α and σ_U, as follows:

$$z_\sigma = \frac{\sigma_U - m_\sigma}{s_\sigma} \tag{2.4}$$

$$z_\alpha = \frac{\alpha - m_\sigma}{s_\sigma} \tag{2.5}$$

Based on these normalized values, we can broadly define four domains according to turbulence and shear as follows:

- $z_\sigma > 0 \cap z_\alpha < 0$: strong turbulence and weak shear
- $z_\sigma > 0 \cap z_\alpha > 0$: strong turbulence and strong shear
- $z_\sigma < 0 \cap z_\alpha < 0$: weak turbulence and weak shear
- $z_\sigma < 0 \cap z_\alpha > 0$: weak turbulence and strong shear

This domain segmentation of wind field characteristics will be repeatedly used in this study when we relate turbine-scale wind field characteristics to various wind turbine load statistics. Studying Figure 2.6 in the context of this segmentation, we see that a large proportion of the simulated SBL flow fields are accompanied either by strong turbulence and weak shear regions or by strong shear and weak turbulence regions. This suggests that shear and turbulence effects are competing effects (this explains the negative correlation between α and σ_U we saw earlier); when either of them is large (they are not likely to both be large at the same time),we see that U_h has higher values (this is also as expected, given the correlation coefficients). Nevertheless, the relationship among these three parameters is by no means a simple one. We note from the figure that simulated SBL wind fields exhibit much strong wind shear (with α as high as 0.53) versus NBL wind fields for which values of 0.2 are more common for α.

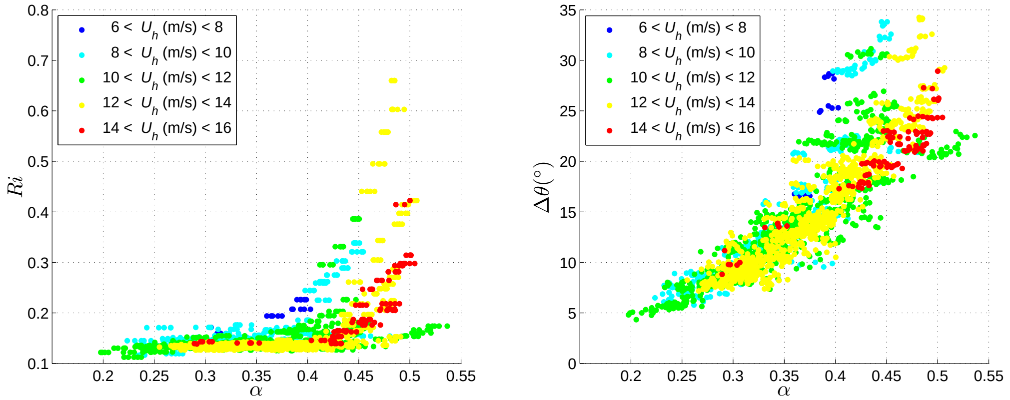

(a) Ri vs. α (b) $\Delta\theta$ vs. α

Figure 2.6: Relationships between (a) U_h, Ri, and α; and (a) U_h, $\Delta\theta$, and α.

We investigate next the relationships among other sets of internal parameters in Figure 2.6. From Fig. 2.6a, we note that strong shear is associated with higher values of Ri; this relationship, however, is not linear—for flow fields where the α values were larger than average, Ri values are seen to increase at a faster rate with increased shear. Figure 2.6b shows that there is strong positive correlation between α and $\Delta\theta$; this again indicates that wind veer accompanies strong wind shear seen in the SBL. Figure 2.6 suggests no strong relationship between U_h and either R_i or $\Delta\theta$.

2.2.3 Low-Level Jets and Correlation with Internal Parameters

As part of the diurnal cycle, shortly before sunset, turbulence decays in what was earlier a well mixed layer; a "residual" layer then forms with characteristics of the decaying mixed layer. In later hours, into the night, the lowest portion of the residual layer is transformed into the stable boundary layer by virtue of contact with the ground. At the ground, winds can be light but at some elevation above ground, winds can be supergeostrophic—this defines a so-called low-level jet (LLJ) [14]. LLJs can have maximum wind speeds of 10 to 30 m/s and are usually located 100 to 300 m above the ground; they can cause damage to wind turbines because they are associated with strong wind shear at elevations that overlap with the rotor swept areas of utility-scale wind turbines. In this study, an LLJ is treated as any simulated LES-SBL flow field that satisfies two conditions: (i) the slope of the mean wind shear profile changes from positive to negative; and (ii) the wind speed at that point is at least 1 m/s higher than the geostrophic wind speed. Based on this criterion, the 2,200 LES-generated wind fields were averaged laterally and in time to yield 440 mean wind profiles; from these, 245 showed the presence of a LLJ. We now examine the relationship of turbine-scale wind field parameters with the formation of LLJs and, specifically, investigate the correlation between the height of the low-level jet, H_{jet}, and these internal parameters.

Table 2.5: Summary statistics of internal parameters and H_{jet} for 245 averaged wind profiles (out of 440 available) that included a LLJ.)

	U_h (m/s)	α	σ_U (m/s)	Ri	$\Delta\theta\,(^\circ)$	H_{jet} (m)
Mean (m)	12.485	0.393	0.517	0.167	16.601	269.8
Std Dev (s)	1.098	0.058	0.172	0.079	6.043	54.3
Max	15.397	0.537	0.944	0.660	34.247	370
Min	8.989	0.255	0.146	0.126	7.339	140

Table 2.5 shows summary statistics on the internal parameters and H_{jet} from simulated wind fields in which LLJs formed. Comparing these statistics with those on the internal parameters based on all 2,200 wind fields (Table 2.3), we make a general observation that, in the subset of wind fields where LLJs form, the mean values of U_h, α, σ_U, Ri, and $\Delta\theta$, are all higher than when all the wind fields are considered together.

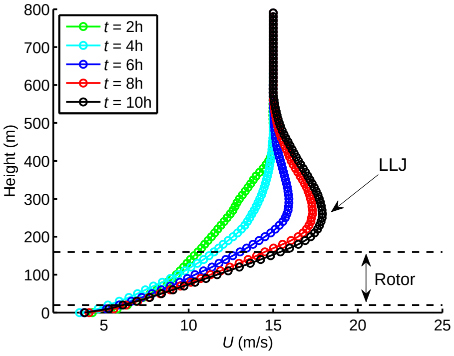

Figure 2.7: Low-level jet evolution with time in the LES-SBL simulations.

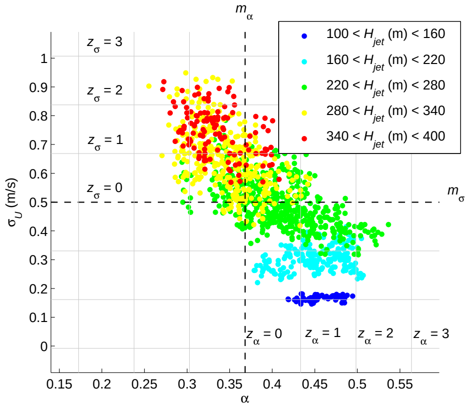

Figure 2.8: Relationship between α, σ_U, and H_{jet} (based on 245 averaged wind profiles where a LLJ formed).

Figure 2.7 shows how the mean wind vertical profile changes with time for a single LES run where a LLJ forms. We note that, at some point in time during the simulation, the mean wind speed at an elevation, referred to as H_{jet}, exceeds the geostrophic wind speed. This process of evolution of the LLJ leads to enhanced shear and faster winds over the rotor plane of the 5-MW turbine used in this study; the vertical extent of this rotor is indicated by the dotted lines.

Figure 2.8 shows conditions during which low-level jets form and associated jet heights, H_{jet}, in those cases. For the 245 averaged wind profiles where jets form, the positions of the points in the figure indicate the levels of shear and turbulence associated with the wind field, the color of the point indicates the jet height, H_{jet}. LLJs are seen to form most commonly in the region of strong shear and weak turbulence, and where the mean wind speed, in general, is higher (see Figure 2.6 to verify this). We also note, from Fig. 2.8, that H_{jet} is negatively correlated with α; a LLJ that forms at lower elevations causes the wind speed to increase more steeply with height, resulting in higher values of α. On the other hand, H_{jet} is positively correlated with σ_U. These observations are confirmed by a study of correlation coefficients of H_{jet} with internal parameters in Table 2.6. Low-level-jets usually form in strongly stratified (stable) atmospheric conditions; thus, H_{jet}, which is negatively correlated with α, is also negatively correlated with Ri and $\Delta\theta$.

Table 2.6: Correlation coefficient between jet height, H_{jet}, and internal parameters (based on 245 LES-SBL averaged wind profiles where a LLJ formed).

	U_h	α	σ_U	Ri	$\Delta\theta$
H_{jet}	0.28	-0.73	0.90	-0.63	-0.91

2.2.4 Large-Scale to Turbine-Scale Influences

The characteristics of wind fields, described by internal parameters, are affected by large-scale environmental conditions described by the combination of external parameters. To understand how these large-scale atmospheric and surface conditions affect turbine-scale characteristics of wind fields, we carry out sensitivity studies that seek to investigate the variation in internal parameters while a single external parameter is changed. As described earlier, the output of a single LES run results in 50 wind fields defined locally around the turbine; hence, we obtain 50 combinations of internal parameters for the same input external parameter set. As a result, we can attempt to assess the influence of the external parameters on the turbine-scale wind fields (and on the internal parameters). Since the internal parameters (from the 50 wind fields in each LES run) result from ten hours of LES-SBL simulations, we can also assess how the internal parameters evolve with time and, hence, better understand characteristics and the evolution of the stable boundary layer. We use the control case (defined in Table 2.2) to assess the influence of two external parameters, geostrophic wind speed and surface cooling rate, on internal parameters.

Table 2.7: LES runs used in studies involving variation of geostrophic wind speed and surface cooling rate.

No.	G(m-s^{-1})	C(K-h^{-1})	z_0(m)	H_i(m)	N(K-m^{-1})	f(s^{-1})	D(m-s^{-1})
G : Geostrophic Wind Speed Trend							
1	**9**	0.75	0.03	200	0.003	0.00010	0
3	**12**	0.75	0.03	200	0.003	0.00010	0
12 **(CONTROL)**	**15**	0.75	0.03	200	0.003	0.00010	0
32	**18**	0.75	0.03	100	0.003	0.00010	0
C : Surface Cooling Rate Trend							
6	15	**0.50**	0.03	200	0.003	0.00010	0
12 **(CONTROL)**	15	**0.75**	0.03	200	0.003	0.00010	0
28	15	**1.50**	0.03	200	0.003	0.00010	0
29	15	**2.00**	0.03	200	0.003	0.00010	0

Table 2.7 shows combinations of external parameters (resulting from different LES runs) that are used to track the influences of the variation of

the geostrophic wind speed and surface cooling rate on internal parameters. In each of the four runs for each parameter sensitivity study, only either the geostrophic wind speed or the surface cooling rate alone is changed while all the other parameters are fixed at the same values as in the control case.

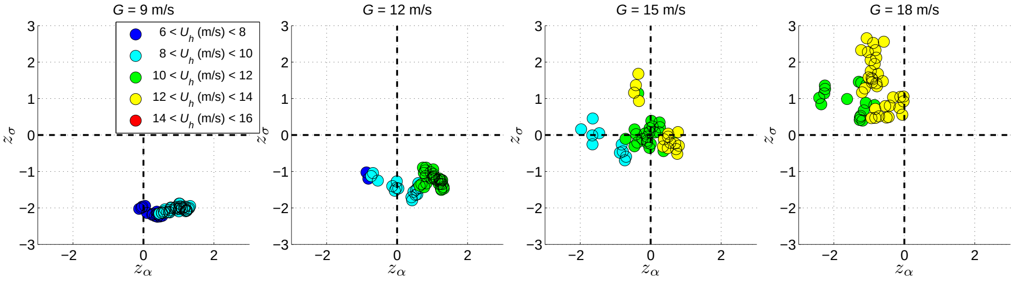

Figure 2.9: Effects of the geostrophic wind speed on internal parameters

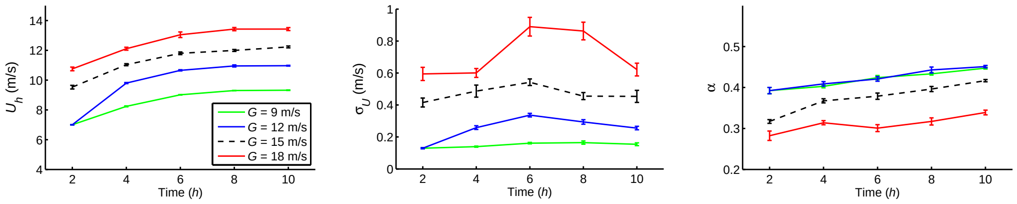

(a) U_h (b) σ_U (c) α

Figure 2.10: Variation of internal parameters with geostrophic wind speed and time.

Figure 2.9 shows how combinations of internal parameters change with changes in the geostrophic wind speed, G. The x-axis and y-axis represent, respectively, normalized α and σ_U values. As the geostrophic wind speed increases, the locations of points in the plots collectively move to the left and upward; this suggests that the level of turbulence increases, while the magnitude of wind shear decreases. In addition, as expected, U_h is seen to increase as the geostrophic wind speed increase.

Figure 2.10 shows how the three internal parameters, U_h, σ_U, and α, all change with time elapsed in the LES-SBL simulations and how these variations are affected by changes in the geostrophic wind speed. In general, U_h increases with time (with slowing rates); increased geostrophic wind speeds raise the U_h levels systematically. No clear time-varying trend is seen for σ_U; in general, σ_U increases with the geostrophic wind speed. We see that α increases almost linearly with time; this suggests that wind shear is intensified with time as the SBL flow field evolves. We note too that α reduces as the geostrophic wind speed increases; this suggests that the higher geostrophic winds tend to disrupt the stratified wind shear profile and, at the same time, increase turbulence levels. In sum, higher geostrophic winds are seen to increases hub-height mean wind speed and turbulence while weakening the wind shear.

Figure 2.11 shows how combinations of internal parameters change with changes in the surface cooling rate, C. As the surface cooling rate increases, the locations of points in the plots collectively move to the right and upward; this suggests that the level of turbulence decreases, while the magnitude of wind shear increases. Also, the points corresponding to higher U_h values make up a greater proportion of the data when the surface cooling rate gets larger. A higher surface cooling rate causes air temperatures to increase more rapidly with height, thus enhancing the stability. As a result of this greater stratification, vertical movement of wind due to buoyancy is suppressed, resulting in reduced levels of turbulence. The reduced turbulence level, in turn, diminishes

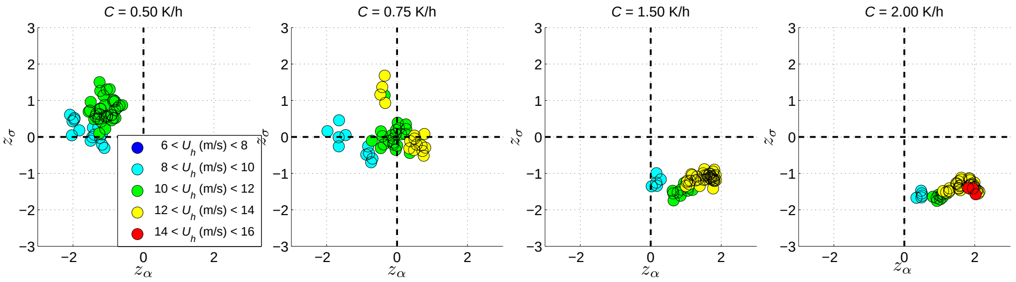

Figure 2.11: Effects of surface cooling rate on internal parameters

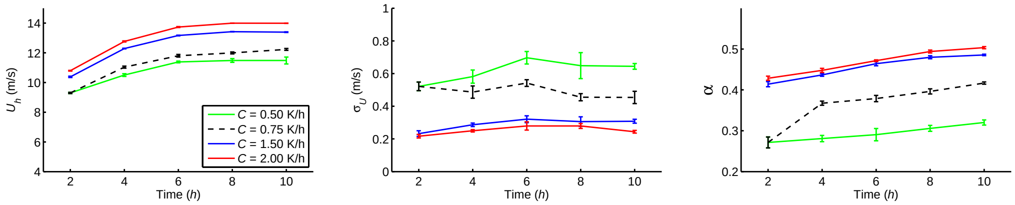

(a) U_h (b) σ_U (c) α

Figure 2.12: Variation of internal parameters with surface cooling rate and time.

the retarding effects of turbulence on mean wind flows and leads to increased wind shear as well as increased wind speeds.

Figure 2.12 shows how the three internal parameters, U_h, σ_U, and α, all change with time elapsed in the LES-SBL simulations and how these time-varying trends are affected by changes in the surface cooling rate. As described above, U_h increases with time; also, higher surface cooling rates increase the general level of U_h.

The dotted lines in Fig. 2.12 represent the control case; thus, we can compare the influences of the geostrophic wind speed and the surface cooling rate on the internal parameters. We note that σ_U does not show any systematic time-varying trend, while the overall σ_U level as well as its variability indicated by error bars increase as the surface cooling rate decreases. We note that α increases with time and it also systematically increases with surface cooling rate. In sum, higher surface cooling rates increases the hub-height mean wind speed and enhances the wind shear, while attenuating the level of turbulence; as expected, it appears that the level of shear and turbulence show opposing general trends.

2.3 The Influence of Turbine-Scale Wind Field Characteristics on Turbine Loads

We now discuss how turbine-scale wind field characteristics (i.e., internal parameters) affect wind turbine loads, by studying in some detail the load processes, OoPBM, TTYM, and FATBM, and the manner in which these internal parameters affect the loads.

2.3.1 Blade Root Out-of-Plane Bending Moment

The strong influence of wind shear on the out-of-plane bending moment along the length of a blade is investigated by first running some controlled stochastic simulations where U_h is set fixed, the turbulence is set to zero, and the wind shear exponent, α, alone is varied. We study the out-of-plane bending moment variation along the length of the blade and as a function of azimuth angle in Fig. 2.13. The upper two color-map plots show the mean wind speed variation that a blade experiences, as a function of azimuthal position, as it

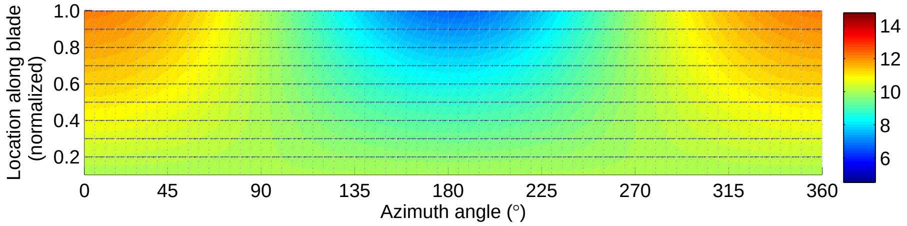

(a) $U_h = 10.0$ m/s, $\alpha = 0.4$, $\sigma_U = 0.0$ m/s

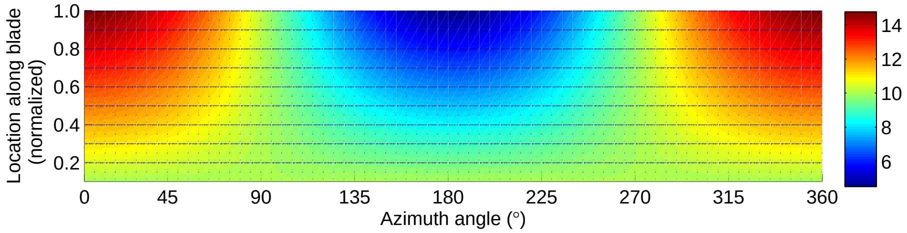

(b) $U_h = 10.0$ m/s, $\alpha = 0.8$, $\sigma_U = 0.0$ m/s

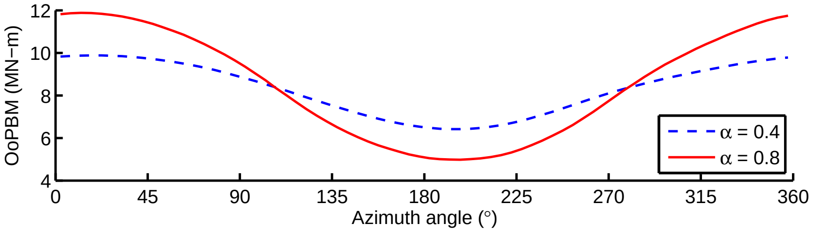

(c) Averaged OoPBM time series

Figure 2.13: The influence of wind shear on the out-of-plane bending moment along a blade (based on controlled stochastic simulation of wind fields).

rotates through two wind fields with wind-shear exponent, α, equal to 0.4 and 0.8. The x-axis represents the azimuth angle, measured from a reference azimuth assumed to zero at the top; the y-axis represents the normalized location along the blade (normalization is such that 0 refers to the blade root; 1 refers to the blade tip). The wind speed variation along a blade is much larger when the wind shear is strong (i.e., in the case where α=0.8); this steeper wind gradient results in larger amplitudes of the blade-root OoPBM cycles, which are shown in the bottom plot of Fig. 2.13 for both wind shear cases. The stronger wind shear case (α=0.8) shows larger fluctuations in OoPBM. Strong wind shear causes a blade to experience steeper wind speed gradients during its rotation, resulting in larger OoPBM amplitudes.

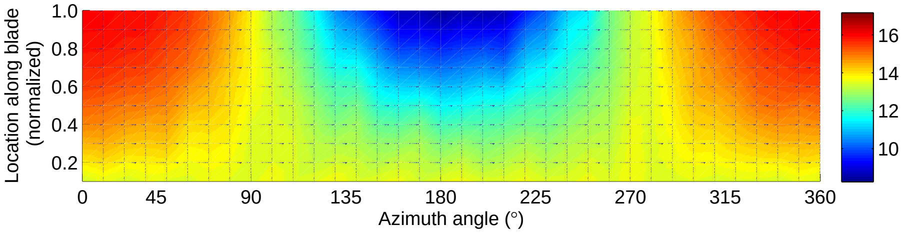

(a) Case 1 : U_h = 12.13 m/s, α = 0.28, σ_U = 0.67 m/s

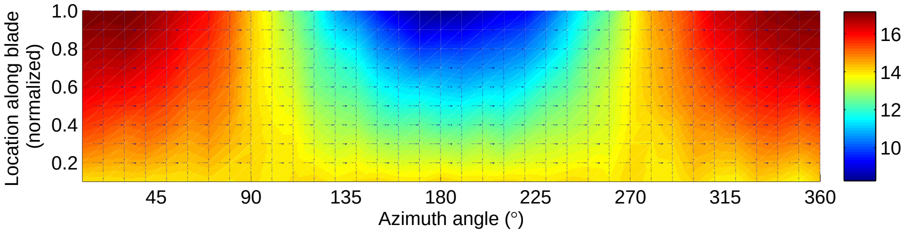

(b) Case 2 : U_h = 12.15 m/s, α = 0.42, σ_U = 0.68 m/s

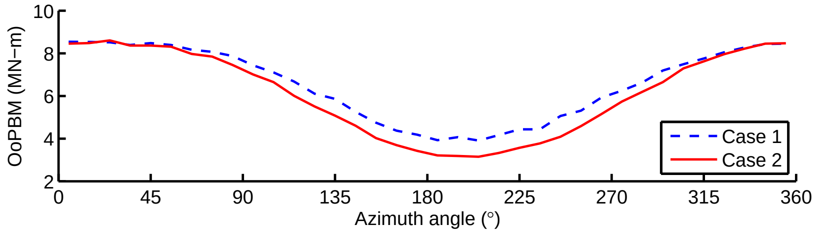

(c) Averaged OoPBM time series

Figure 2.14: The influence of wind shear on the out-of-plane bending moment along a blade (based on LES-generated wind fields for the SBL).

While the controlled stochastic simulations allow us to easily assess the effect of wind shear on OoPBM, we return now to our LES-SBL wind fields. To verify that an enhanced wind shear indeed increases the amplitude of OoPBM in the LES-SBL wind fields, we selected two LES-generated wind fields (from among all the 2,200 LES wind fields) whose U_h and σ_U values are almost identical but where the estimated shear exponent values, α, from the LES output time series are different. Similar results as for the controlled simulations in Fig. 2.13 are presented in Fig. 2.14. Because the differences in α from 0.28 to 0.42 (as well as the magnitude of shear at the upper end of this range) are not as dramatic as with the controlled simulations (where α was changed from 0.4 to 0.8), smaller differences in the OoPBM load are seen. Still, it is easy to verify the effect of wind shear on the OoPBM cycle amplitudes.

2.3.2 Tower-Top Yaw Moment and Base Fore-Aft Tower Bending Moment

In the cases of the TTYM and FATBM load processes, it is the turbulence level, indicated by σ_U, that has a dominant influence on these loads. To confirm this, we plot hub-height wind speed time series along with associated TTYM and FATBM times series for the two wind fields obtained from controlled stochastic simulations where σ_U is different but U_h and α values are the same. The time series for both TTYM and FATBM in Fig. 2.15 clearly show the same large fluctuations that the wind speed times series show; this suggests these two loads are strongly influenced by turbulence in the wind field. We shall see that the TTYM process is influenced by asymmetric loading over the rotor plane, which results from interaction between the rotating blades and coherent turbulence structures.

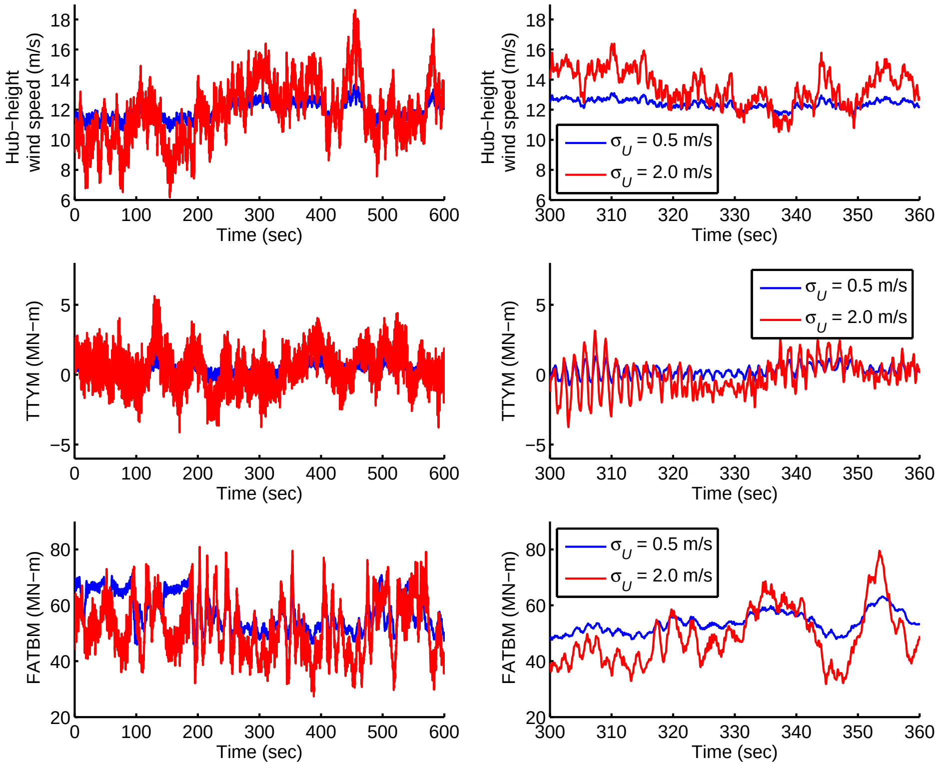

Figure 2.15: The influence of turbulence on TTYM and FATBM (based on controlled stochastic simulation of wind fields, where $U_h = 12$ m/s and $\alpha = 0.2$).

While the controlled stochastic simulations allow us to easily assess the effect of turbulence on TTYM and FATBM, we return now to our LES-SBL. To verify that increased turbulence indeed increases the TTYM and FATBM loads in the LES-SBL wind fields, we selected two LES-generated wind fields (from among all the 2,200 LES wind fields) whose U_h and α values are almost identical but where the estimated hub-height longitudinal turbulence standard deviation values, σ_U, from the LES output time series are different. Similar results as for the controlled simulations in Fig. 2.15 are presented in Fig. 2.16. While the differences in σ_U from 0.39 m/s to 0.80 m/s (as well as the degree of turbulence at the upper end of this range) are not as dramatic as with the controlled simulations (where σ_U was changed from 0.5 m/s to 2.0 m/s), clear differences in the TTYM and FATBM loads are seen. These loads are both increased when the turbulence level (i.e., σ_U) is larger.

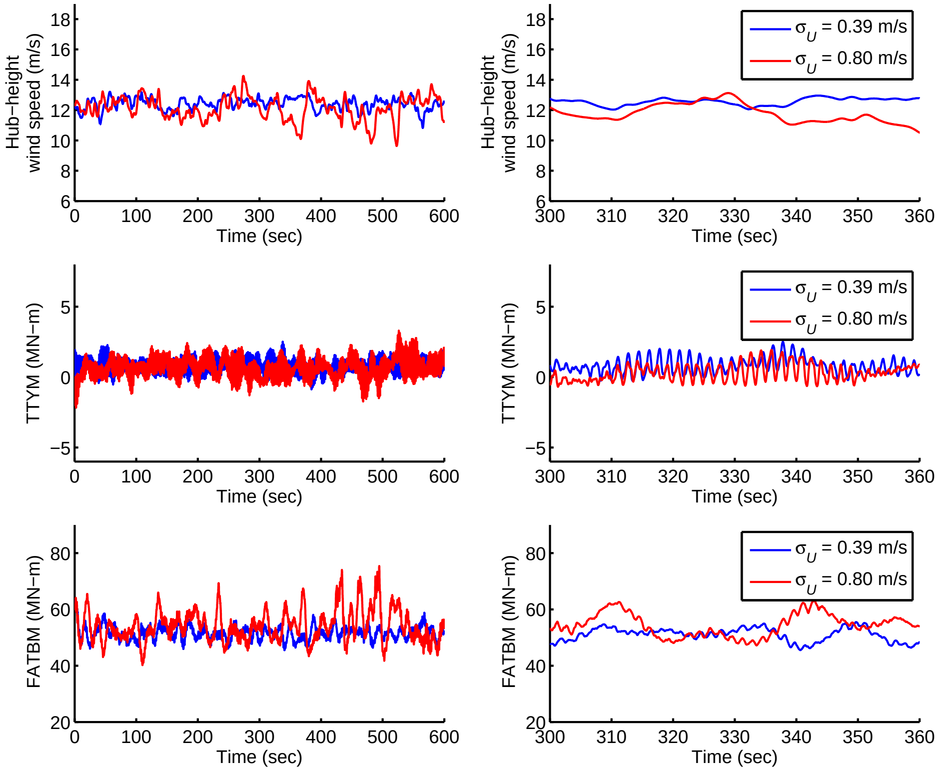

Figure 2.16: The influence of turbulence on TTYM and FATBM (based on based on LES-generated wind fields for the SBL, where $U_h$and α are almost identically matched at values close to 12.3 m/s and 0.38, respectively).

2.4 The Influence of Large-Scale Environmental Conditions on Turbine Loads

2.4.1 Characteristics of Wind Fields and Load Statistics in SBL

We now discuss the general characteristics of wind fields in the stable boundary layer and how they relate to wind turbine loads. We first summarize characteristics of the 2,200 wind fields extracted from the 44 LES runs and corresponding wind turbine load statistics. In particular, we investigate two distinct load statistics—the EFL (equivalent fatigue load) and the 10-min maximum load—for three wind turbine load variables: blade root out-of-plane bending moment (OoPBM), tower top yaw moment (TTYM) and fore-aft tower base moment (FATBM). The 3D boxes in Figs. 2.17, 2.19, and 2.21 represent both characteristics of the LES-generated wind fields and the corresponding load statistics. The wind field characteristics are described by normalized versions of the three wind field (internal) parameters, U_h, σ_U and α, that are mapped on the x, y and z axes of this 3D domain. Any point in this 3D box represents a specific set of wind field parameters; turbine load statistics are mapped by color to represent the magnitude of the relevant load statistic. This graphical mapping technique allows us to understand, at the same time, general characteristics of the simulated wind fields and corresponding wind turbine load statistics under stable boundary layer conditions.

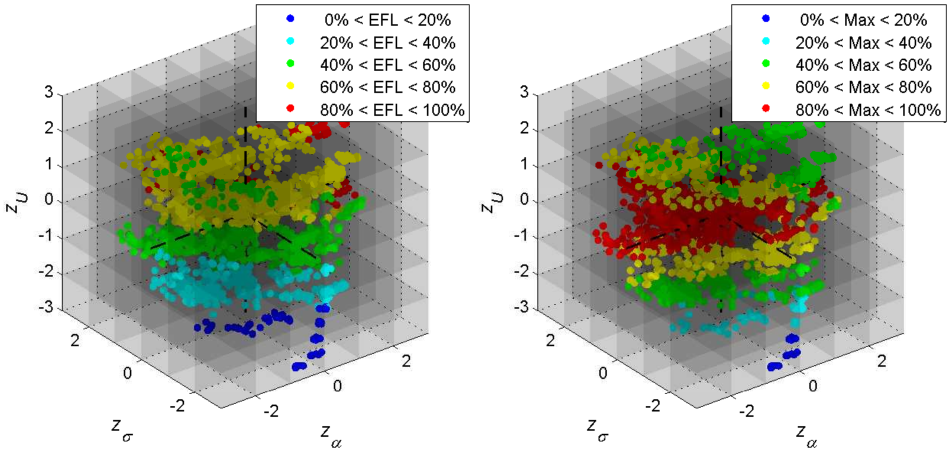

(a) EFL (b) Maximum load

Figure 2.17: Load statistics of OoPBM mapped on the internal parameter-domain (representing a total of 2,200 LES-generated wind fields).

2.4.1.1 Blade-Root Out-of-Plane Bending Moment in SBL

Figure 2.17 shows how the EFL and 10-minute maximum OoPBM are distributed in the 3D-domain whose axes represent normalized U_h, σ_U and α values. Figure 2.18 is a 2D-converted view based on divided U_h bins. The top plots of Fig. 2.18 show the sorted values of the EFL and maximum loads, based on which the colors of dots are assigned. The higher EFL values (red dots) are evident in the strong shear region or the strong turbulence region. Particulary when U_h is high, wind shear contributes to the higher EFL values. In the case of maximum load, U_h appears to have the dominant influence, regardless of σ_U and α. Above the rated wind speed (11.4 m/s), maximum loads start to decrease due to the turbine's pitch control.

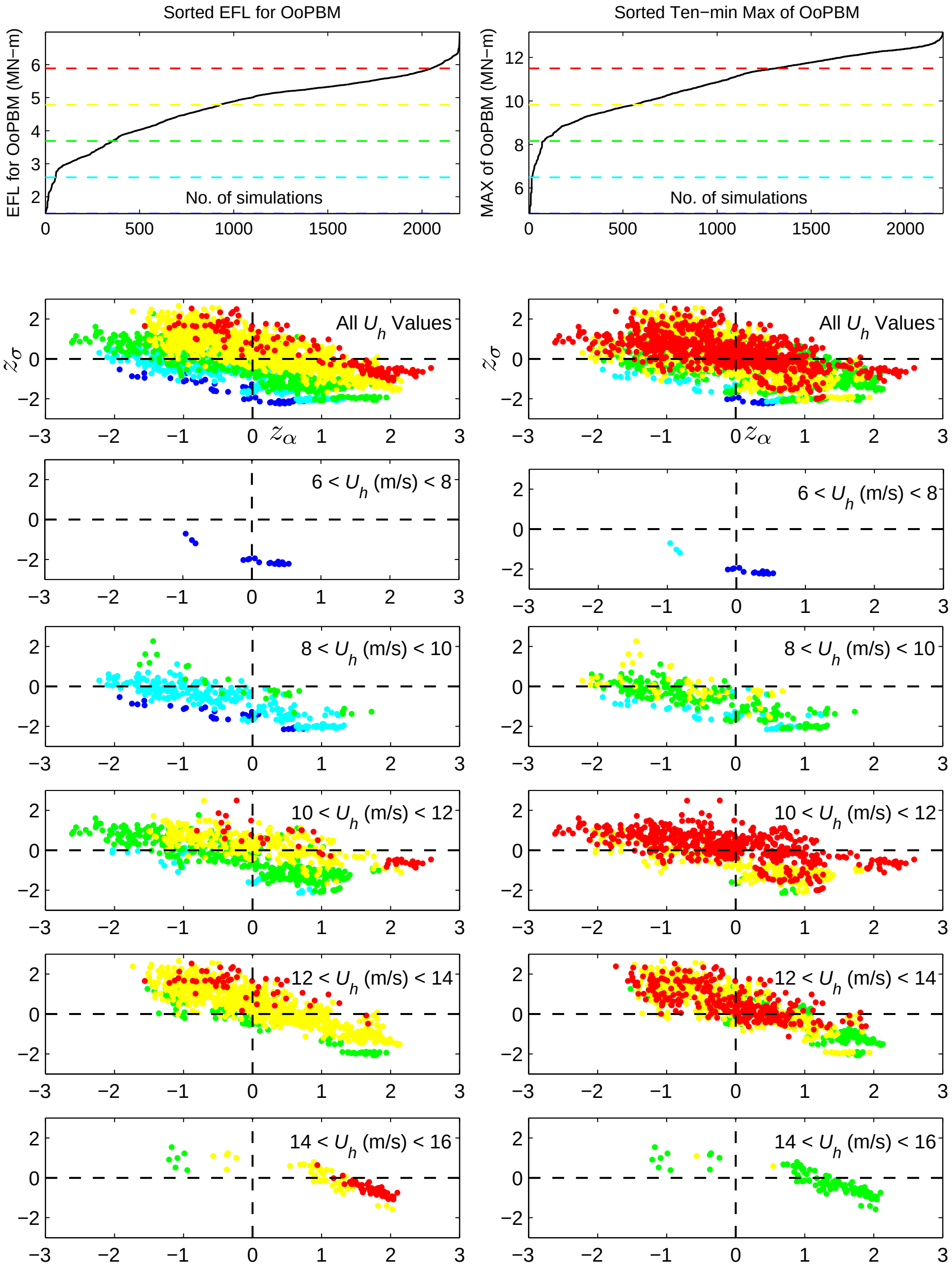

Figure 2.18: Load statistics of OoPBM mapped on the internal parameter-domain.

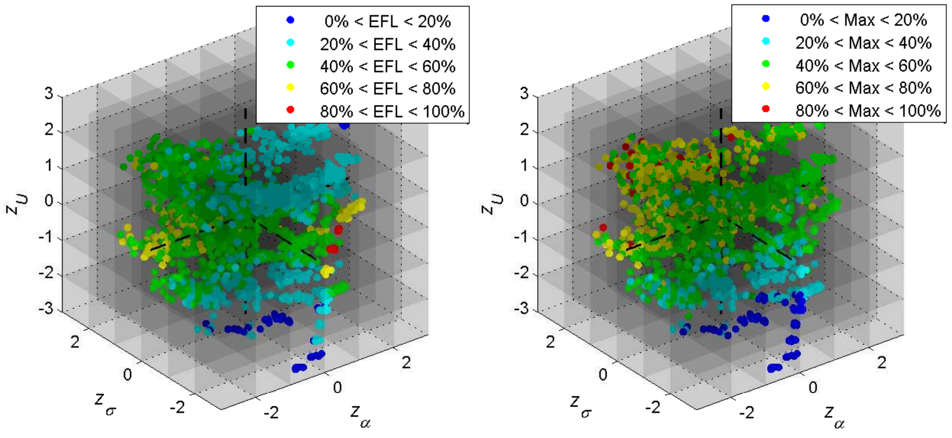

(a) EFL

(b) Maximum load

Figure 2.19: Load statistics of TTYM mapped on the internal parameter-domain (representing a total of 2,200 LES-generated wind fields).

2.4.1.2 Tower Top Yaw Moment in SBL

Figures 2.19 and 2.20 show how the EFL and 10-min maximum TTYM are distributed in the 3D and 2D wind field parameter domains, respectively. In Fig. 2.20, there are only a small number of very high EFL values that occur in the slightly stable region; the next higher range of EFL values are mostly associated with the region where the turbulence is high and U_h is below the rated wind speed. In the case of 10-min maxima, most of the higher values are associated with the high turbulence region, and U_h seems not to affect these maximum loads. This is because TTYM is mainly influenced by asymmetric loads acting on the rotor plane; such asymmetric loads are increased by turbulence rather than by U_h and α.

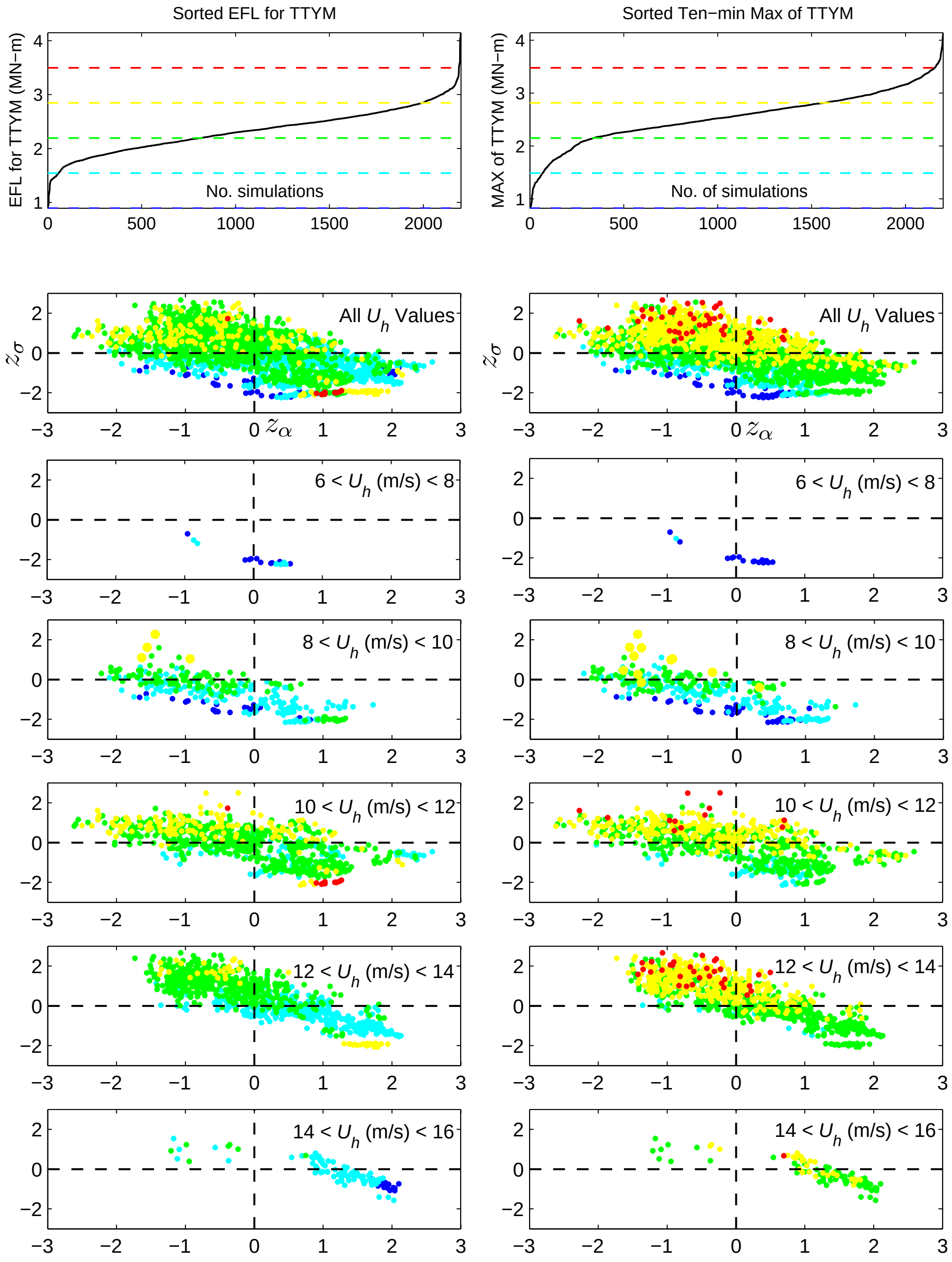

Figure 2.20: Load statistics of TTYM mapped on the internal parameter-domain (spread).

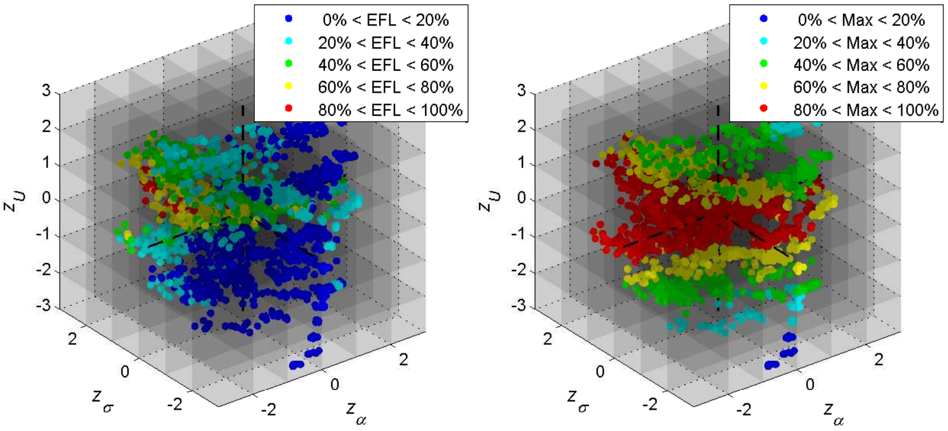

(a) EFL

(b) Maximum load

Figure 2.21: Load statistics of FATBM mapped on the internal parameter-domain (representing a total of 2,200 LES-generated wind fields).

2.4.1.3 Fore-Aft Tower Base Moment in SBL

Figures 2.21 and 2.22 show how the EFL and 10-min maximum FATBM are distributed in the 3D and 2D wind field characteristic domains, respectively. According to Fig. 2.22, higher EFL values are associated with the domain where the level of turbulence is high and U_h is around the rated wind speed (11.4 m/s). We also see that the EFL of FATBM decreases as the atmosphere become more stable for the same U_h. In the case of 10-min maximum load, U_h seems to have the dominant influence, regardless of σ_U and α. In addition, at higher wind speeds, the 10-min maximum loads start to decrease (due to the turbine's pitch control) above the rated wind speed (11.4 m/s). This trend is almost identical to that for the OoPBM case.

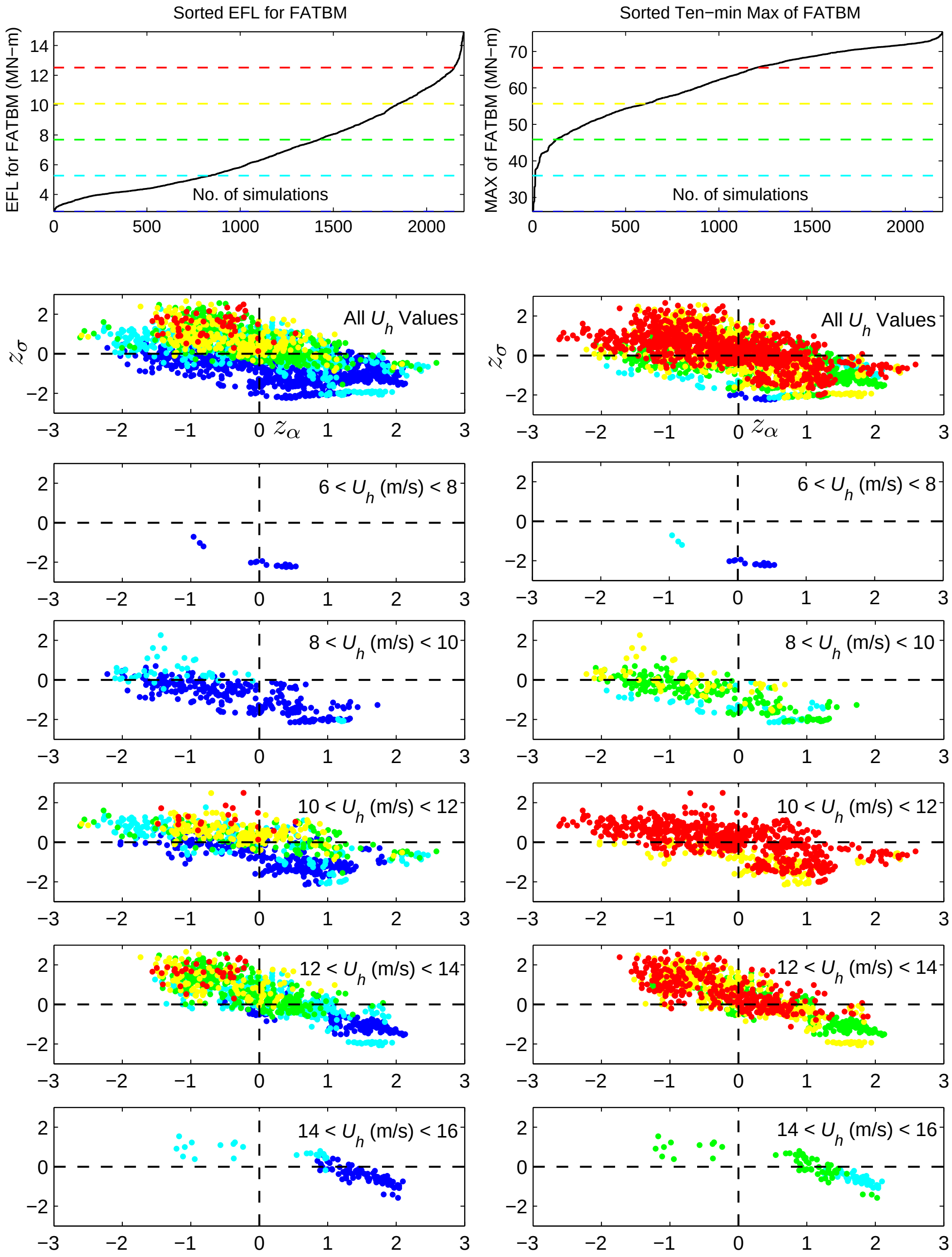

Figure 2.22: Load statistics of FATBM mapped on the internal parameter-domain (spread).

2.4.2 Wind Turbine Load Statistics Conditional on Environmental Conditions

As described in the previous section, a certain environmental condition can affect the turbine-scale wind field characteristics and thus affect wind turbine load statistics. We now address the direct relationship between environmental conditions, which are expressed as the combination of external parameters, and load statistics for the three types of wind turbine loads: OoPBM, TTYM and FATBM. To note the influence of a single external parameter on wind turbine load statistics, we systematically change that parameter, while fixing other parameters as in the control case and track time-varying trend of load statistics. Particularly, we investigate the influences of the geostrophic wind speed and surface cooling rate on load statistics since these two external parameters have the greatest influence on turbine-scale wind field characteristics. The LES runs and the corresponding external parameter values listed in Table 2.7 were selected and used in this analysis.

Due to the complex interactions among the internal parameters, it is difficult to exactly interpret time-varying trends of load statistics with the variation of internal parameters. Therefore, we focus here on describing how environmental conditions affect general time-varying trends in load statistics.

2.4.2.1 Time-Varying Trend of OoPBM Statistics Conditional on Environment

Figure 2.23 compares the influence of geostrophic wind speed on the time-varying trends in the EFL and 10-min maximum OoPBM. In general,

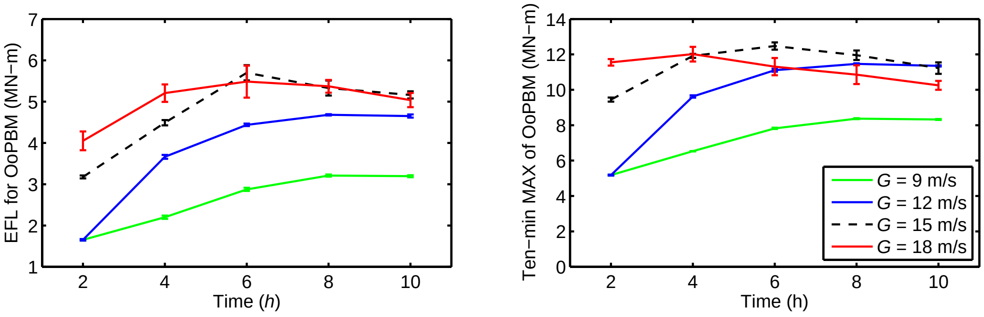

(a) EFL (b) MAX

Figure 2.23: Influences of the geostrophic wind speed on the time-varying trend of OoPBM statistics.

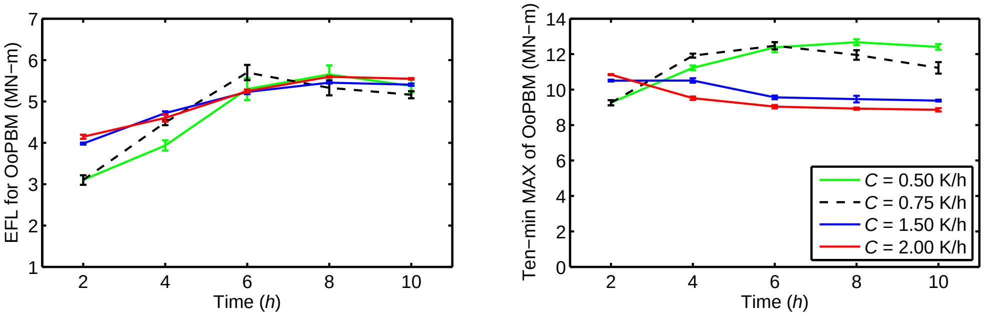

(a) EFL (b) MAX

Figure 2.24: Influences of the surface cooling rate on the time-varying trend of OoPBM statistics.

the EFL increases with time, and this trend is similar with the time-varying trend of U_h. The increasing trends in U_h and α with SBL evolution are likely contributors to the increasing trend of EFL with time. Consistent with this time-varying trend, geostrophic wind speed increases the general level of EFL. Higher geostrophic wind speeds (G = 15 m/s, 18 m/s), however, cause EFL to decrease because of the turbine's pitch control—geostrophic wind speeds above 15m/s cause U_h to exceed the rated wind speed (11.4 m/s). The 10-

min maximum OoPBM increases with time for the same reason as was the case for the EFL. These time-varying trends also show similar dependence on geostrophic wind speed as for the case with the EFL.

Figure 2.24 compares the influence of surface cooling rate on the time-varying trends of EFL and 10-min maximum values of OoPBM. Compared with the control case (dotted line), higher surface cooling rates do not change the time-varying trends of EFL significantly, except only raising the overall mean value of EFL. The higher surface cooling rates make the 10-min max values decrease with time; this is because reduced turbulence levels have a stronger influence than the increased mean wind speed at hub, both of which are caused by the increased surface cooling rate and the evolution of the SBL.

2.4.2.2 Time-Varying Trend of TTYM Statistics Conditional on Environment

Figure 2.25 compares the influence of the geostrophic wind speed on the time-varying trends of EFL and 10-min maximum TTYM. The EFL does not show any clear time-varying trend. This is because the EFL of TTYM is predominantly influenced by the level of turbulence and σ_U was seen to also not display any clear time-varying trend. The overall mean of EFL is raised with an increase in the geostrophic wind speed because higher geostrophic wind speeds are associated with higher turbulence levels that, in turn, magnify the level of EFL. As was seen with the EFL, there is no obvious time-varying trend in the maximum value of TTYM. The overall maximum TTYM values increase

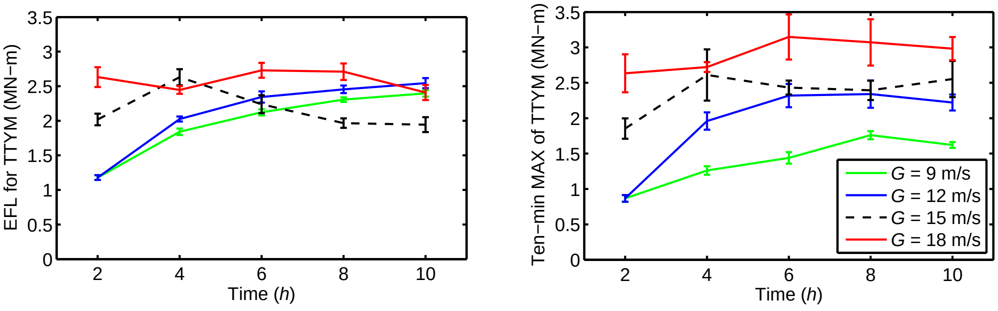

(a) EFL (b) MAX

Figure 2.25: Influences of the geostrophic wind speed on the time-varying trend of TTYM statistics

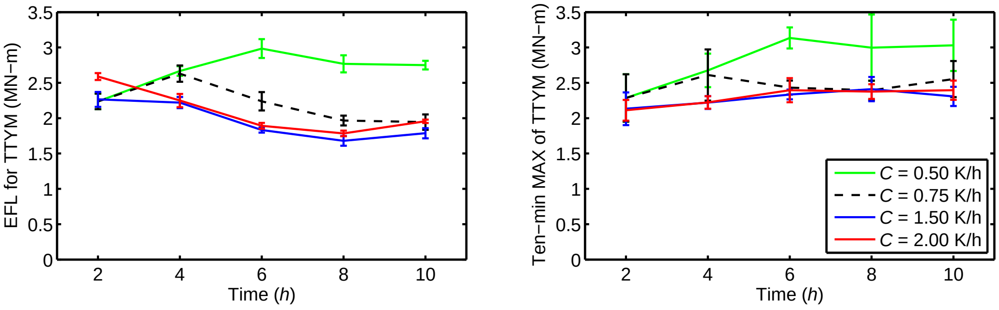

(a) EFL (b) MAX

Figure 2.26: Influences of the surface cooling rate on the time-varying trend of TTYM statistics

with geostrophic wind speed because higher turbulence levels associated with the higher geostrophic wind speeds increase the maximum value of TTYM.

Figure 2.26 compares the influence of the surface cooling rate on the time-varying trends of EFL and 10-min maximum TTYM. The higher surface cooling rates suppress the level of turbulence and in turn lower the general level of EFL values. The time-varying tends of EFL are very similar the time-varying trends of σ_U for different surface cooling rates (see Figure 2.12b). The maximum values show similar trends as was seen with the EFL; the lower surface cooling rate is associated with higher maximum values because of the higher turbulence levels at these lower surface cooling rates.

2.4.2.3 Time-Varying Trend of FATBM Statistics Conditional on Environment

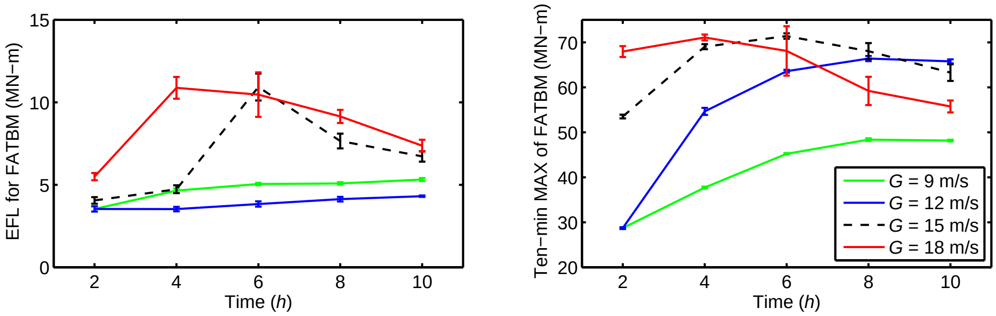

(a) EFL (b) MAX

Figure 2.27: Influences of the geostrophic wind speed on the time-varying trend of FATBM statistics

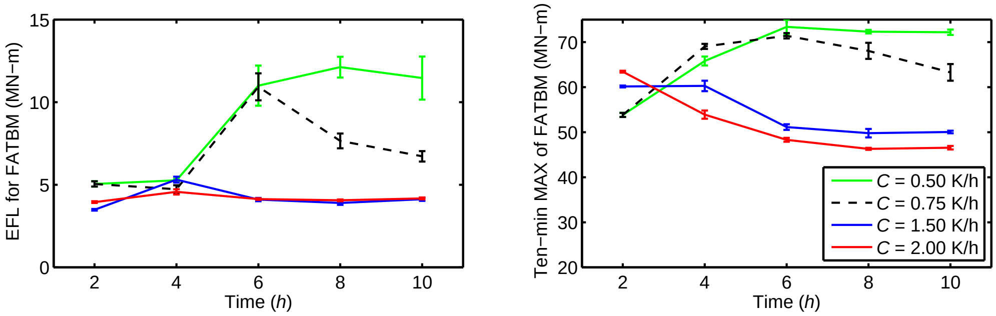

(a) EFL (b) MAX

Figure 2.28: Influences of the surface cooling rate on the time-varying trend of FATBM statistics

Figure 2.27 compares the influence of geostrophic wind speed on the time-varying trends of EFL and 10-min maximum FATBM. The EFL of FATBM is predominantly influenced by σ_U; therefore, the time-varying trend of EFL is similar to that of σ_U. The higher geostrophic wind speed leads to higher U_h and σ_U values, both of which contribute to increase the general level of EFL. The maximum loads for FATBM increase with time because of increasing U_h; higher geostrophic wind speeds than 15 m/s cause maximum values to decrease due to the turbine's pitch control. In general, the mean of maximum FATBM values is higher when the geostrophic wind speed is high.

Figure 2.28 compares the influence of surface cooling rate on the time-varying trends of EFL and 10-min maximum value of FATBM. Higher surface cooling rates are associated with reduced turbulence levels; this, in turn, leads to lower overall EFL values. The reduced turbulence level due to the higher surface cooling rates, also, lowers the overall maximum value of FATBM. The decreasing time-varying trend is due to the turbine's pitch control; higher surface cooling rates are associated with higher values of U_h, which initiates the blade pitching.

2.4.3 Load Distribution Conditional on Environmental Conditions

We investigate next how external parameters affect time-varying trends in turbine load distributions. To assess the influence of a single environmental parameter on the variation of load distributions with time, we systematically change a single external parameter—again, we only consider the geostrophic wind speed and surface cooling rate—while fixing other parameters as in the control case and track load distributions with time. The LES runs and associated external parameter values that were selected and used in this analysis are listed in Table 2.7.

The complementary cumulative distribution (or probability of exceedance of any level, l, by load, L in ten minutes) can be estimated from block maxima as follows:

$$P(L > l) = 1 - [1 - P(L_{block} > l)]^n \tag{2.6}$$

where L_{block} is a block maximum value over a shorter duration than ten minutes, and n is the number of blocks in ten minutes. We use one-minute blocks; hence, $n = 10$.

From a single LES run, we extract 50 load time series for any load measure, L—these result from 5 time series obtained from each of 5 lateral representing the LES computational domain, taken from every hour out of a 10-hour simulation. Representing each hour, then, we obtain 50 one-minute block maxima and estimate time-varying load distributions using Eq. 2.6. We study these load distribution variations with time and by examining how changes in external parameters affect these trends. We discuss only the influences of the geostrophic wind speed and surface cooling rate here because the influence of other parameters was not found to be significant.

Figure 2.29 shows time series of the hub-height longitudinal wind speed and three different loads (OoPBM, TTYM, and FATBM) corresponding to an

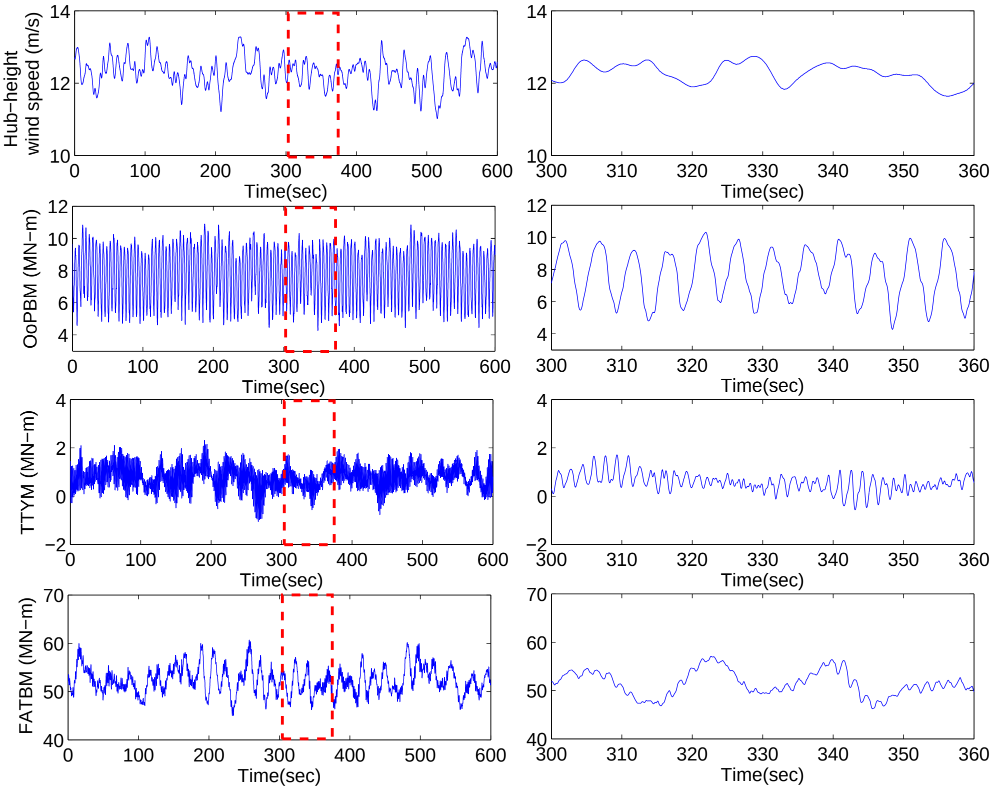

Figure 2.29: Wind velocity and load time series corresponding to the control case.

LES-SBL wind field extracted from the last hour of a 12-hour simulation and taken from the central slice in the lateral direction. These time series are for the control case (U_h = 12.30 m/s, σ_U = 0.41 m/s, and α = 0.42). The plots in the right columns are zoomed-in views of the red boxes from the plots in the left column. The atmospheric conditions at this point in the simulations correspond very stable conditions; as a result, there are not large fluctuations in the wind speed time series, which in turn cause the turbine loads to be distributed over a narrow range. Among the three loads, TTYM shows the greatest variability in one-minute block maxima because this load is influenced by spatially organized and coherent turbulence structures rather than by simpler averaged quantities such as the hub-height wind speed and turbulence. The variability in the two other loads, which are very small in this case, are influenced by the level of turbulence at hub height.

2.4.3.1 Time-Varying Trends in OoPBM Load Distributions

Figure 2.30 compares time-varying trends in load distributions for the blade root out-of-plane bending moment (OoPBM) for different geostrophic wind speeds. Generally, with time, the load distribution curves move to the right (towards higher load levels) due to the increased wind speed and steeper shear gradients resulting from the evolution of the SBL. At a certain time, however, the load distribution curves corresponding to higher geostrophic wind speeds start to move to the left (towards lower load levels) because of the turbine's pitch control. The gaps between the curves in each plot highlight the influence of the geostrophic wind speed—U_h, which is proportional to the geostrophic wind speed establishes the general load distribution level (i.e., the location of the curve horizontally), while σ_U, which is also proportional to the geostrophic wind speed, influences the range of the load distribution (i.e., the separation between the largest and smallest loads in a single curve). Note that there is not large variability in the OoPBM distributions at lower geostrophic wind speeds; this is because of the lower turbulence levels associated with

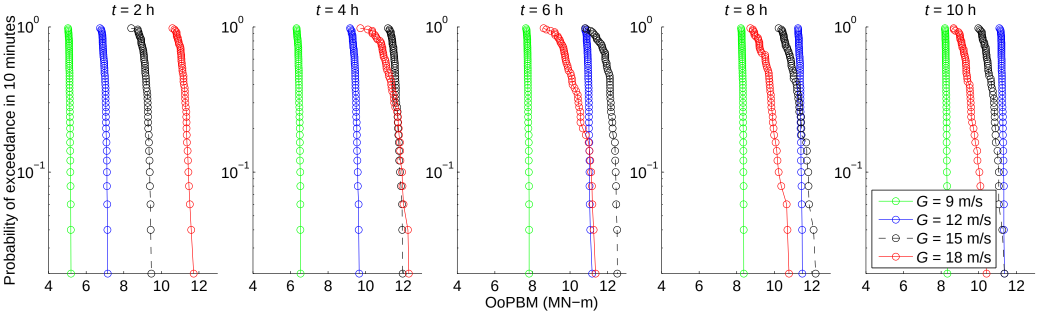

Figure 2.30: Time-varying OoPBM load distributions and influence of geostrophic wind speed.

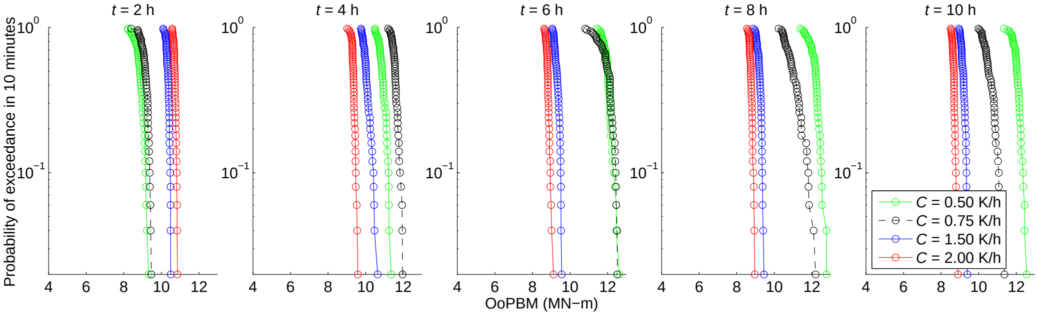

Figure 2.31: Time-varying OoPBM load distributions and influence of surface cooling rate.

these lower geostrophic wind speeds.

Figure 2.31 compares time-varying trends and the influence of surface cooling rate on distributions for OoPBM. Higher surface cooling rates are associated with higher U_h values that exceed the rated wind speed; this make the load distribution curves move to the left (towards lower load levels). The curves corresponding to the lower surface cooling rates are located towards higher load levels and, also exhibit greater variability.

2.4.3.2 Time-Varying Trends in TTYM Load Distributions

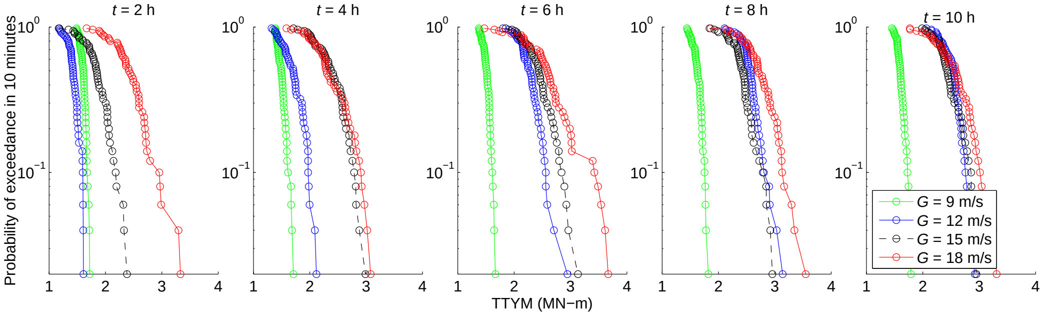

Figure 2.32: Time-varying TTYM load distributions and influence of geostrophic wind speed.

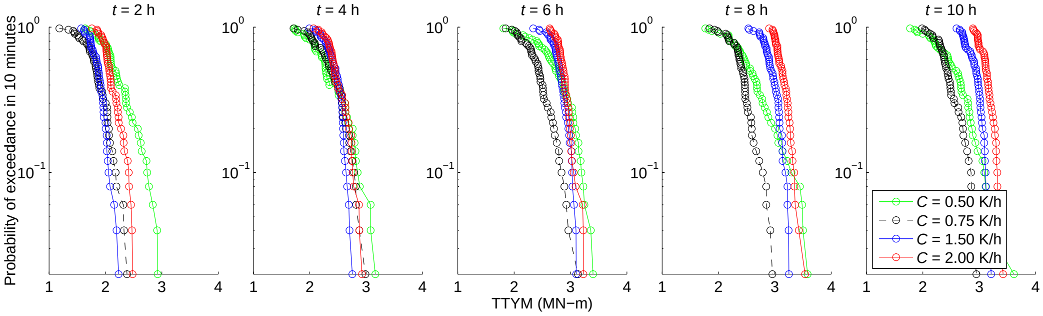

Figure 2.33: Time-varying TTYM load distributions and influence of surface cooling rate.

Figure 2.32 compares time-varying trends in distributions for the tower-top yawing moment (TTYM) for different geostrophic wind speeds. Generally, the load distribution curves move slightly to the right with time. This is because the wind shear, which directly influences the mean TTYM (see Figure **??**), is enhanced with time. The differences among the load distribution curves are caused by the different turbulence levels, which have the greatest influence on the level of the TTYM maxima. Turbulence levels increase with geostrophic wind speed; hence, the higher geostrophic wind speeds are associated with higher loads.

Figure 2.33 compares time-varying trends and the influence of surface cooling rate on distributions for TTYM. It is difficult to tell how surface cooling rates influence the load distributions. The general mean levels of the distribution curves increase with increases in surface cooling rate due to the enhanced wind shear, which increases the mean TTYM levels; the variability in each curve is greater, however, when surface cooling rates are lower, due to the increased turbulence levels that cause large fluctuations in the TTYM load process.

2.4.3.3 Time-Varying Trends in FATBM Load Distributions

Figure 2.34 compares time-varying trends in distributions for the base fore-aft tower bending moment (FATBM) for different geostrophic wind speeds. The overall load level for FATBM is most influenced by U_h; hence, the load distribution curves move to the right with increased U_h during the SBL evolution. However, as with the OoPBM maxima, the distribution curves corresponding to higher geostrophic wind speed start to move to the left (towards lower levels) due to the turbine's pitch control. The overall level of these load distribution curves is directly proportional to the geostrophic wind speed, but this trend is reversed when pitch control is required at the higher geostrophic wind speeds. Load variability increases with geostrophic wind speed because

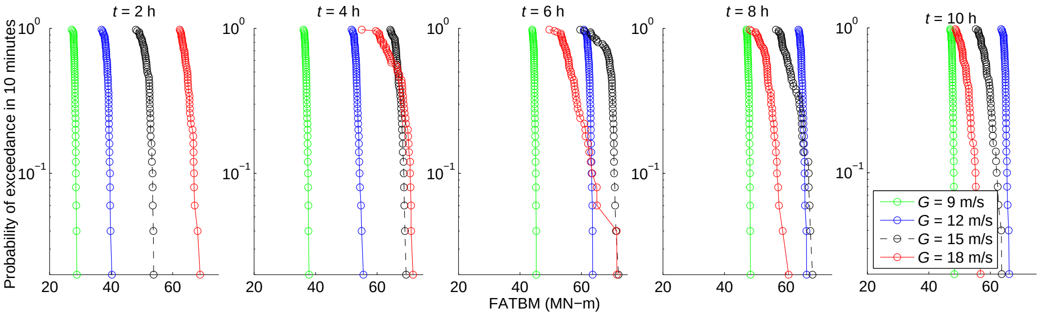

Figure 2.34: Time-varying FATBM load distributions and influence of geostrophic wind speed.

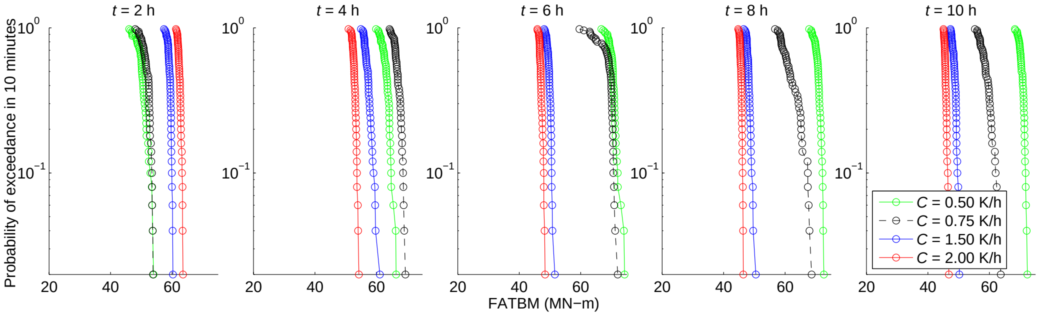

Figure 2.35: Time-varying FATBM load distributions and influence of surface cooling rate.

of the corresponding increase in turbulence levels.

Figure 2.35 compares time-varying trends and the influence of surface cooling rate on distributions for FATBM. Early in the simulations, higher surface cooling rates are associated with higher load levels because of higher U_h levels that are associated with these higher surface cooling rates. As time passes, however, the load levels corresponding to lower surface cooling rates exceed those corresponding to higher surface cooling rates. This is because, with the lower surface cooling rate cases, U_h keeps increasing with time without reaching the rated wind speed; also turbulence levels are higher—both of these effects contribute to increasing FATBM load levels significantly.

2.5 Summary and Conclusions

In this chapter, we saw how large-scale atmospheric and surface conditions affect the characteristics of wind fields as well as the wind turbine loads.

We studied how a single external parameter affects the characteristics of wind fields (internal parameter) by conducting selected parametric sensitivity studies. The major findings are as follows:

- Turbine-scale wind field characteristics (internal parameters) continue to change during the evolution of the stable boundary layer.
- Increases in the geostrophic wind speed leads to an increase in the mean and standard deviation of the longitudinal hub-height wind speed but it reduces wind shear.
- Increases in the surface cooling rate strengthens wind shear and increase the hub-height mean wind speed but it reduces turbulence levels.

We also sought to establish direct relationships between environmental conditions (large-scale atmospheric and surface conditions) and wind turbine load statistics. Among all the environmental parameters, the geostrophic wind speed and surface cooling rate have the greatest influence on wind turbine load statistics. Investigating those large-scale environmental conditions at planned wind turbine sites can provide us with insights into likely turbine-scale wind field characteristics and wind turbine loads at those sites.

Chapter 3

Toward Understanding of Wind Turbine Load Characteristics in the Stable Boundary Layer

3.1 Introduction

Characteristics of wind fields associated with the atmospheric stable boundary layer (SBL) are known to be distinct from those associated with near-neutral conditions exclusively used to simulate inflow wind fields in wind turbine design. For instance, it has been noted that wind fields in the SBL have more strongly sheared mean wind profiles (i.e., steeper mean wind speed gradients with elevation above ground) and they also exhibit wind veer (i.e., wind direction change with elevation). Both of these features can have a great influence on power produced as well as loads experienced by utility-scale wind turbines with large rotor swept areas [5, 9, 11]. Such SBL flow fields cannot be simulated using conventional Fourier-based stochastic procedures. Large-eddy simulation (LES) can be used to generate the SBL flow fields [1, 12, 13] while stochastic simulation [6] is widely accepted for the generation of neutral boundary layer (NBL) flow fields and its use with spectral methods is well documented in design standards and guidelines. In addition to contrasting wind shear profiles and no intrinsic way in which wind veer is modeled which limit the use of simpler stochastic methods for simulating SBL flows, NBL flow fields employed in practice for wind turbine loads studies often employ simplifying assumptions such as that proposed in the IEC 61400-1 standard [2] which specifies constant turbulence standard deviation values at all points above the ground. Our goal in this study is to compare NBL- and SBL-related wind turbine loads by attempts to isolate differences in key turbine-scale flow characteristics—wind shear, wind veer, and turbulence variation over the rotor plane—through generation first of SBL flow fields using LES and comparison with controlled NBL stochastic simulations that seek to highlight differences in these key characteristics.

3.1.1 Procedure of Analysis

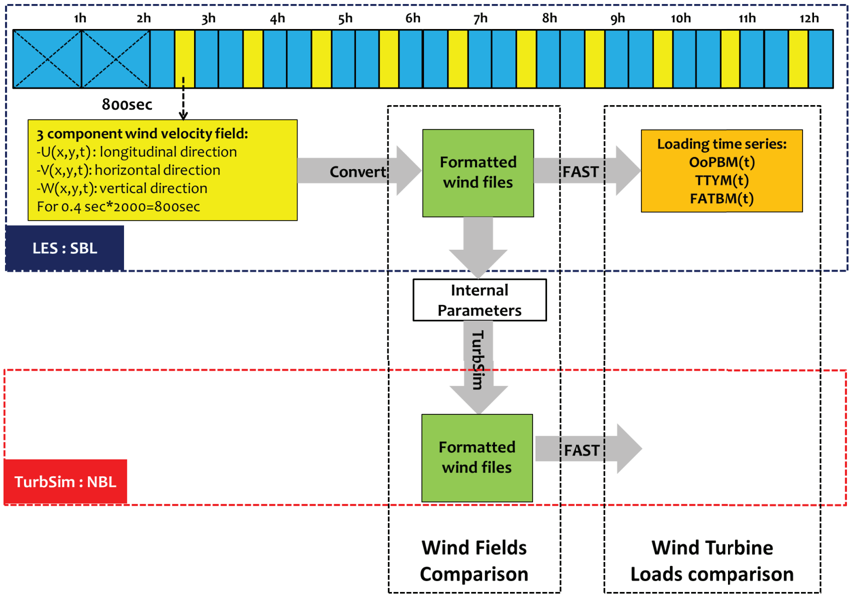

Figure 3.1: Procedure for comparing two wind field simulation methods in wind turbine loads studies.

Figure 3.1 shows a schematic flow chart describing the comparison study that we undertake with SBL and NBL flow fields. The LES-SBL flow fields provide 12 hours of output—for loads computed using the open-source software, FAST [7], inflow is provided by 800-second time series of three wind velocity components generated every hour beginning from the third to the twelfth hour over the rotor plane of the selected 5-MW turbine model [8]. From each turbine response simulation using FAST, we evaluate loads—three different loads are considered here; they include the blade root out-of-plane bending moment (OoPBM), the tower-top yawing moment (TTYM), and the base fore-aft tower bending moment (FATBM). Extremes (Max) and fatigue loads are evaluated. The stochastic NBL flow fields are generated using TurbSim [6] by matching the "internal parameters," which are turbine-scale wind field characteristics such as hub-height wind speed and wind shear resulting from the SBL run to which comparison will be made. The NBL flow fields are also applied to the turbine model using FAST and loads are compared. A total of 2,200 SBL runs provide 10-minute load time series (200 seconds out of the available 800 seconds from each FAST simulation are discarded to avoid the influence of dynamic vibratory response transients). The 2,200 SBL flow field time series arise from 44 separate environmental conditions listed in Table 2.2 that we also refer to as "external parameters." In our NBL versus SBL flow and load comparisons, we will often seek to separate out flow regimes into subsets. Based on normalized values of shear and turbulence (see Eqs. 2.4, 2.5), these subsets are defined as follows:

- $z_\sigma > 0 \cap z_\alpha < 0$: strong turbulence and weak shear
- $z_\sigma > 0 \cap z_\alpha > 0$: strong turbulence and strong shear
- $z_\sigma < 0 \cap z_\alpha < 0$: weak turbulence and weak shear
- $z_\sigma < 0 \cap z_\alpha > 0$: weak turbulence and strong shear

3.2 Wind Field Characteristics in the SBL and in the NBL

First we address how different are SBL and NBL wind field characteristics. From each of the 2,200 SBL wind fields, the hub-height longitudinal mean wind speed, U_h, and standard deviation, σ_U, were determined; with matching U_h and σ_U, 2,200 stochastic simulations were generated for NBL flow fields (assuming Kaimal turbulence power spectra, exponential coherence functions, constant turbulence variation over the rotor, and a power-law wind shear exponent, α, of 0.2).

3.2.1 Wind Shear

Figure 3.2 compares the ensemble-averaged mean wind profiles for the SBL and NBL wind fields. In each plot, the green circles represent the ensemble-averaged mean wind speed at elevation, z, above the ground for the NBL wind fields while the blue circles represent that for the SBL wind fields. The error bars indicate one standard deviation of the mean wind speed for the SBL wind fields. The mean wind profiles for the SBL deviate from

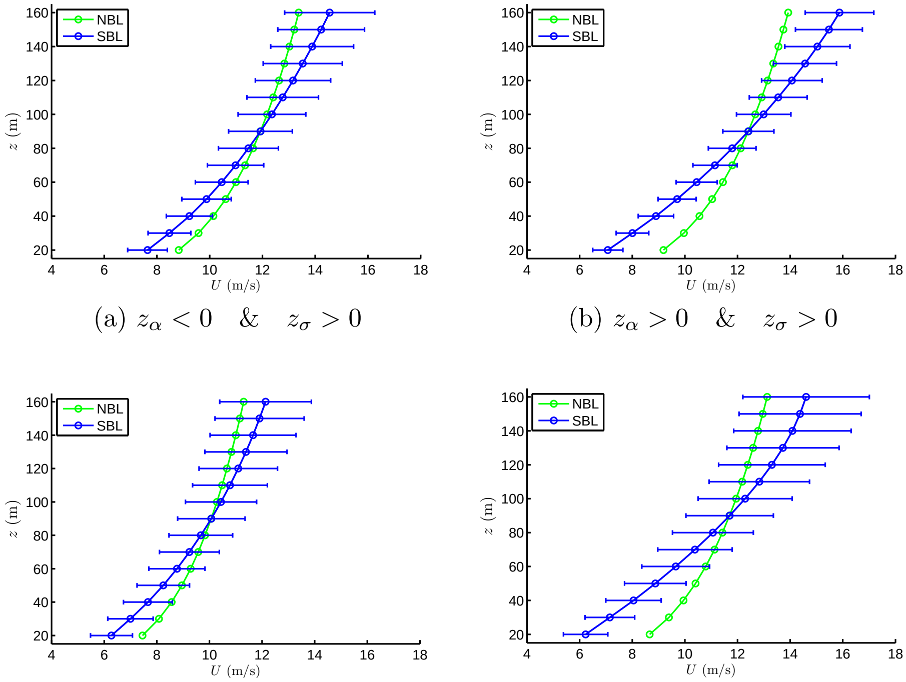

(a) $z_\alpha < 0 \quad \& \quad z_\sigma > 0$ (b) $z_\alpha > 0 \quad \& \quad z_\sigma > 0$

(c) $z_\alpha < 0 \quad \& \quad z_\sigma < 0$ (d) $z_\alpha > 0 \quad \& \quad z_\sigma < 0$

Figure 3.2: Comparison of mean wind speed profiles.

those for the NBL case in those LES runs (see Figs. 3.2b and 3.2d) where stronger shear results from environmental conditions associated, for example, with faster surface cooling rates. In the SBL case, the mean wind speed variation between the rotor top and bottom is almost twice as much as that in the NBL case.

3.2.2 Vertical Mean Wind Direction Profile

Figure 3.3 compares the ensemble-averaged mean wind direction profiles for the SBL and NBL wind fields. The green circles represent the ensemble-

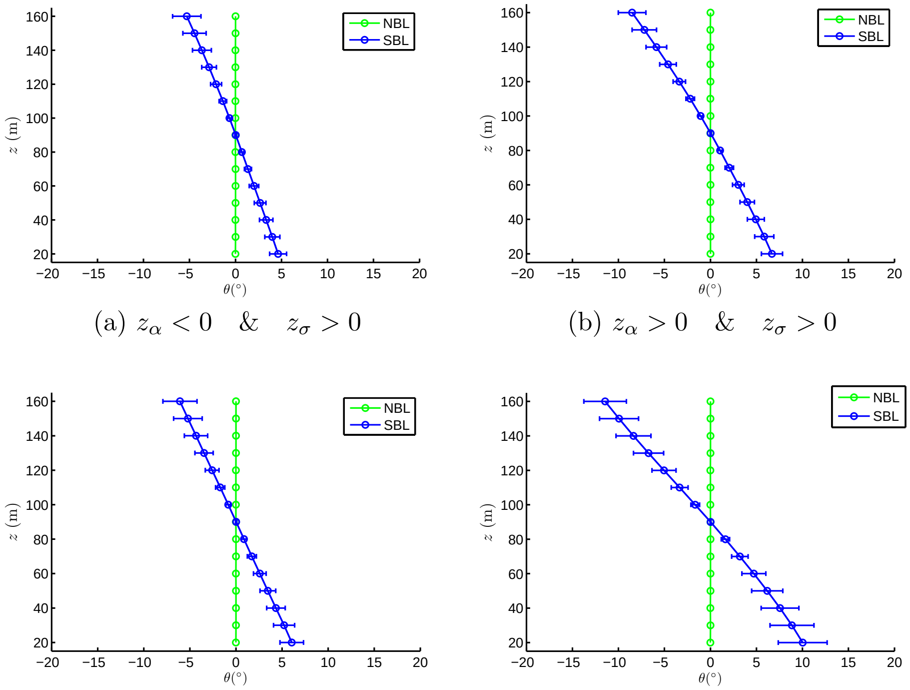

(a) $z_\alpha < 0 \quad \& \quad z_\sigma > 0$ (b) $z_\alpha > 0 \quad \& \quad z_\sigma > 0$

(c) $z_\alpha < 0 \quad \& \quad z_\sigma < 0$ (d) $z_\alpha > 0 \quad \& \quad z_\sigma < 0$

Figure 3.3: Comparison of mean wind direction profiles.

averaged mean wind direction at elevation, z, above the ground for the NBL wind fields while the blue circles represent that for the SBL wind fields. The error bars indicate one standard deviation of the mean wind direction for the SBL wind fields. We note that there is a mean wind direction variation with elevation only in the SBL case; this wind veer is expected in the stable boundary layer. While the SBL mean wind direction variation is almost linear with elevation, there is no mean wind direction variation with height for the NBL. Note that the NBL flow fields were generated after the SBL runs were completed. The LES-generated SBL flow fields were rotated so as to have a zero-mean lateral velocity component at the hub height; this is why both the SBL and NBL cases have a zero wind direction at hub height. In loads studies that follow, the yaw misalignment differences between the NBL and SBL cases are minimized as a resultant of the rotation imposed on the SBL flow field.

Comparing mean wind direction profiles between the left and right plots in Fig. 3.3, the gradients in cases (b) and (d) are larger than those in (a) and (c). This indicates that stronger wind shear is accompanied by stronger wind veer. Comparing the mean wind direction profiles between the top and bottom plots, the gradients in the stronger turbulence domains, (a) and (b), are somewhat smaller than those for weaker turbulence (cases (c) and (d)).

3.2.3 Vertical Standard Deviation profile

Figure 3.4 compares ensemble-averaged profiles of the standard deviation of the longitudinal wind velocity, U, for the SBL and NBL wind fields. The green circles the ensemble-averaged standard deviation of U at elevation z above the ground, for the NBL wind fields, while the blue circles represent that for the SBL wind fields. The error bars indicate one standard deviation on the profiles for the SBL wind fields. Turbulence levels for the SBL case clearly decrease with elevation, whereas they are constant at all elevations for the NBL case. Larger turbulence levels that decrease with elevation are more realistic due to surface friction effects at the ground. Wind velocity standard deviation profiles in the stronger turbulence domains, i.e., cases (a) and (b), show somewhat different gradients; below the rotor hub, the turbulence in-

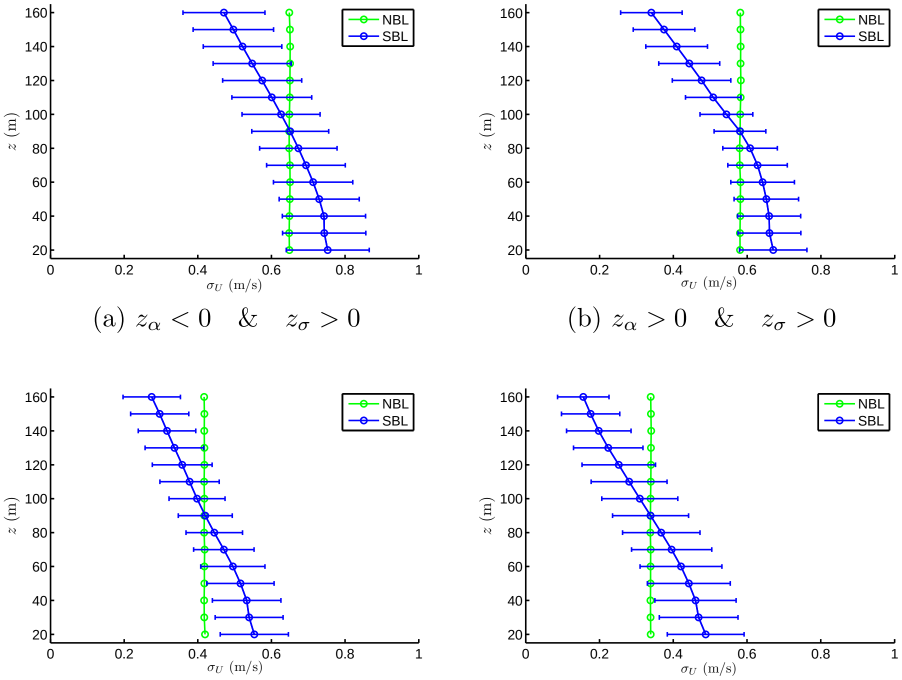

(a) $z_\alpha < 0 \quad \& \quad z_\sigma > 0$

(b) $z_\alpha > 0 \quad \& \quad z_\sigma > 0$

(c) $z_\alpha < 0 \quad \& \quad z_\sigma < 0$

(d) $z_\alpha > 0 \quad \& \quad z_\sigma < 0$

Figure 3.4: Comparison of variation in the standard deviation of the longitudinal wind velocity over the rotor plane.

creases at a lower rate than the rate of decrease above the rotor hub. Note that the NBL flow fields were generated so as to have the same longitudinal mean wind speed and standard deviation at hub height as that of the SBL flow fields.

3.3 Isolation of SBL flow field features on NBL fields

Based on the preceding observations regarding profiles of the wind speed, wind direction, and standard deviation, which we denote, respectively, as $\overline{U}(z)$, $\overline{\theta}(z)$, and $\sigma(z)$ (such that at hub height, z_h, we have $\overline{U}(z_h) = U_h$, $\overline{\theta}(z) = 0$, and $\sigma(z) = \sigma_U$), we can make linear least-squares fits of SBL-generated profiles using three parameters, $\hat{\alpha}$, $\hat{S}_\theta$, and $\hat{S}_\sigma$. Thus, we can express $\overline{U}(z)$, $\overline{\theta}(z)$, and $\sigma(z)$ as follows:

$$\overline{U}(z) = U_h \left(\frac{z}{z_h}\right)^{\hat{\alpha}} \tag{3.1}$$

$$\overline{\theta}(z) = \hat{S}_\theta (z - z_h) \tag{3.2}$$

$$\sigma(z) = \hat{S}_\sigma (z - z_h) + \sigma_U \tag{3.3}$$

where Eq. 3.3 can use two different slopes, $\sigma(z)$, one for $z < z_h$ and another for $z > z_h$, if necessary. We assume no dependence of these profiles on the lateral coordinate, y.

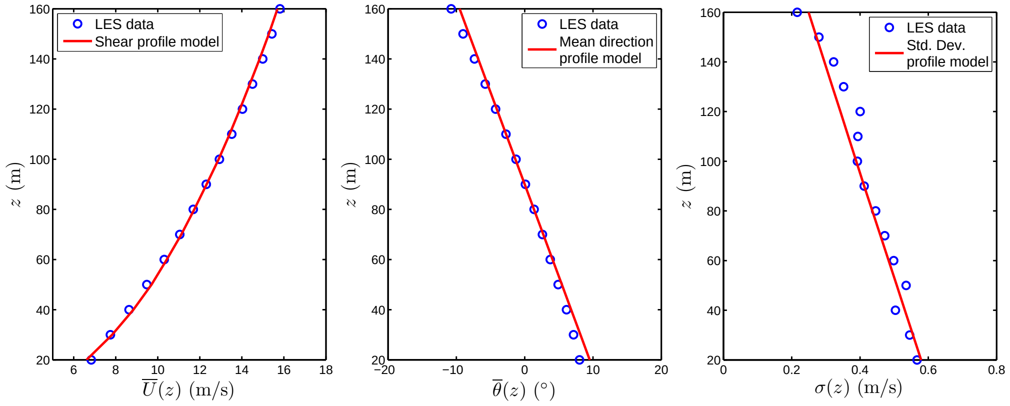

(a) fit using $\hat{\alpha}$ (b) fit using $\hat{S}_\theta$ (c) fit using $\hat{S}_\sigma$

Figure 3.5: Shear, direction, and turbulence profiles and least squares fits for SBL flow fields from a single LES run.

For a single LES run (taken from the last hour of a 12-hour simulation for the control case in Table 2.2), profiles based on fits using Eqs. 3.1, , and are shown along with the data in Figure 3.5. The three slope parameters, $\hat{\alpha}$, $\hat{S}_\theta$, and $\hat{S}_\sigma$, serve to describe distinct SBL-associated wind field characteristics. From each of the 2,200 LES runs, such parameters are estimated; the NBL flow fields previously discussed are now modified by correction their shear, direction, and turbulence profiles, one at a time to render them more "similar" to the SBL flows. By studying wind turbine loads from the SBL flow fields with those from the incrementally adjusted NBL flow fields, we seek to identify those flow characteristics that influence the loads.

3.3.1 Modification of NBL wind fields with adjustments for shear, direction, and turbulence

Figure 3.6 conceptually illustrates the procedure of adjusting NBL flow fields by successively enhancing wind shear (Step 1) using $\hat{\alpha}$; introducing wind veer (Step 2) using $\hat{S}_\theta$ (note that this step introduces a non-zero lateral wind velocity component, $\overline{V}(z)$); and suppressing or enhancing turbulence (Step 3) using $\hat{S}_\sigma$ (possibly at different slopes above and below the hub height).

3.3.2 Illustration of each modification procedure

The single LES case presented in Fig. 3.5 is considered to discuss the fitted slope parameters, $\hat{\alpha}$, $\hat{S}_\theta$, and $\hat{S}_\sigma$, first. These slope parameters are summarized in Table 3.1. The three steps incrementally add one, then two, and finally three adjustments to the NBL flow field to attempt to target the SBL flow field by use of the slope parameters in Table 3.1. In each step, the modifications made for shear, direction, and turbulence are based on the

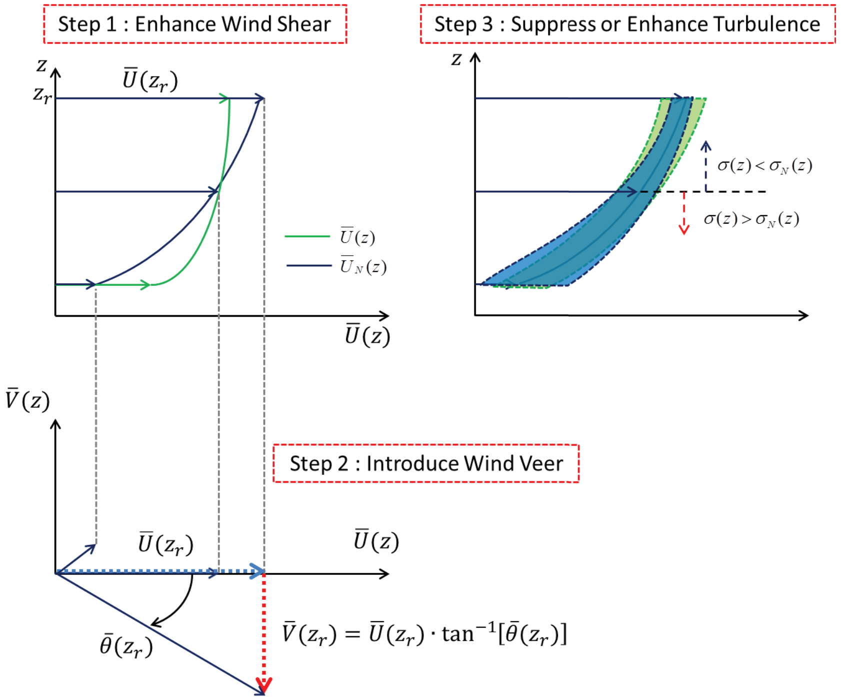

Figure 3.6: NBL wind field modification to match SBL in three steps that modify profiles for mean wind speed, wind direction, and turbulence variation.

estimated slope parameters; the red lines in Fig. 3.7a, 3.7b, and 3.7c show the modified NBL profiles which are seen to closely follow the SBL data indicated by the blue circles. The green line shows the original unmodified NBL profiles.

3.3.3 Comparison of Single Wind Turbine Load History

For three loads—blade root out-of-plane bending moment (OoPBM), tower-top yawing moment (TTYM), and base fore-aft tower bending moment (FATBM)—we compare time series, power spectrum density functions, and stress range histograms for the SBL wind fields and the NBL wind field, un-

Table 3.1: Step-wise correction of profiles for shear, direction, and turbulence for a single LES run (taken from the last hour of a 12-hour simulation for the control case in Table 2.2).

	NBL	Step 1	Step 2	Step 3	SBL
U_h (m/s)	12.288	12.288	12.288	12.288	12.304
σ_U (m/s)	0.392	0.392	0.392	0.392	0.412
$\hat{\alpha}$		0.417	0.417	0.417	0.417
$\hat{S}_\theta (°/m)$			-0.136	-0.136	-0.136
$\hat{S}_\sigma$ ((m/s)/m)				[-0.0024, -0.0023]	[-0.0024, -0.0023]

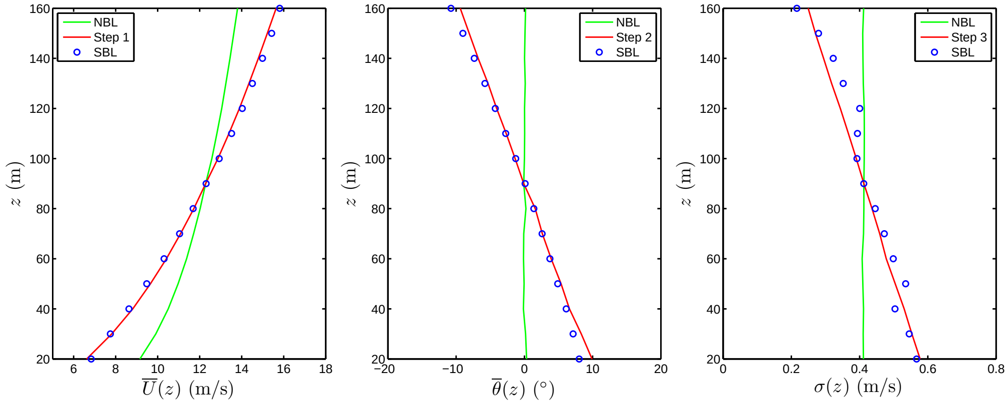

(a) $\overline{U}(z)$ (b) $\overline{\theta}(z)$ (c) $\sigma(z)$

Figure 3.7: Modification of NBL-based profiles of wind speed, direction, and turbulence based on SBL linear fits for a single LES run.

modified as well as with incremental modifications in three steps for the single LES run also presented in Table 3.1.

3.3.3.1 Blade-Root Out-of-Plane Bending Moment

Figure 3.8 compares OoPBM time series for the SBL and NBL cases, all represented by different color lines; the top plot is a 10-minute time series while

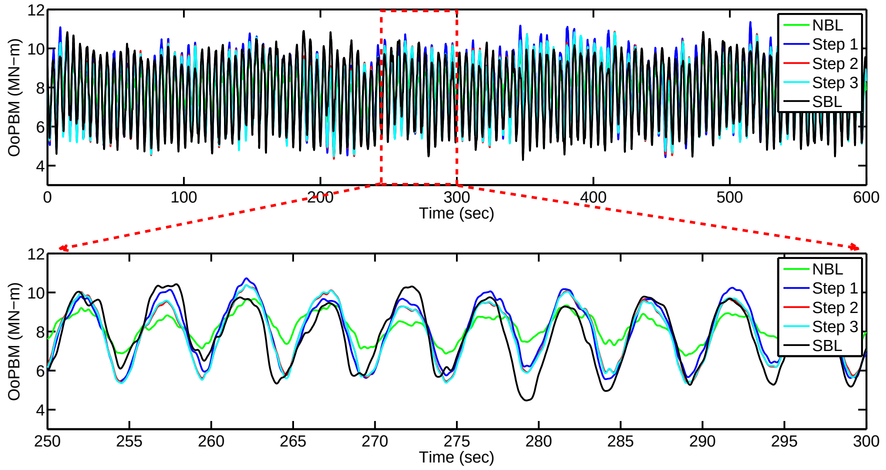

Figure 3.8: Comparison of OoPBM time series for a single case (control).

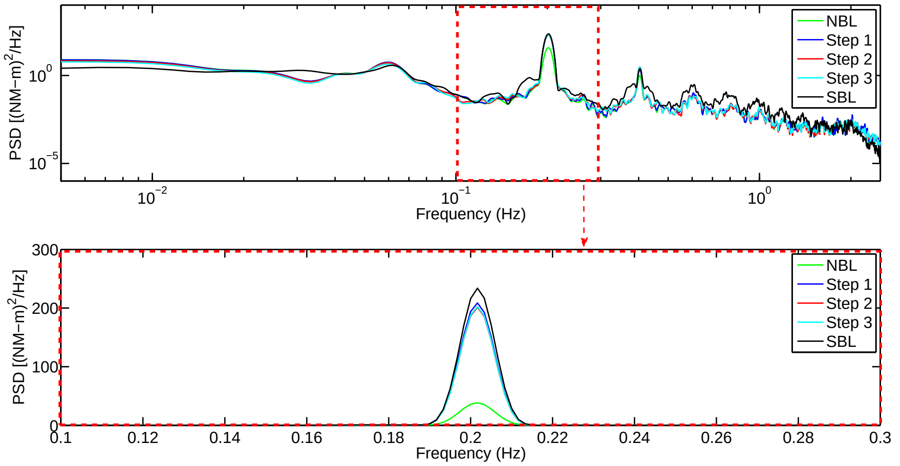

Figure 3.9: Comparison of OoPBM power spectra for a single case (control).

the bottom one is for a 50-sec segment. Figure 3.9 compares OoPBM power spectra for the SBL and NBL cases; the top plot is for a wider frequency range while the bottom is for a narrow range and is plotted using a linear scale. In general, the OoPBM based on the SBL wind field (black line) exhibits stronger

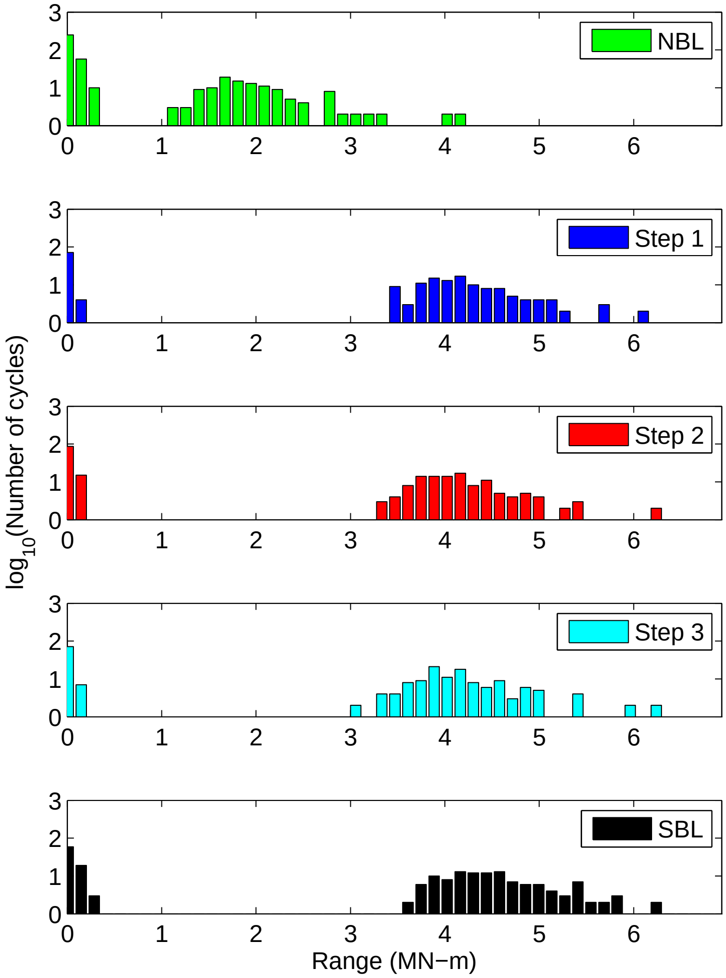

Figure 3.10: Comparison of OoPBM range histograms for a single case (control).

periodic behavior than the NBL cases; it is more narrow-banded. The shear-enhancing modification in Step 1 makes a significant correction to the base

NBL case by increasing OoPBM amplitudes as can be seen in the increased power spectrum peak. Subsequent modifications from Steps 2 and 3 do not significantly change the OoPBM process. Figure 3.10 compares OoPBM range histograms for the SBL and NBL cases where it is seen even more clearly that the Step 1 modification, which increases the shear in the base NBL flow field, leads to a very similar range histogram as in the SBL case; again Steps 2 and 3 do not significantly add to the change from Step 1.

3.3.3.2 Tower-Top Yaw Moment

Figure 3.11 compared TTYM time series and Fig. 3.12 compares OoPBM power spectra for the SBL and NBL cases. The Step 1 (shear-enhancing) modification to the NBL flow field increases both the mean value and amplitude of the TTYM process. The increased amplitude is clear from the increased energy seen over a range of frequencies in the PSD plot. Step 2 (wind direction correction) further increases the amplitude of the TTYM process, making the time series and PSD plots more comparable to those for the SBL case. The TTYM process appears to be influenced by both wind shear and wind direction change over the rotor swept area. Figure 3.13 compares TTYM range histograms for the SBL and NBL cases. Step 1 increases the number of some high-amplitude cycles; Step 2 makes slight corrections to the histograms. Even after all three steps of modification (accounting for shear, direction, and turbulence profile matching), the TTYM histograms are very different for the NBL case compared to the histogram from the SBL case, which has significantly

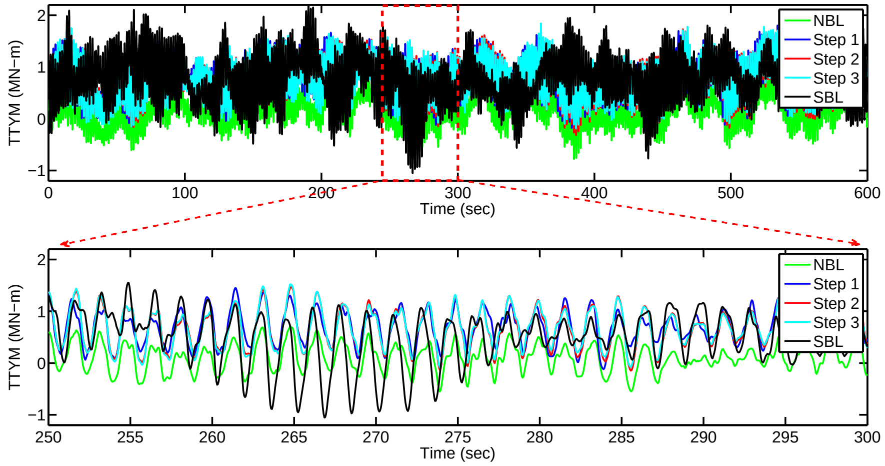

Figure 3.11: Comparison of TTYM time series for a single case (control).

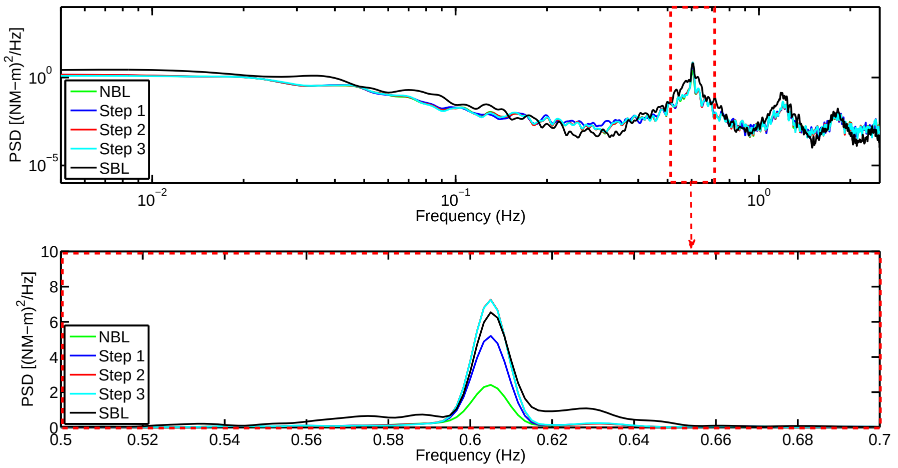

Figure 3.12: Comparison of TTYM power spectra for a single case (control).

more high-amplitude cycles. This deviation in TTYM range histogram, which will influence fatigue loads, is investigated further by comparing NBL and SBL turbulent wind fields in some detail next.

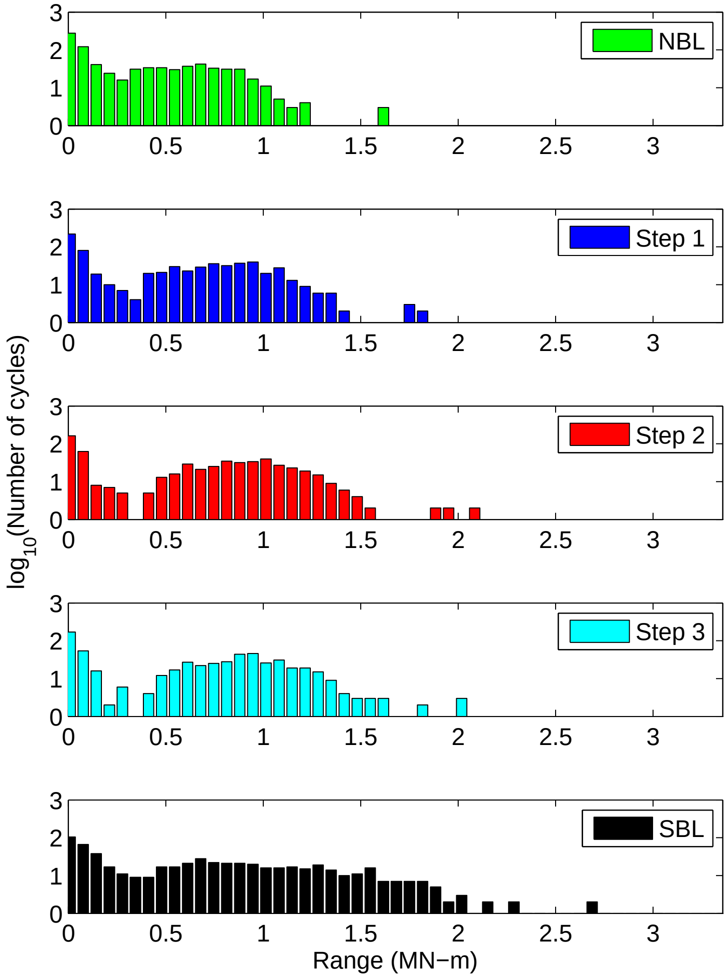

Figure 3.13: Comparison of TTYM range histograms for a single case (control).

Figure 3.14 shows the variation in time and space (over the rotor swept area) of the longitudinal turbulence in the NBL and SBL flow fields and their impact on TTYM loads, which are compared in the bottom plot. We first

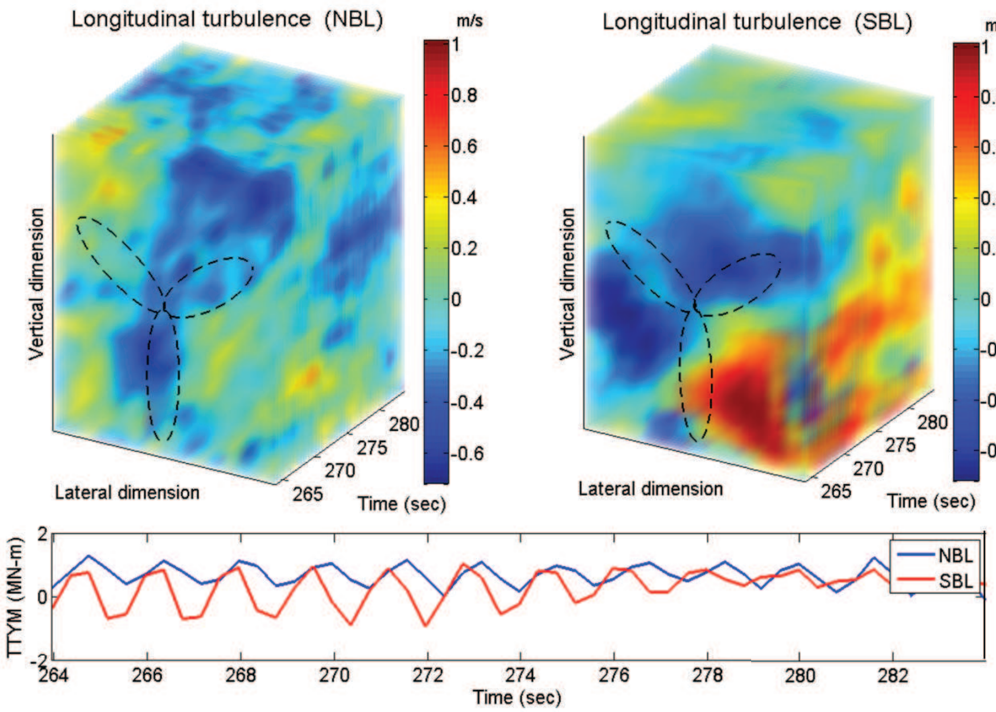

Figure 3.14: Effect of turbulent wind field on TTYM process for a single run (control).

extracted ≈20-second portions of the time series of TTYM, from the two cases where deviations were large and then compared turbulence levels during that time. The mean wind fields are the same in the two cases; therefore, the contrasting variation in turbulence for the two cases is the main reason why the TTYM process for the SBL case has higher amplitudes. Studying the 3-D turbulence distribution plots, it is seen that the SBL wind field has more locally concentrated (coherent) and organized turbulence structures. These turbulence structures are sustained for a while, during which the corresponding

TTYM process cycles are large. Such locally concentrated turbulence causes strong asymmetric forces on the rotor and, in turn, bring about large tower-top yawing moments, TTYM, that are enhanced by asymmetric loading effects.

3.3.3.3 Fore-Aft Tower Base Moment

Figure 3.15 compares FATBM time series and Fig. 3.16 compares power spectra for SBL and NBL cases. In contrast with the blade loads, there is greater influence of low-frequency energy on the FATBM process and greater differences between the SBL and NBL wind fields in that range. Because the SBL wind fields have lower energy in the low-frequency region, the FATBM process also has lower energy levels there for SBL relative to NBL wind fields. Figure 3.17 compares FATBM range histograms for the SBL and NBL cases. The low-amplitude cycles (or ranges) in the histogram are somewhat smaller for the SBL wind field compared to the base NBL and modified NBL wind fields; this is because the SBL wind fields have reduced turbulence energy over high frequencies that are responsible for the low-amplitude load cycles. We shall see later that the small-amplitude cycles differences do not greatly influence fatigue loads on the tower. The FATBM range histogram shows smaller differences for large-amplitude cycles.

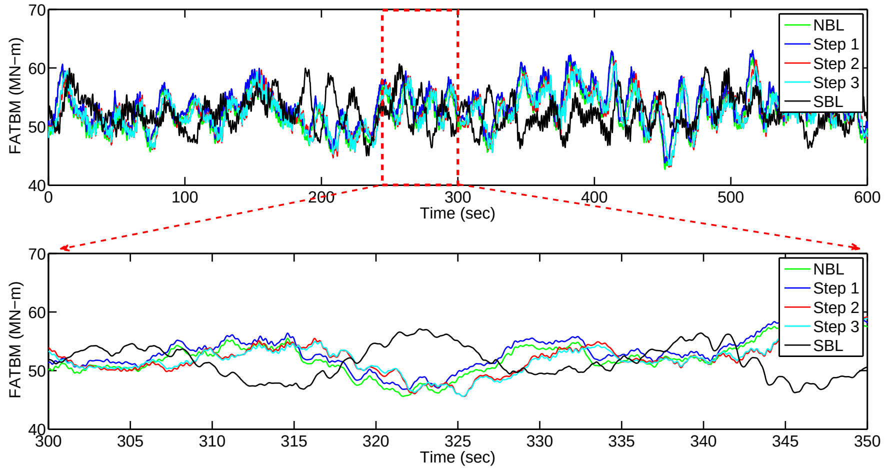

Figure 3.15: Comparison of FATBM time series for a single case (control).

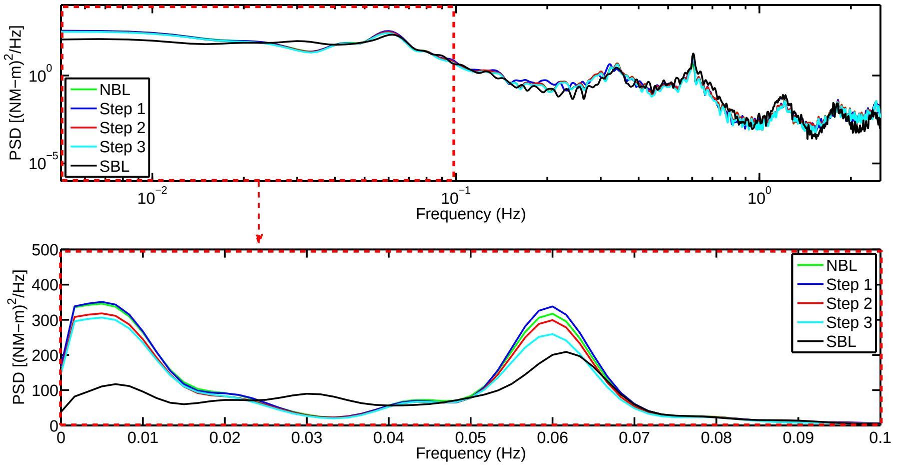

Figure 3.16: Comparison of FATBM power spectra for a single case (control).

3.4 Comparison of Time-Varying Wind-Related Processes and Wind Turbine Load Processes

We examine next how the probability distributions of processes describing the longitudinal wind velocity, U, the lateral wind velocity, V, the

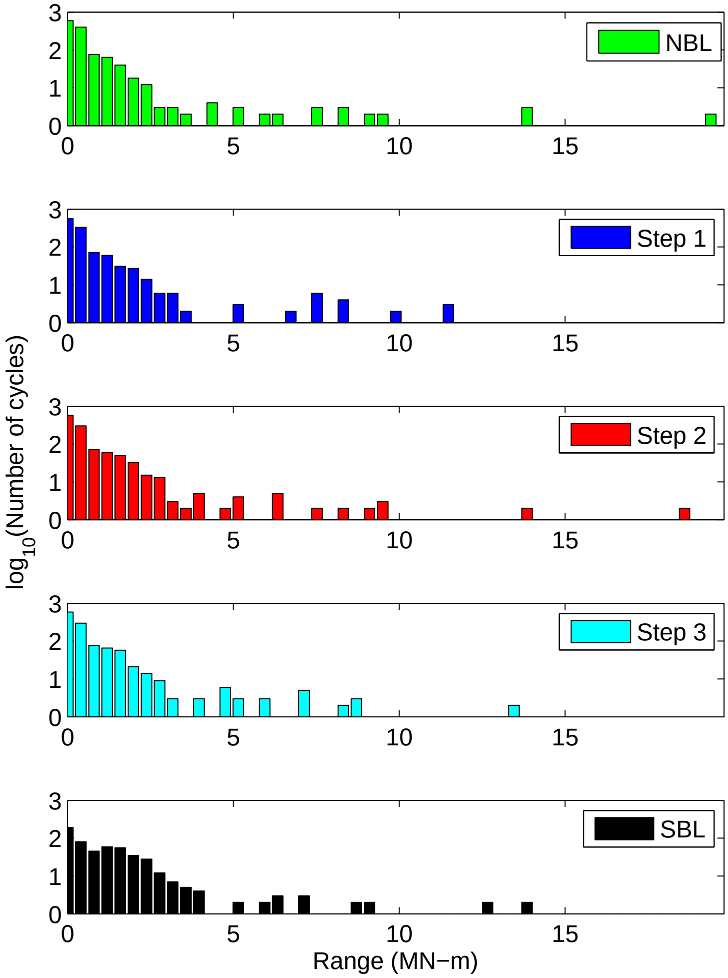

Figure 3.17: Comparison of FATBM range histograms for a single case (control).

Reynolds stress, uv, and the wind direction, θ compare for the base NBL wind field, the modified NBL wind fields, and the SBL wind field. We also examine these various processes at different elevations including the top, center (hub), and bottom of the rotor swept area. The probability density functions (PDFs) will be accordingly studied first for U, V, uv, and θ. After this, we compare PDFs for the three load processes (OoPBM, TTYM, an FATBM) for the various NBL and SBL wind fields.

3.4.1 Wind Field Process

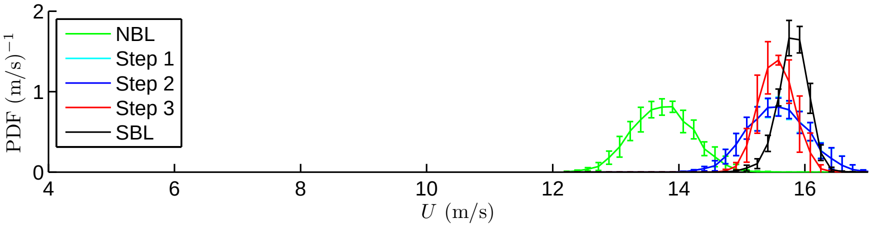

(a) Rotor top

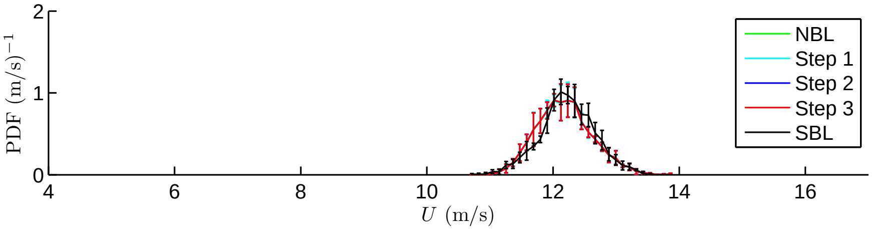

(b) Rotor hub

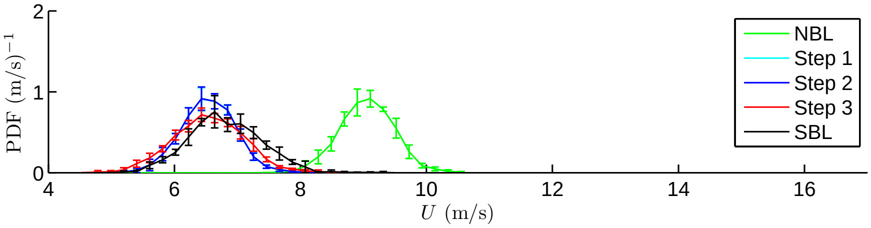

(c) Rotor bottom

Figure 3.18: Probability density functions for the longitudinal wind velocity, U, for a single case (control).

Figure 3.18 compares PDFs for the longitudinal wind velocity time series at the three locations—at the rotor top, the rotor hub, and rotor bottom. The PDFs are based on a averages from the five wind fields extracted from the last stage (twelfth hour of the LES run) of the control LES case and corresponding NBL base and modified wind fields. Error bars indicate one standard deviation on each indicated PDF ordinate. Step 1 (enhancing shear) is seen to move the PDF for U, at the rotor top, towards higher wind speeds and, at the rotor bottom, towards lower wind speeds. Nor much change results at the rotor hub since U_h and σ_U were matched there for the SBL and NBL cases. Step 2 results in no change to the PDFs for U since it only influences V. Step 3, which suppresses turbulence at the top and enhances turbulence at the bottom, causes the PDF to be narrower at the rotor top and more disperse at the rotor bottom. We note that the PDF for U for the NBL wind field becomes more and more similar to that of the SBL field with each modification step.

Figure 3.19 compares PDFs for the lateral wind velocity time series at the same three locations as before. Steps 1 and 3 do not affect the PDF for V because they only modify longitudinal wind velocity, U. Step 2 (including wind direction change or wind veer), however, has an effect on the PDF of V at the rotor top and bottom as expected. This is the result of introducing a non-zero mean lateral velocity component, $\overline{V}(z)$, to the NBL wind field. We see that Step 2 effectively modifies the PDF of V so that it is more similar to that of the SBL wind field than was the case with the NBL base wind field.

Figure 3.20 compares PDFs for the Reynolds stress time series at the

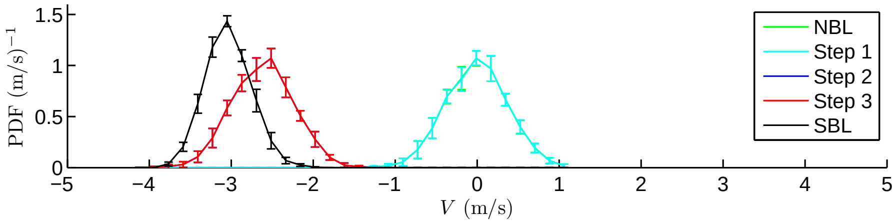

(a) Rotor top

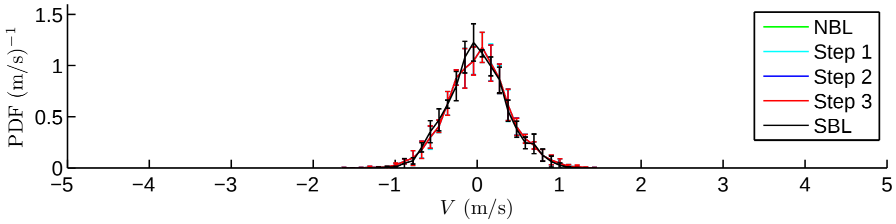

(b) Rotor hub

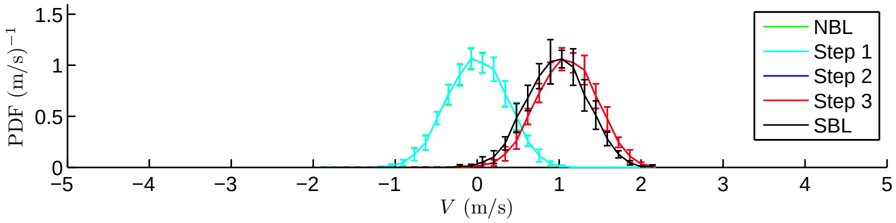

(c) Rotor bottom

Figure 3.19: Probability density functions for the lateral wind velocity, V, for a single case (control).

same three locations as before. The mean values of the turbulence components, u and v, are zero; thus, the peaks of the PDF for the Reynolds stress, uv, are zero at all three locations. Steps 1 and 2 do not influence the PDF of the Reynolds stress because they only modify the mean wind field. Step 3 decreases the dispersion in the PDF for uv at the rotor top, and increases it at the rotor bottom; this causes the PDF curve after Step 3 to become more

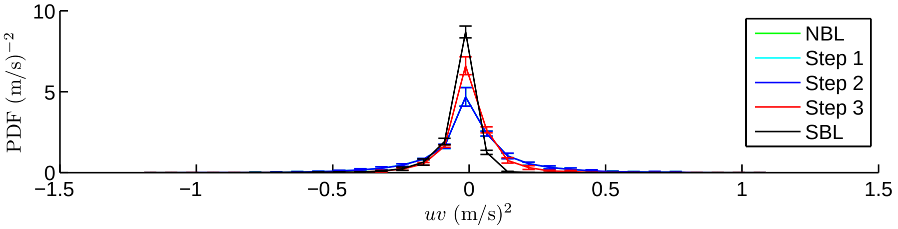

(a) Rotor top

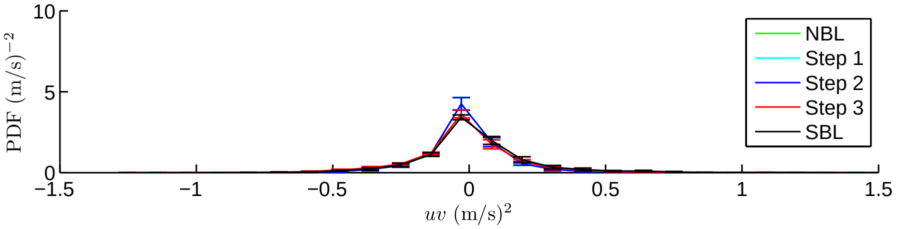

(b) Rotor hub

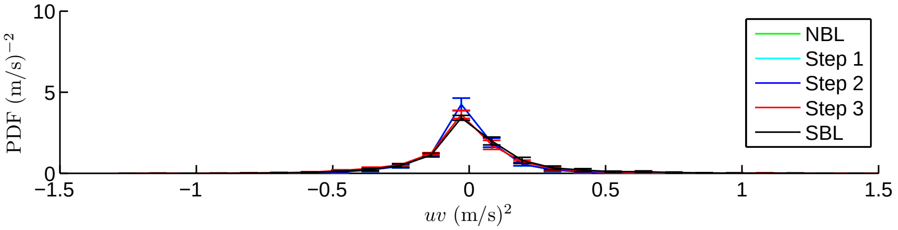

(c) Rotor bottom

Figure 3.20: Probability density functions for the Reynolds stress, uv, for a single case (control).

similar to that with the SBL wind field.

Figure 3.21 compares PDFs for the wind direction time series at the same three locations as before. Step 1 does not significantly affect the PDF for θ; it slightly widens the PDF at the rotor bottom due to adjustments to the mean longitudinal wind speed there. Step 2 significantly modifies the PDF for θ so that it closely resembles that for the SBL wind field. The small

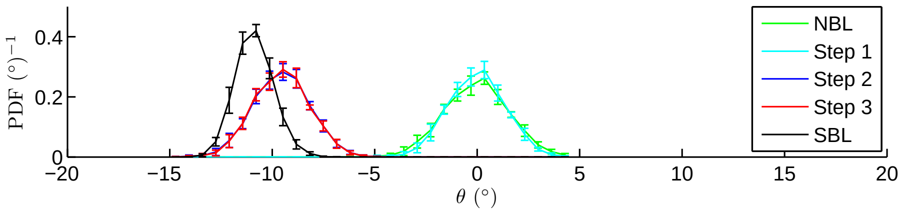

(a) Rotor top

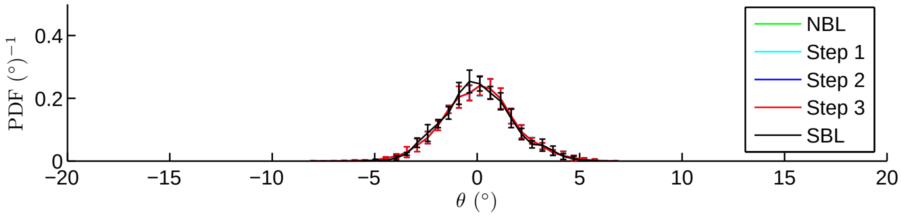

(b) Rotor hub

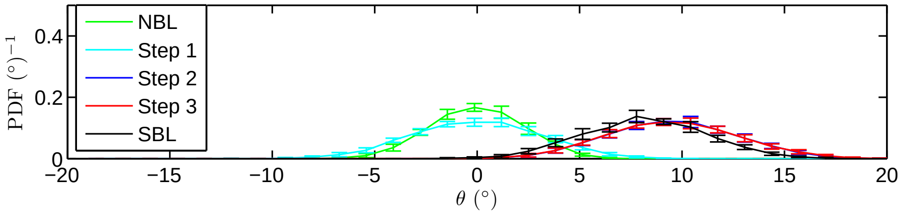

(c) Rotor bottom

Figure 3.21: Probability density functions for the wind direction, θ, for a single case (control).

differences between the PDFs from the NBL-modified (Step 3) wind field and the SBL wind field are due to the approximated linear model assumed for the mean wind direction profile. Step 3 has little effect on the PDF for θ because although the longitudinal turbulence is scaled, is relatively very small compared to U to greatly influence the time-varying wind direction.

3.4.2 Comparison of Wind Turbine Load Processes

We compare PDFs of wind turbine load processes for the base NBL wind field, the modified NBL wind fields, and the SBL wind field in order to assess the influence of SBL wind field characteristics related to wind shear, wind veer, and turbulence gradients. We average PDF curves estimated from five wind fields generated from the twelfth hour of the LES-SBL control case. Similarly, we obtain averaged PDF curves for the base NBL wind field and for the modified NBL wind fields. A comparison of these PDF curves enables us to understand the effect of each SBL-associated wind field characteristic on the load processes. In this comparison exercise, we use the same wind fields that were used in the time-varying wind-related process PDF comparisons (summarized in Fig. 3.18, 3.19, 3.20 and 3.21). Figures 3.22, 3.23 and 3.24 present PDFs for three different turbine load processes—blade-root out-of-plane bending moment (OoPBM), the tower-top yawing moment (TTYM), and the base fore-aft tower bending moment (FATBM).

3.4.2.1 Blade Root Out-of-Plane Bending Moment

Figure 3.22 compares OoPBM PDFs. We note that the shape of the PDF for the NBL base wind field is completely different from that for the SBL wind field. However, the three modification steps cause the NBL wind field to have an OoPBM PDF that is quite similar to that resulting from the SBL wind field. Step 1 changes the uni-modal PDF to a bimodal one; the difference in the load levels at the two modes represent a dominant amplitude of the load

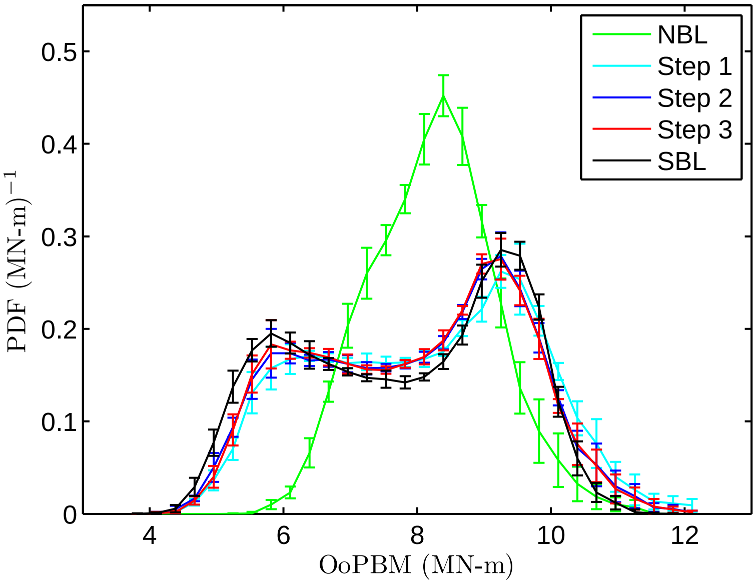

Figure 3.22: Probability density functions for the blade root out-of-plane bending moment, OoPBM, for a single case (control).

process. This suggests that the enhanced wind shear changes the OoPBM from a broad-banded process to a somewhat more narrow-banded one with a stronger periodic component. This trend can be easily verified in the OoPBM time series (Figure 3.8) which show increases in OoPBM process amplitude, and in the PSD plots (Figure 3.9) which show that 1P (1 per rev) energy peak is significantly increased with the Step 1 shear enhancement. Note that the asymmetry in the PDF curve results from the different wind velocity variation that blade experiences when it rotates in upper half of the rotor plane versus in the lower half. Velocity differences between the rotor hub and bottom are larger than those between the rotor hub and top due to the power-law shear profile; this causes an asymmetric periodic OoPBM process and, also, an asymmetric PDF. Steps 2 and 3 lead to somewhat smaller adjustments to the OoPBM PDF. In summary, by merely enhancing the wind shear, OoPBM loads from the NBL wind field become quite similar to those from the SBL wind field.

3.4.2.2 Tower-Top Yawing Moment

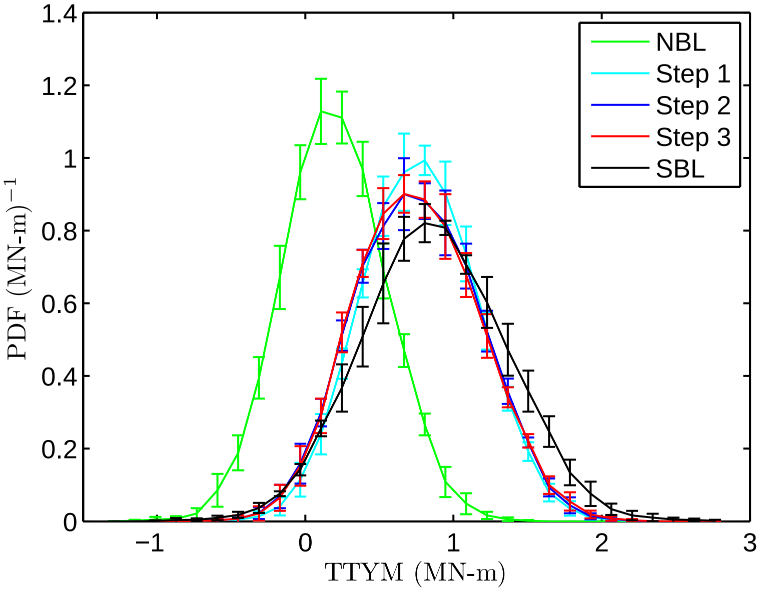

Figure 3.23: Probability density functions for the tower-top yawing moment, TTYM, for a single case (control).

Figure 3.23 compares TTYM PDFs. The Step 1 modification to the NBL base wind field shifts the TTYM PDF curve towards larger load levels, and the moves the mode and mean TTYM closer to that for the SBL wind field. Steps 2 and 3 have little apparent influence on the PDF for TTYM. Even after all the NBL field modifications, there are still deviations in the TTYM PDF curve relative to that from the SBL wind field whose PDF has a more significant upper tail; these larger TTYM values are associated with larger amplitude cycles that. Fatigue of the nacelle yaw bearing will likely be influenced by these large-amplitude TTYM cycles. The differences in the PDFs for the modified NBL wind fields and the SBL wind field arise, at least in part, from localized and sustained turbulent structures that cause highly asymmetric force over the turbine rotor plane that drive the TTYM process.

3.4.2.3 Base Fore-Aft Tower Bending Moment

Figure 3.24 compares FATBM PDFs. The PDF for the NBL wind field has a more significant upper tail compared to that for the SBL wind field. Step 1 moves the FATBM PDF in the opposite direction instead of approaching the PDF for the SBL wind field. Steps 2 and 3 reverse this trend to some degree but there still remains a significant difference in the FATBM PDFs for the modified NBL wind fields versus the SBL wind field. It is worth noting that, on a relative scale, the deviations in the FATBM are not very large compared to the mean or center of the FATBM PDF; we note that the deviation in the TTYM loads were significantly larger relative to the mean TTYM value.

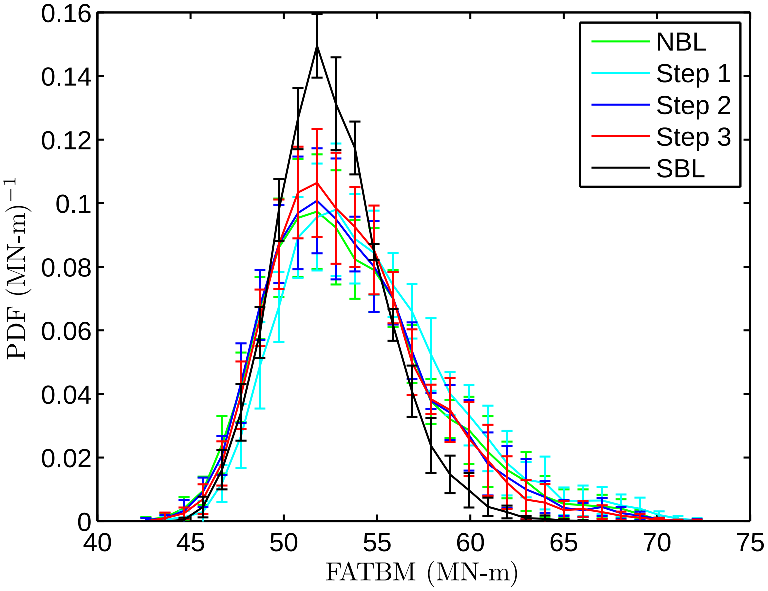

Figure 3.24: Probability density functions for the base fore-aft tower bending moment, FATBM, for a single case (control).

3.5 Extreme and Fatigue Load Statistics

The entire suite of 2,200 SBL wind fields generated from 44 LES runs is considered next. The same procedure described for a single control case is now repeated for all of the 2,200 wind fields. Thus, base NBL wind fields are first generated with matching mean wind speed and standard deviation values at hub height. Then, necessary modifications are made in three steps where wind shear, direction, and turbulence as discussed. Figure 3.25 shows a schematic flow chart that explains the procedure adopted for assessing the influence of SBL-related wind field characteristics on wind turbine loads.

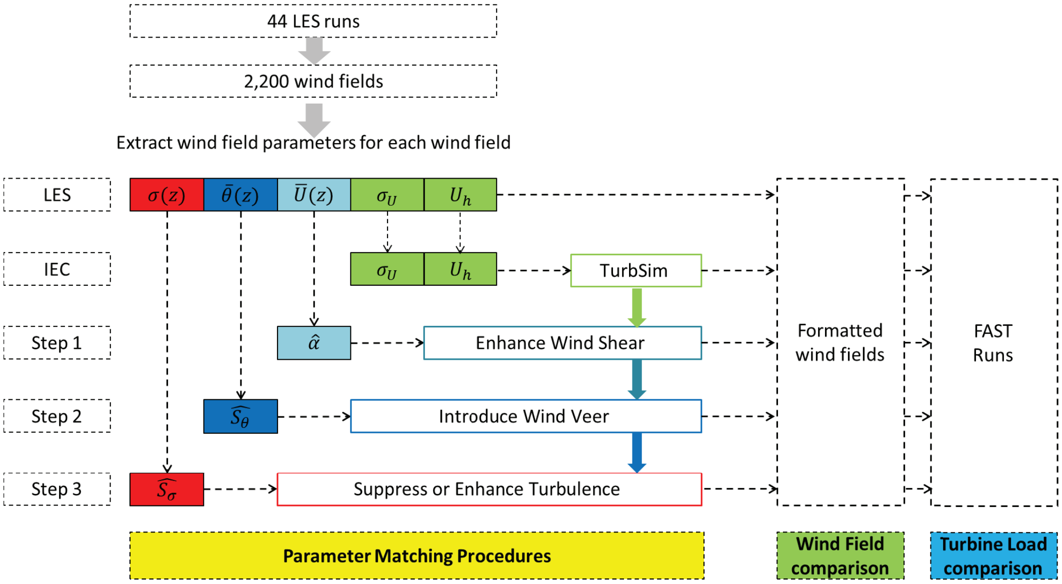

Figure 3.25: Procedure for isolating SBL-related wind field characteristics and comparing their influences on wind fields and turbine loads.

3.5.1 The Comparison of Wind Field Parameters' Contribution to Extreme Load Statistics

Equivalent fatigue load (EFL) and the maximum load for a 10-min loading time history are used to compare each wind field parameter's contribution and importance in a turbine load estimation. These two loading statistics corresponding to 2,200 wind fields generated from the 44 LES runs, 2,200 wind fields generated from TurbSim based on the IEC standard, and each set of 2,200 modified wind fields for three parameter matching steps are compared. We compare these statistics in each wind field characteristic domain segmented by the relative magnitude between shear and turbulence to evaluate the contribution of each wind field parameter on turbine loads depending on the level of shear and turbulence. In addition, this categorical comparison gives insight into how extreme turbine load statistics are affected by the level of turbulence and shear.

Figures 3.26 - 3.31 compare the equivalent fatigue load (EFL) values (corresponding to 1,000 load cycles in each case) and maximum values from ten-minute time series of OoPBM, TTYM and FATBM. We compare these load statistics for four different domains:(a) strong turbulence and weak shear; (b) strong turbulence and strong shear; (c) weak turbulence and weak shear; and (d) weak turbulence and strong shear. Box plots in each of these four groups summarize the median value (red line), 25% and 75% fractiles (boundary of blue box), and the minimum and maximum values (extended black bar) for the EFL and ten-minute maximum values for loads evaluated for wind fields from the available 2,200 that are contained in that group. The red crosses represent outliers.

3.5.1.1 Blade-Root Out-of-Plane Bending Moment

Figure 3.26 compares statistics of EFL for OoPBM. Step 1 (wind shear enhancing) significantly increases the median of EFL, making the NBL case comparable to that of the SBL case. This improvement is especially evident in the strongly stratified (stable) groups, (b) and (d). The other modification steps affect the EFL for OoPBM only very slightly. Thus, correct representation of the wind shear in the stable boundary layer is critical to estimate OoPBM fatigue loads. Figure 3.27 compares statistics of the 10-min maximum

OoPBM. Each modification step has a small influence on the maximum load; Step 1 slightly increases the median of the ten-minute maximum load, and this increased median is comparable to that for the SBL case. The small changes are because maximum values are not influenced by modifications (as in the three steps) to the entire load process but are affected mostly by instantaneous large values. Such instantaneous effects are correlated more strongly with the level of turbulence; hence, the higher turbulence regions, (a) and (b), are associated with larger maximum loads than the lower turbulence regions, (c) and (d).

3.5.1.2 Tower-Top Yaw Moment

Figure 3.28 compares statistics of EFL for TTYM. Each modification step gradually increases the EFL values; however, the median of EFL for the SBL wind field is still much higher than that for the NBL base and modified wind fields. In the more stable cases, (b) and (d), the effects of each modification are more apparent because enhanced wind shear and wind veer are more significant in these cases and, thus, the mean wind fields in these regions are modified more significantly compared with the wind fields in other cases. Compared with EFL in the less stable cases, (a) and (c), we notice small improvements with modifications to the base NBL winds and large differences relative to the SBL winds. This suggests that some other factor in the SBL wind field, that is not accounted for in our NBL field modification, possibly contributes the EFL for TTYM. We saw earlier that these EFL deviations for

NBL versus SBL are likely caused by significantly different spatial and temporal turbulence structures in the wind fields. Figure 3.29 compares statistics of ten-minute maximum loads for TTYM. The variation in the statistics for the ten-minute maximum TTYM in each case is similar to that for the EFL. It is important to point out that the large TTYM values seen with the SBL wind fields cannot be estimated by stochastic simulation, even if modifications for wind shear, veer, and turbulence variation over the rotor plane are taken into consideration.

3.5.1.3 Fore-Aft Tower Base Moment

Figures 3.30 and 3.31 compare the statistics of the EFL and ten-minute maximum values, respectively, for the FATBM. Both the EFL and ten-minute maximum values of FATBM corresponding to the NBL base wind field are already comparable to those for the SBL wind field; this suggests that the hub-height mean longitudinal wind speed and standard deviation alone, i.e., U_h and σ_U, are sufficient to predict the EFL and ten-minute maximum values of FATBM, regardless of atmospheric stability conditions. This trend can also be seen by comparing load statistics in the less stable cases, (a) and (c), with those in the more stable cases, (b) and (d). The median values for the EFL and ten-minute maximum value do not vary depending on the level of stability but show some variation with the level of turbulence; the medians of EFL and ten-min maxima are significantly larger in the strong-turbulence cases, (a) and (b). This can be simply explained by the cantilever analogy for this tower base moment: fluctuations in wind speed are converted into fluctuations in forces exerted at the wind turbine tower tip, which cause overturning moment variation at the tower base. In this manner, the wind turbine hub height of 90 m acts as a moment arm, converting enhanced wind speed fluctuations (turbulence levels) to significantly amplified FATBM levels.

3.5.2 Summary on Load Statistics

Table 3.2: EFL statistics from 2,200 wind fields (SBL versus NBL base and modified cases).

	OoPBM				
	NBL	Step 1	Step 2	Step 3	SBL
μ (MN-m)	3.096	4.555	4.492	4.493	4.748
σ (MN-m)	0.809	0.946	0.8944	0.900	0.957
	TTYM				
	NBL	Step 1	Step 2	Step 3	SBL
μ (MN-m)	1.420	1.600	1.728	1.765	2.333
σ (MN-m)	0.362	0.331	0.381	0.346	0.406
	FATBM				
	NBL	Step 1	Step 2	Step 3	SBL
μ (MN-m)	6.828	6.910	6.957	6.658	6.872
σ (MN-m)	2.921	2.940	2.831	2.826	2.695

Table 3.2 summarizes the comparison of EFL statistics for all three wind turbine loads, OoPBM, TTYM and FATBM, based on the 2,200 SBL fields and associated base and modified NBL wind fields. The mean and standard deviation of the EFL values are presented. First, for the OoPBM

case, Step 1 is seen to increase the mean EFL by almost 50% compared with base NBL wind field; also, this increased mean value is almost comparable to that for the SBL case. The standard deviation of the OoPBM EFL value is not significantly affected by modifications to the NBL base wind field. Second, for the TTYM case, though each step slightly improves the mean EFL, these values do not reach the same level as seen for the SBL wind field. As mentioned before, this deviation between NBL (even after modifications) and SBL wind fields is because of different characteristics of the turbulence fields such as the coherence and local energy distribution over the rotor plane. Finally, for the FATBM case, the mean EFL is seen to be relatively stable for the NBL base and modified wind fields and comparable with that for the SBL wind field. This is because the base fore-aft tower bending moment is influenced primarily by the longitudinal mean wind speed and turbulence, both of which are matched for the NBL and SBL cases. The complex interactions between the blades and wind field characteristics such as the influence of shear, wind direction, and turbulence variation over the rotor do not appear to transfer to loads at the tower base.

Table 3.3 summarizes statistics on ten-min maximum values for OoPBM, TTYM, and FATBM, based on the 2,200 SBL wind fields and associated base and modified NBL wind fields. The mean and standard deviation of the ten-minute maximum values are presented. First, for the OoPBM case, the mean of the ten-minute maximum values are similar for all the NBL and SBL wind fields. The ten-minute maximum load appears to be most directly influenced

Table 3.3: Ten-minute maximum load statistics from 2,200 wind fields (SBL versus NBL base and modified cases).

	OoPBM				
	NBL	Step 1	Step 2	Step 3	SBL
μ (MN-m)	10.374	11.102	10.939	10.847	10.819
σ (MN-m)	1.400	1.367	1.334	1.331	1.413
	TTYM				
	NBL	Step 1	Step 2	Step 3	SBL
μ (MN-m)	1.444	1.934	1.973	2.060	2.557
σ (MN-m)	0.413	0.402	0.382	0.430	0.484
	FATBM				
	NBL	Step 1	Step 2	Step 3	SBL
μ (MN-m)	62.665	63.551	63.045	62.711	61.680
σ (MN-m)	9.284	9.304	9.285	9.306	9.319

by hub-height mean wind speed, U_h, and standard deviation, σ_U, and all the wind field cases share the same values of U_h and σ_U). Second, for the TTYM case, Step 1 significantly increases the mean of ten-minute maximum TTYM. We saw before how an enhanced wind shear leads to an increase in the overall load level for TTYM. Thus, the Step 1 modification helps to make the maximum TTYM closer to that from the SBL wind field. Note, however, that the mean ten-minute maximum TTYM for the SBL case is still considerably larger that those for all the NBL wind fields. Finally, for the FATBM case, the mean of the ten-minute maximum shows a similar trend to that of the OoPBM; the mean and standard deviation of the maximum TTYM are similar for all the SBL and NBL wind fields. This, again, suggests that the maximum base fore-aft tower bending moment is primarily influenced by the hub-height mean wind speed and standard deviation, U_h and σ_U.

3.5.3 Summary on SBL and NBL differences

Table 3.4: Summary on relationships between SBL wind field characteristics and percentile differences in the extreme wind turbine loads estimated from NBL and SBL wind fields; Q_1 and Q_3 represent the first and third quartiles, respectively; diff. (%) = $100 \cdot (L_{NBL} - L_{SBL})/L_{SBL}$ where L represents an equivalent fatigue load (EFL) or a ten-minute maximum load(MAX).

Case		$z_\alpha < 0$, $z_\sigma > 0$		$z_\alpha > 0$, $z_\sigma > 0$		$z_\alpha < 0$, $z_\sigma < 0$		$z_\alpha > 0$, $z_\sigma < 0$	
No. of data		837		265		291		807	
Quartiles		Q_1	Q_3	Q_1	Q_3	Q_1	Q_3	Q_1	Q_3
SBL	$\hat{\alpha}$	0.29	0.34	0.38	0.42	0.30	0.35	0.40	0.45
	$\Delta\theta$ (°)	7.48	10.54	12.19	15.50	8.98	12.44	16.57	22.58
	$\Delta\sigma$ (m/s)	0.25	0.37	0.31	0.39	0.24	0.33	0.29	0.37
		Differences for SBL and NBL							
EFL diff. (%)	OoPBM	-30.5	-21.0	-38.7	-29.4	-37.5	-28.1	-51.9	-39.0
	TTYM	-36.8	-27.7	-37.6	-28.8	-44.6	-36.5	-54.6	-38.9
	FATBM	-6.5	14.5	-2.4	19.5	-9.7	8.7	-24.5	5.7
MAX diff. (%)	OoPBM	-6.0	-0.9	-7.9	-3.5	-4.0	-0.5	-7.6	-2.1
	TTYM	-44.2	-30.0	-48.7	-35.6	-47.4	-35.6	-58.6	-47.0
	FATBM	-1.3	3.6	-0.8	3.8	-0.1	3.9	-0.7	3.0
		Differences for SBL and modified-NBL (Step 3)							
EFL diff. (%)	OoPBM	-12.1	-3.9	-8.2	-1.8	-9.8	-3.5	-4.6	0.3
	TTYM	-28.1	-18.4	-23.1	-12.5	-32.4	-23.1	-31.3	-19.0
	FATBM	-10.6	8.5	-6.3	13.5	-16.3	2.4	-20.6	3.0
MAX diff. (%)	OoPBM	-3.6	1.1	-2.2	1.4	-1.8	1.7	0.2	3.7
	TTYM	-27.8	-12.4	-23.1	-7.5	-31.0	-16.1	-24.7	-12.9
	FATBM	-1.4	3.6	-0.5	3.5	-0.1	3.7	-0.2	3.6

We finally seek to understand trends between the wind field conditions, grouped into four cases based on levels of shear and turbulence, and SBL-related wind field characteristics such as the enhanced wind shear, the wind direction difference between the rotor top and bottom ($\Delta\theta = \hat{S}_\theta \cdot D_{rotor}$ where D_{rotor} is the rotor diameter), and the standard deviation difference between the rotor top and bottom ($\Delta\sigma = \hat{S}_\sigma \cdot D_{rotor}$. Table 3.4 provides statistics on those parameters; we use the 25- and 75-percentile values, Q_1 and Q_3, to assess the extent of variation in these different wind field characteristics where the number of data sets varies for each of the four groups. In general, the values of $\Delta\theta$, $\Delta\sigma$ and $\hat{\alpha}$ are all higher when shear is strong, $z_\alpha > 0$, which is for very stratified (stable) conditions.

We have focused on three SBL-related wind field characteristics and attempted to include them in modifications to base NBL wind fields. For all the SBL and NBL wind fields, we estimated EFL and ten-minute maximum loads for OoPBM, TTYM and FATBM. The percentile differences in these load statistics estimated by SBL and NBL base wind fields are presented. The negative differences seen in so many of the load statistics suggest that, in general, the NBL base wind fields underestimate load statistics compared to the SBL case. In particular, the EFL for OoPBM and both the EFL and ten-minute maximum for TTYM are grossly underestimated; the differences are most severe when the shear is strong ($z_\alpha > 0$).

All three of the wind field modifications are applied to the NBL wind fields in Step 3; therefore, by investigating percentile differences in the load statistics estimated from SBL and NBL wind fields after Step 3, we can learn about the importance of three wind field characteristics (wind shear, wind direction, and turbulence variation) on loads. Also, the previously provided percentile differences on loads between the SBL and NBL base case provides a useful reference for this comparison. After three steps of modifications to the base NBL wind fields, the percent differences in load statistics relative to the SBL case are, in general, decreased; this suggests that although modified NBL wind fields still underestimate loads, the wind field characteristics modified in the base NBL fields do have some influence on the turbine loads. In particular, the EFL for OoPBM under stable conditions is greatly improved; in the strong shear and weak turbulence case, the percentile difference (Q_1; Q_3) range changed from (-51.9; -39.0) to (-4.6; 0.3). In the case of TTYM, the improvements are slight, not significant.

The percentile differences in ten-min maximum loads are smaller than those in EFL values, and they do not show clear improvements after NBL wind field modifications. This is because maximum values are most related to turbulence and wind speed rather than to shear and direction profiles. In the case of TTYM, however, percentile errors are reduced after NBL wind field modification, particularly when shear is strong; this appears to be due to the increased mean values of TTYM that result due to enhanced wind shear. The significant difference in TTYM loads SBL and NBL wind fields is an interesting topic for further study; SBL conditions clearly make these loads higher.

3.6 Discussion and Conclusion

SBL and NBL wind fields were compared in terms of the characteristics of the wind fields and associated loads on a 5MW wind turbine. LES can generate more realistic wind inflow fields by accounting for atmospheric stability. The major differences between SBL and NBL wind fields are summarized in

Table 3.5: Summary of the differences in SBL and NBL wind fields

	SBL	**NBL**
Mean longitudinal wind velocity profile	Shear profile is influenced by the level of stability	Set by a power law
Mean wind direction profile	Accounts for wind direction change	No wind turning is assumed
Standard deviation of longitudinal wind velocity profile	Turbulence level changes with elevation	Turbulence level is usually assumed constant over the rotor plane

Table 3.5.

To isolate SBL-related wind field characteristics and their influence on wind turbine loads, we attempted modifications of NBL wind fields generated by stochastic simulation so as to match wind field characteristics with those from SBL wind fields. Statistics and probability distributions for the NBL-modified wind fields and the SBL wind fields were compared and were generally found to be in good agreement. Each load type of a wind turbine is differently affected by the SBL-related wind field characteristics. By comparing the extensive wind turbine load statistics on EFL and ten-minute maxima for different load types (including OoPBM, TTYM, and FATBM), we evaluated the contribution of each wind field characteristic (related to shear, veer, and turbulence) to wind turbine loads. The results are summarized as follows:

- The EFL and maximum value for the blade root out-of-plane bending moment (OoPBM) is mainly influenced by U_h and σ_U. In the case of

EFL, wind shear significantly changed the EFL level.

- The EFL and maximum value for the tower-top yawing moment (TTYM) are significantly increased by spatially and temporally organized turbulence structures, which are difficult to include in any stochastic wind modeling method.

- The EFL and maximum value for the base fore-aft moment tower bending moment are mainly influenced by U_h and σ_U.

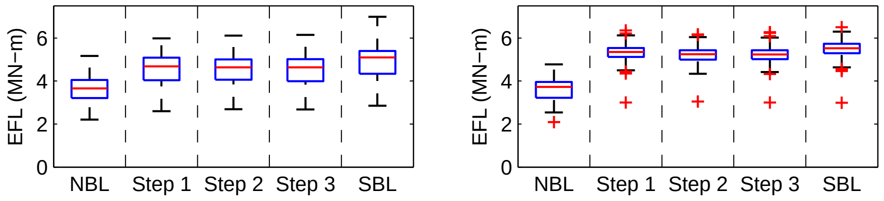

(a) $z_\alpha < 0 \quad \& \quad z_\sigma > 0$ (b) $z_\alpha > 0 \quad \& \quad z_\sigma > 0$

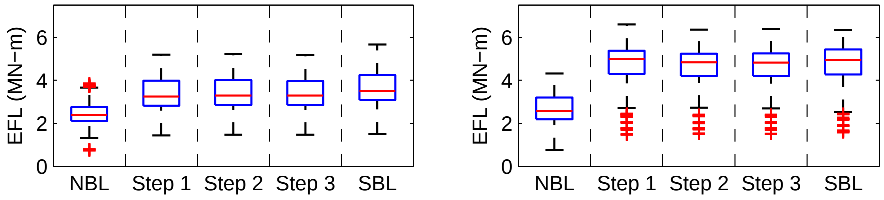

(c) $z_\alpha < 0 \quad \& \quad z_\sigma < 0$ (d) $z_\alpha > 0 \quad \& \quad z_\sigma < 0$

Figure 3.26: EFL statistics for OoPBM from 2,200 wind fields (SBL versus NBL base and modified cases).

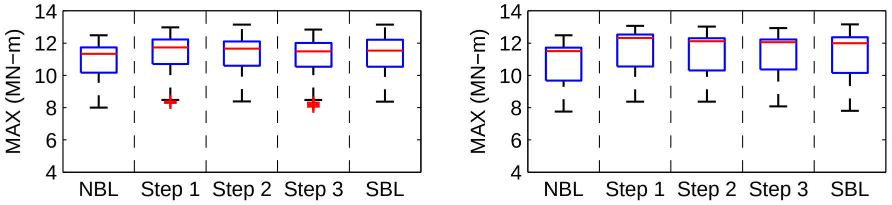

(a) $z_\alpha < 0 \quad \& \quad z_\sigma > 0$ (b) $z_\alpha > 0 \quad \& \quad z_\sigma > 0$

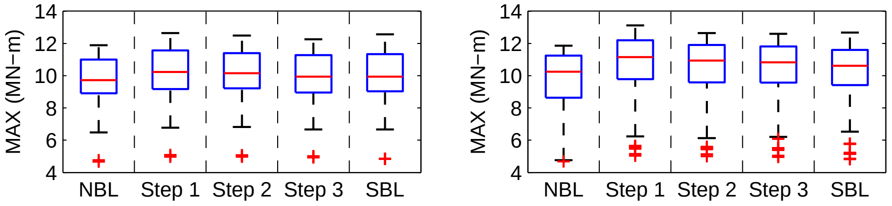

(c) $z_\alpha < 0 \quad \& \quad z_\sigma < 0$ (d) $z_\alpha > 0 \quad \& \quad z_\sigma < 0$

Figure 3.27: Ten-minute maximum statistics for OoPBM from 2,200 wind fields (SBL versus NBL base and modified cases).

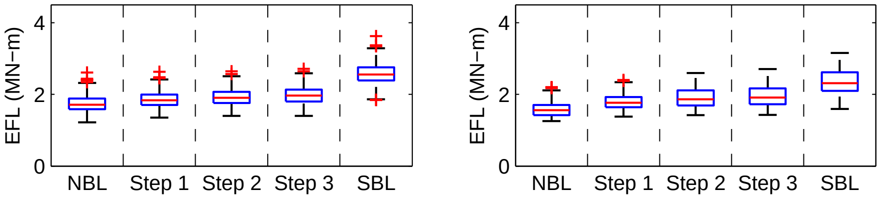

(a) $z_\alpha < 0 \quad \& \quad z_\sigma > 0$

(b) $z_\alpha > 0 \quad \& \quad z_\sigma > 0$

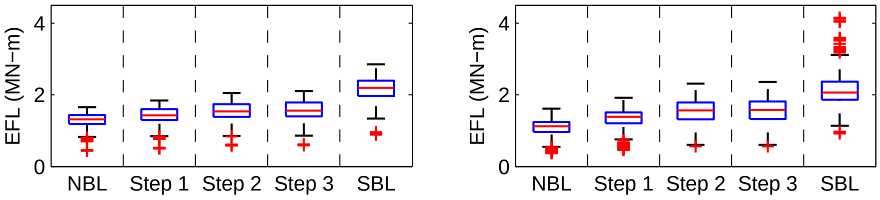

(c) $z_\alpha < 0 \quad \& \quad z_\sigma < 0$

(d) $z_\alpha > 0 \quad \& \quad z_\sigma < 0$

Figure 3.28: EFL statistics for TTYM from 2,200 wind fields (SBL versus NBL base and modified cases).

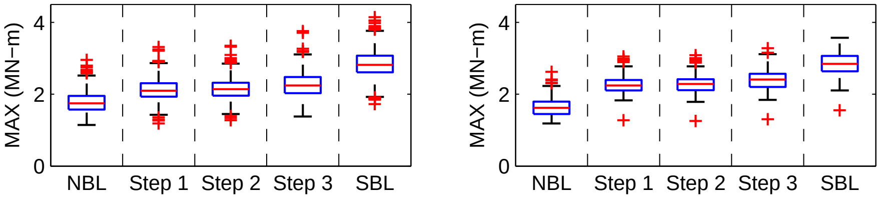

(a) $z_\alpha < 0 \quad \& \quad z_\sigma > 0$

(b) $z_\alpha > 0 \quad \& \quad z_\sigma > 0$

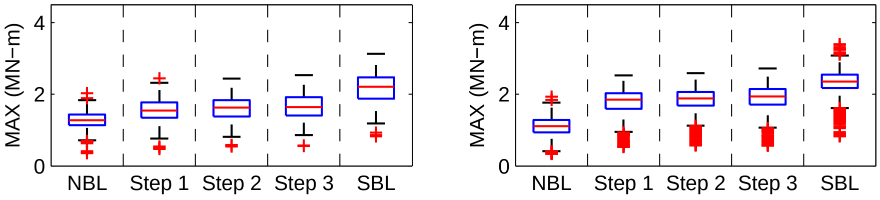

(c) $z_\alpha < 0 \quad \& \quad z_\sigma < 0$

(d) $z_\alpha > 0 \quad \& \quad z_\sigma < 0$

Figure 3.29: Ten-minute maximum statistics for TTYM from 2,200 wind fields (SBL versus NBL base and modified cases).

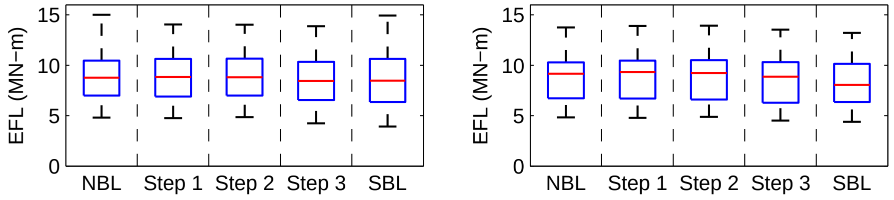

(a) $z_\alpha < 0 \quad \& \quad z_\sigma > 0$ (b) $z_\alpha > 0 \quad \& \quad z_\sigma > 0$

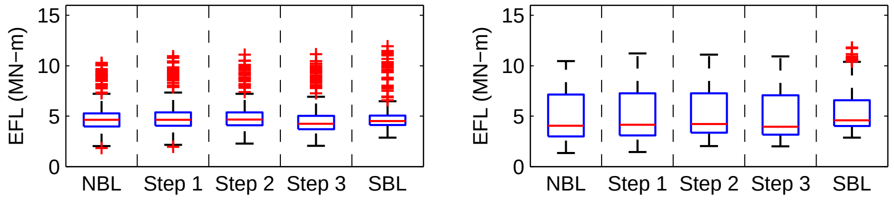

(c) $z_\alpha < 0 \quad \& \quad z_\sigma < 0$ (d) $z_\alpha > 0 \quad \& \quad z_\sigma < 0$

Figure 3.30: EFL statistics for FATBM from 2,200 wind fields (SBL versus NBL base and modified cases).

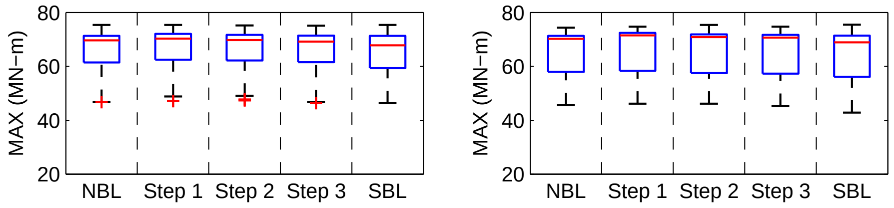

(a) $z_\alpha < 0 \quad \& \quad z_\sigma > 0$ (b) $z_\alpha > 0 \quad \& \quad z_\sigma > 0$

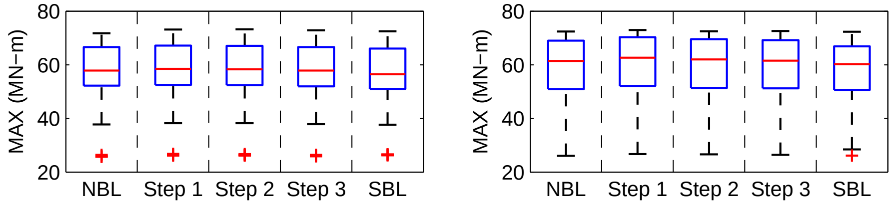

(c) $z_\alpha < 0 \quad \& \quad z_\sigma < 0$ (d) $z_\alpha > 0 \quad \& \quad z_\sigma < 0$

Figure 3.31: Ten-minute maximum statistics for FATBM from 2,200 wind fields (SBL versus NBL base and modified cases).

Chapter 4

Conclusions

4.1 The Stable Boundary Layer and its Effects

Large-eddy simulation (LES) can be used not only to generate wind flow fields in the stable boundary layer, but also to study characteristics of such wind fields. In LES, large-scale atmospheric conditions are set and then wind fields are generated based on solution of the Navier-Stokes equations. By relating external parameters describing the large-scale environmental conditions and internal parameters describing turbine-scale wind field characteristics, we investigated the influences of atmospheric conditions on wind flow fields. The following are conclusions based on our analysis:

- Geostrophic wind speed and surface cooling rate have the most significant influences on the characteristics of wind flows, while other large-scale environmental conditions, such as surface roughness, boundary layer height, inversion strength, Coriolis force frequency, and geostrophic departure have comparatively less influence on wind flow fields.

- Turbine-scale wind field characteristics (internal parameters) continue to change during the evolution of the stable boundary layer.

- An increases in the geostrophic wind speed leads to an increase in the mean and standard deviation of the longitudinal hub-height wind speed, but it reduces wind shear.
- An increase in the surface cooling rate enhances wind shear and also increases the hub-height mean wind speed, but it reduces turbulence levels.

4.2 Relationship between Wind Field Characteristics and Wind Turbine Loads

Both the influence of large-scale environmental conditions on turbine-scale wind fields and the influence of these turbine-scale wind field characteristics on wind turbine loads were investigated. The following points represent the major conclusions from the analysis:

- The geostrophic wind speed and surface cooling rate are the most influential factors among the external large-scale parameters on wind turbine load statistics.
- Higher geostrophic wind speeds increase the mean and standard deviation of the longitudinal wind speed, while attenuating wind shear. This generally increases fatigue and maximum loads on the wind turbine.
- A higher surface cooling rate makes the atmosphere more strongly stratified and, subsequently, increases the wind shear and decreases the level

of turbulence. This generally decreased the fatigue and maximum tower-top yawing moment and the base fore-aft tower bending moment. In the case of the blade root out-of-plane bending moment, however, higher surface cooling rates increased fatigue loads due to the enhanced shear which magnified the amplitude of this blade bending moment.

4.3 Comparison of the Characteristics of SBL and NBL wind fields

We compared characteristics of wind fields generated by the two methods—LES and stochastic simulation. The stochastic method constructs a mean wind profile based on a simple power law, and describes turbulence energy levels using standard spectra and coherence functions. These simplifications in the stochastic method result in wind field characteristics in the NBL (where such methods are commonly used) that are different from those of the SBL wind fields as follows:

- The wind shear is stronger in the stable boundary layer, which is effectively accounted for in LES wind field generation.
- The level of turbulence decreases with height in the LES-generated SBL wind fields, while the level of turbulence is often assumed to remain constant over the rotor plane in stochastic simulation of NBL wind fields.
- The wind direction variation with elevation is accounted for in the SBL wind fields and LES can account for this effect; NBL wind fields gen-

erated using stochastic simulation cannot taken into consideration such wind veer.

4.4 Comparison of Wind Turbine Loads Estimated from SBL and NBL wind fields

Flow features specific to the SBL that are present only in the wind fields generated using LES affect the wind turbine load types differently. We investigated how these features affect a wind turbine structure through turbine-scale wind field parameter-matching steps. The following are conclusions based on this analysis:

- The blade root out-of-plane bending moment is significantly amplified by strong shear in the stable boundary layer. Thus, modifying the mean wind profile by increasing the power-law shear exponent value leads to load statistics from stochastic simulation that are comparable to those for the SBL case.
- Tower-top yawing moments are much higher in the stable boundary layer as seen in LES-generated wind fields; matching turbine-scale wind field parameters in stochastic simulation is unable to match these load levels.
- The base fore-aft tower base moment is almost identical in both the SBL and NBL cases because this load is mainly influenced by the mean and standard deviation of the longitudinal wind speed at the hub height of the wind turbine.

Bibliography

[1] S. Basu, E. Foufoula-Georgiou, and F. Porté-Agel. Synthetic turbulence, fractal interpolation, and large-eddy simulation. *Physical Review*, E 70, 026310, 2004.

[2] International Electotechnical Commission. Wind Turbines - Part 1: Design Requirements. IEC 61400-1, Edition 3.0, 2005.

[3] American Society for Testing and Materials Standards. Standard practices for cycle counting in fatigue analysis. E1049-85, 1993.

[4] B. J. Geurts. *Elements of Direct and Large-Eddy Simulation.* R.T. Edwards, Inc., 2004.

[5] M. M. Hand, N. D. Kelley, and M. J. Balas. Identification of wind turbine responses to turbulent inflow structures. Technical Report NREL/CP-500-33465, National Renewable Energy Laboratory, Golden, Co, 2003.

[6] B. J. Jonkman and M. L. Buhl. TurbSim User's Guide. Technical Report NREL/EL-500-41136, National Renewable Energy Laboratory, Golden, Co, 2007.

[7] J. M. Jonkman and M. L. Buhl. FAST User's Guide. Technical Report NREL/EL-500-38230, National Renewable Energy Laboratory, Golden, Co, 2005.

[8] J. M. Jonkman, S. Butterfield, W. Musical, and G. Scott. Definition of a 5MW reference wind turbine for a offshore system development. Technical Report NREL/TP-500-38060, National Renewable Energy Laboratory, Golden, Co, 2007.

[9] N. D. Kelley. A case for including atmospheric thermodynamic variables in wind turbine fatigue loading parameter identification. Technical Report NREL/CP-500-26829, National Renewable Energy Laboratory, Golden, Co, 1999.

[10] N. D. Kelley, R. M. Osgood, J. T. Bialasiewicz, and A. Jakubowski. Using time-frequency and wavelet analysis to assess turbulent/rotor interactions. Technical Report NREL/CP-500-27151, National Renewable Energy Laboratory, Golden, Co, 1999.

[11] N.D. Kelley, M. Shirazi, D. Jager, S. Wilde, J. Adams, M. Buhl, P. Sullivan, and E. Patton. Lamar low-level jet project interim report. Technical Report NREL/TP-500-34593, National Renewable Energy Laboratory, Golden, Co, 2004.

[12] C. Sim. *Simulation and Anlysis of Wind Turbine loads for Neutrally Stable Inflow Turbulence.* M.S. Thesis, University of Texas at Austin, 2009.

[13] C. Sim, S. Basu, and L. Manuel. The influence of stable boundary layer flows on wind turbine fatigue loads. *47th AIAA Aerospace Sciences*

Modeling Including The New Horizons Forum and Aerospace Exposition, Orlando, Florida, AIAA 2009-1405, 2009.

[14] R. B. Stull. *An Introduction to Boundary Layer Meteorology.* Kluwer Academic Publishers, 1988.

[15] H. J. Sutherland. On the fatfigue analysis of wind turbines. Technical Report SAND99-0089, Sandia National Laboratories, Albuquerque, New Maxico, 1999.

[16] H. J. Sutherland. U.S. Department of Energy Workshop Report: Reserach needs for wind resource characterization. Technical Report NREL/TP-500-43521, National Renewable Energy Laboratory, Golden, Co, 2008.

Vita

Jinkyoo Park was born in Jinju-si, Republic of Korea on 10 May 1982, the son of Mr. Jaemyung Park and Mrs. Jungsook Lee. He received the Bachelor of Science degree in Engineering from Seoul National University in 2009 with the honor of first class in the Department of Architecture & Architectural Engineering. He served in the Republic of Korean Army from April, 2004 to April, 2006 and was discharged as a sergeant. As a recipient of the Graduate School Recruitment Fellowships, he started his graduate studies at the Department of Civil, Architectural and Environmental Engineering of the University of Texas at Austin in August 2009. He continues his PhD studies at Stanford University from September, 2011

Permanent address: 113-201 Greenvill Apt, Gajwa-dong
Jinju-si, Korea 660-779

This thesis was typeset with LaTeX[†] by the author.

[†] LaTeX is a document preparation system developed by Leslie Lamport as a special version of Donald Knuth's TeX Program.